Thomas Kronberg

Properties of raw glazes – The impact of composition, firing and functional coatings

Åbo Akademi University

Properties of raw glazes – The impact of composition, firing and functional coatings

Thomas Kronberg

Inorganic Chemistry
Faculty of Science and Engineering
Åbo Akademi University
Åbo, Finland, 2020

Supervisor

Professor Leena Hupa

Åbo Akademi University

Opponent and reviewer

Professor Delia Brauer

Friedrich-Schiller-Universität Jena

Reviewer

Professor Bo Jonson

Linnaeus University

ISBN 978-952-12-3978-6 (printed)

ISBN 978-952-12-3979-3 (digital)

Painosalama Oy – Turku, Finland 2020

"Science, like nature must also be tamed

With a view towards its preservation

Given the same state of integrity

It will surely serve us well"

Neil Peart/Rush, Natural Science

Preface

The work described in this thesis was carried out as part of my work at Geberit Production Oy (Ido Kylpyhuone Oy) during years 2001-2010 and at the Laboratory of Inorganic Chemistry, Åbo Akademi University, as part of the Johan Gadolin Process Chemistry Centre during years 2018-2020. Funding for the doctoral activities was provided by the Finnish Funding Agency for Technology and Innovation (Tekes), Johan Gadolin Process Chemistry Centre, Rector at Åbo Akademi University, Pukkila Oy and Ido Kylpyhuone Oy.

I would like to express my gratitude to everyone that has helped and supported me during this journey. First, I am deeply grateful to my supervisor Professor Leena Hupa. Your expertise, interest in my research topic and valuable help in writing made this happen. Without your help, this thesis had never been finalized. The help and all the valuable discussions with late Kaj Fröberg, especially in the beginning of this journey, is also highly acknowledged.

I would like to thank all my co-authors and the personnel at the Laboratory of Inorganic Chemistry. Your strong help and guidance made this thesis possible. Especially, the help from Linda Fröberg-Niemi and Minna Piispanen in laboratory work and co-writing is highly acknowledged. A special thanks to Jaana Paananen for carrying out a lot of laboratory work for this thesis. Clifford Ekholm and Linus Silvander are acknowledged for their help with SEM/EDX analysis.

I like to thank all my former colleagues at Ido Kylpyhuone Oy, for learning me how to produce ceramics and helping me to understand the difference between theory and practise.

Finally, I want to thank my friends and family who have always supported and accompanied me. My wife Maarit and my sons, Fredrik and Sebastian for supporting and pushing me forward. Remember it is never too late to fulfil your dreams!

Turku , May 2020

Thomas Kronberg

Abstract

Raw glazes, i.e. glazes mixed from oxides and minerals, are cost-effective alternatives to fritted compositions for ceramics fired at a high peak temperature (> 1150 °C). Raw glazes are mainly used for sanitary ware and porcelain, but also e.g. for dense floor tiles. Typically, many of the raw materials come from local mining plants and thus are cost-efficient alternatives.

New demands like replacing raw materials to more environmentally friendly ones, using lower top firing temperatures, or going to shorter firing cycles all require an adjustments of the glaze composition. For achieving a high-quality surface, a thorough understanding of the influence of different raw materials on the sintering, the melting as well as on the crystallization behaviour of the glaze is essential. The phase composition of the fired raw glaze depends on the kinetics of the various raw material reactions during the heating and soaking periods at the top firing temperature as well as on the phase changes taking place during the cooling period.

Although ceramics are considered to provide easy-to-clean surfaces, considerable effort and money are spent on cleaning the soiled surfaces. Exposure to chemical agents or mechanical wear can alter the surface structure and thereby diminish the cleanability during the life cycle. Functional surfaces have been developed to increase the anti-soiling and cleanability properties of traditionally glazed surfaces.

These new requirements and changes have led to the need for a better understanding of the melting behaviour and surface modification to achieve surfaces with desired appearance and performance.

In this work, the melting behaviour was estimated from sintering curves and characteristic sample points measured with hot-stage microscopy (HSM). Altogether seventy-five compositions were mixed from seven different raw materials (Series I). All the compositions were also applied on raw tiles and fired in an industrial kiln for fast-firing (50 min) to verify the melting behaviour and characteristics of the final glaze (gloss, surface hardness and phase composition). The goal was to explore whether the typical sample shapes and sintering curves measured with HSM can be used to describe the melting behaviour of raw glazes. The temperatures describing the sintering and melting of the glazes were mathematically modelled as functions of the raw material composition. For each point, a model of the compositional dependence was established. A correlation between the gloss of the fast-fired glazes and the melting characteristics at higher temperatures of the HSM measurement could be found.

Thus, the melting behaviour obtained by HSM can also be used to predict the melting behaviour in the industrial fast-firing kiln when optimizing glossy glazes.

The effect of soaking time on phase composition and topography was estimated from tiles fired in a laboratory kiln with different soaking times. The same tiles were also fired in an industrial fast-fired kiln. Fifteen experimental glaze compositions were used in this study (Series II). The goal was to establish the changes in phase composition and topography of raw glazes within the compositional field for tiles and sanitary ware when firing cycle varied from fast to traditional. The results showed that the phase composition and topography changed with the firing cycle. In short firing, the surface morphology depended on initial raw material reactions and melt formation. At prolonged firing, the surface morphology correlated with the total oxide composition and the equilibrium phase condition at high temperatures. The results also indicated that the soaking time of raw glazes can be shortened if the total glaze composition is adjusted to provide desired surface properties.

The results from the study of the melting behaviour showed that dolomite and wollastonite in the recipe enhanced the melting behaviour of the glaze at around 1200 °C. However, when the amount of the alkaline earths CaO and MgO increased, a matte surface appearance was obtained. The effect of adding these alkaline earths through dolomite and wollastonite on the melting behaviour and surface properties was explored. Twenty-five experimental glaze compositions (Series III) were used in this study. Both the total content and the ratio between wollastonite and dolomite were found to control the melting behaviour. The fusibility was increased with wollastonite, and thus, the CaO content in the glaze. Also, MgO introduced as dolomite increased the fusibility of the glazes. In fast-firing, the most pronounced effect was found when the MgO content was around 2 wt%. The main crystalline phases in the Series III glazes were wollastonite and diopside. The chemical durability of the glazes containing wollastonite crystals at the surface was poor in acidic solutions. The wollastonite crystals were rapidly attacked and reacted through incongruent dissolution of calcium and leaving a silica-rich remnant at the surface. The diopside crystals showed excellent durability in all acidic to alkaline the solutions. However, the amorphous phase in the glazes with high contents of alkaline earths was heavily attacked in the acidic solutions. Although the overall acid durability of the wollastonite-containing glazes was low, the excellent properties of the diopside crystals are encouraging for further studies of manufacture of diopside-based matted raw glazes, especially in a modified composition range with higher silica contents to ensure better durability.

Increasing demands for improved surface properties, such as easier cleanability, have led to applying also functional coatings on traditional glaze surfaces. However, the functionality, as well as the mechanical and chemical durability of these coatings are not yet fully understood or controlled. In this study, traditional white sanitary ware glazes were coated with commercial fluoropolymers and experimental hybrid sol-gel functional coatings. The cleanability and the resistance to mechanical and chemical wear of the coated surfaces were measured. The results showed that the additional functional coatings improved the cleanability of glazes. However, the increased cleanability by the additional functional films was lost for the surfaces, which were partially or totally destroyed by mechanical or chemical wear.

The results obtained in this study give valuable additional information and new tools to design glaze compositions with desired surface characteristics for different firing schedules. The models can be utilized when designing new glaze compositions for changed requirements or when comparing the melting behaviour of different raw glazes. Also, the calculated trends can directly be adapted to practical glaze firing processes. The results can also be applied to adjust the glaze composition for given firing cycles in order to improve the chemical durability and to achieve the desired microstructure through controlled surface composition. The results can also be used to estimate the criteria for tailoring additional functional coatings and glaze surfaces for a long-term effect on cleanability in everyday environments.

Keywords: glaze, melting behaviour, phase composition, chemical durability, functional coatings

Svensk sammanfattning

Råglasyrer, dvs glasyrer tillverkade från oxider och naturliga mineral, är ett lönsamt alternativ istället för frittor (finmalt glas) för keramiska produkter brända vid en hög topptemperatur (> 1150 °C). Råglasyrer används främst för sanitets- och hushållsporslin, men kan även användas för t.ex. tätsintrade golvplattor. Flera av råmaterialen kommer vanligtvis från lokala anläggningar och blir därmed kostnadseffektiva.

Nya krav, såsom användning av mera miljövänliga råmaterial, lägre topptemperaturer eller förkortade bränntider i brännugnen, kräver alla en justering av glasyrsammansättningen. För att uppnå en glasyryta av högsta kvalitet är det nödvändigt att ha en grundlig förståelse av hur de olika råmaterialen inverkar på glasyrens sintrings-, smält- samt kristallisationsegenskaper. Den brända glasyrens fassammansättningen beror på de olika råmaterialens reaktionskinetik under upphettningsperioden, hålltiden vid topptemperaturen samt på olika fasförändringar som kan ske under kylningsperioden.

Även om en keramisk yta anses vara lätt att rengöra, läggs stora ansträngningar och pengar på att rengöra nedsmutsade glasyrytor. Då ytorna utsätts för kemikalier eller mekaniskt slitage kan ytstrukturen påverkas och därmed minskar även rengörbarheten under produktens livslängd. Funktionella ytor har utvecklats för att förbättra rengöringsegenskaperna även för traditionella glasyrer.

Dessa nya krav och förändringar har lett till ett behov av bättre förståelse för glasyrens smältbeteende och hur man kan modifiera glasyrytan. Detta för att erhålla ytor med önskat utseende och prestanda.

I detta arbete har smältbeteendet för olika glasyrsammansättningar uppskattas från sintringskurvor och karakteristiska mätpunkter uppmätta med upphettningsmikroskopi. Totalt 75 sammansättningar bestående av 7 olika råmaterial användes i denna försöksserie (Serie 1). Dessa sammansättningar applicerades även på obrända kakelplattor, varefter plattorna brändes i en industriell ugn för snabb bränning (50 min) för att kunna verifiera glasyrens smältbeteende samt övriga egenskaper (glans, hårdhet och fassammansättning). Målet var att undersöka om de karakteristiska mätpunkterna uppmätta med upphettningsmikroskopi kan användas för att beskriva smältbeteendet för råglasyrer. Temperaturerna för de olika mätpunkterna som beskriver glasyrens sintring och smältning modellerades matematiskt som funktion av råmaterialsammansättningen. För varje mätpunkt upprättades en modell som beskriver inverkan av råmaterialsammansättningen. En

korrelation identifierades mellan glansvärdet för industriellt, snabb brända glasyrer och smältbeteendet vid de högre temperaturerna från upphettningsmikroskopi. Därmed kan upphettningsmikroskopi även användas för att kunna förutse smältbeteendet i industriell, snabb bränning när man vill optimera glansiga glasyrer.

Inverkan av bränningens hålltid vid topptemperaturen på fassammansättning och topografi uppskattades från glasyrsammansättningar brända i en laboratorieugn med olika hålltider samt i en industriell ugn för snabb bränning. I denna försöksserie användes 15 olika glasyrsammansättningar (Serie II). Resultaten visade att fassammansättningen och topografin ändrade med bränntiden. I snabb bränning beror morfologin på de första reaktionerna mellan råmaterialen samt på smältbildningen. Vid en längre bränntid korrelerar morfologin med den totala oxidsammansättningen samt med fasjämviktsförhållanden vid högre temperaturer. Resultaten antydde också att hålltiden kan förkortas om den totala glasyrsammansättningen kan justeras så att önskade egenskaper för glasyrytan erhålls.

Resultaten från Serie I visade att en tillsats av dolomit och wollastonit i glasyrreceptet förbättrade glasyrens smältbarhet vid ca 1200 °C. En noggrannare undersökning utfördes för att studera effekten av att tillsätta dolomit och wollastonit på glasyrens smältbeteende och ytans egenskaper. 25 olika glasyrsammansättningar undersöktes i denna studie (Serie III). Både den totala andelen samt förhållandet mellan wollastonit och dolomit inverkade på smältbeteendet. Smältbarheten ökade med andelen wollastonit och därmed andelen CaO i glasyren. Smältbarheten ökade även med andelen MgO från dolomit. I snabb bränning hade en MgO andel på ca 2 vikt-% den största effekten. När CaO och MgO mängden i receptet var högt erhölls en matt glasyryta. I dessa glasyrer bestod de kristallina faserna främst av wollastonit och diopsid.

För glasyrer med wollastonit partiklar på ytan var den kemiska beständigheten i sura lösningar dålig. Wollastonit kristallerna attackerades snabbt och reagerade genom en inkongruent upplösning av kalcium och lämnade kvar en kiselrik rest på ytan. Diopsid kristallerna däremot hade en utmärkt kemisk beständighet i både sura och basiska lösningar. I glasyrer med en hög andel av både CaO och MgO blev den amorfa glasyrfasen hårt angripen av sura lösningar. Även om wollastonit hade en dålig beständighet i sura lösningar så är diopsidens utmärkta kemiska beständighet lovande för fortsatta studier av diopsid baserade matta råglasyrer. Genom att justera sammansättningen med en högre mängd kisel torde även den kemiska beständigheten öka.

Högre krav på ytans egenskaper, såsom rengörbarhet, har lett till att även funktionella ytor har applicerats på traditionella glasyrytor. Funktionaliteten, liksom den mekaniska och kemiska hållfastheten för dessa ytor är fortfarande inte helt kända. I denna studie har kommersiella och experimentella funktionella ytor applicerats på traditionella, vita sanitetsglasyrer. Rengörbarheten samt den mekaniska och kemiska hållbarheten för de olika ytorna har undersökts. Resultaten visade att de funktionella ytorna förbättrade glasyrernas rengörbarhet. Rengörbarheten försämrades dock för de funktionella ytor som hade en dålig kemisk och mekanisk beständighet.

Resultaten som erhållits i detta arbete ger värdefull information och nya verktyg för att utveckla nya glasyregenskaper. Modellerna kan utnyttjas för att utveckla nya glasyrsammansättningar eller när man vill jämföra smältbeteendet för olika glasyrer. Resultaten kan även användas för att justera glasyrsammansättningen för en given bränntid för att förbättra den kemiska beständigheten och för att uppnå en önskad kontrollerad mikrostruktur på ytan. Resultaten ger även riktlinjer för att framställa funktionella ytor och glasyrytor med en långsiktig effekt på rengörbarheten.

List of original publications

This dissertation is based on the following scientific publications:

I. T. Kronberg, L. Hupa, Melting behavior of raw glazes, J. Eur. Ceram. Soc. 39 (2019), 4404-4416.

II. L. Fröberg, T. Kronberg, L. Hupa, Effect of soaking period on phase composition and topography and surface microstructure in vitrocrystalline whiteware glazes, J. Eur. Ceram. Soc. 29 (11) (2009), 2153-2161.

III. T. Kronberg, L. Hupa, K. Fröberg, Melting behaviour and surface structure of glazes containing wollastonite and dolomite, Adv. Sci. Technol. 45 (2006), 590-595, Trans Tech Publications, Switzerland.

IV. T. Kronberg, L. Hupa, The impact of wollastonite and dolomite on chemical durability of matte fast-fired raw glazes, J. Eur. Ceram. Soc. 40 (2020), 3327- 3337.

V. T. Kronberg, A.C. Ritschkoff, R. Mahlberg, J. Mannila, M. Kallio, M., A. Vesa, L. Hupa, Soil-resistant surfaces for traditional ceramics, J. Eur. Ceram. Soc. 27 (2007), 1775-1780.

VI. M. Piispanen, T. Kronberg, S. Areva, L. Hupa, Effect of mechanical and chemical wear on soil attachment and cleanability of sanitaryware with additional coatings, J. Am. Ceram. Soc. 94(3) (2011), 951-958.

Other publications from the author with relevance to this thesis:

T. Kronberg, L .Hupa, K. Fröberg, Optimizing of glaze properties, Ceram. Eng. Sci. Proc. **22** (2) (2001), 179-189.

T. Kronberg, K. Fröberg, The melting behavior in the wollastonite – feldspar – quartz system, Ceram. Eng. Sci. Proc. **22** (2) (2001), 167-177.

L. Fröberg, T. Kronberg, L. Hupa, M. Hupa, Influence of firing parameters on phase composition of raw glazes, J. Eur. Ceram. Soc. **27** (2007), 1671-1675.

L. Fröberg, T. Kronberg, L. Hupa, K. Fröberg, M. Hupa, Working towards better raw glazes, Proc. 10th ECerS 2007, Berlin, Germany, ISBN-3-87264-022-4 (CD-Rom), 2008.

T. Kronberg, L. Hupa, K. Fröberg, Durability of mat glazes in hydrochloric acid solution", 8th European Ceramic Society Conference and Exhibition, 29.6 – 3.7.2003, Istanbul, Turkey. Key Eng. Mat. Vols. 264-268 (2004), 1565-68.

L. Fröberg, T. Kronberg, S. Törnblom, L. Hupa, Chemical durability of glazed surfaces, J. Eur. Ceram. Soc. **27** (2007), 1811-1816.

S. Vane-Tempest, T. Kronberg, L. Fröberg, L. Hupa, Chemical resistance of fast-fired raw glazes, Qualicer 2004, Proc. of VIII World Congress on Ceramic Tile Quality, Castellón, Spain (2004), Vol. I, P.GI-155

L. Hupa, R. Bergman, L. Fröberg, S. Vane-Tempest, M. Hupa, T. Kronberg, E. Pesonen-Leinonen, A. M. Sjöberg, Chemical resistance and cleanability of glazed surfaces, Surf. Sci. (2005), 584, 113-118.

L. Fröberg, T. Kronberg, L. Hupa, K. Fröberg, M. Hupa, Working towards better raw glazes, Proc. 10th ECerS 2007, Berlin, Germany, ISBN-3-87264-022-4 (CD-Rom), 2008

T. Kronberg, M. Piispanen, S. Areva, L. Hupa, Cleanability of functional and traditional ceramic surfaces. Proc. 10th ECerS 2007, Berlin, Germany, ISBN-3-87264-022-4 (CD-Rom), 2008

M. Piispanen, T. Kronberg, S. Areva, J. Pimenoff, L. Hupa, Easy-to-clean coatings on glass and glazed surfaces, Adv. Sci. Technol. 66 (2010), 150-155.

M. Piispanen, L. Fröberg, T. Kronberg, S. Areva, L. Hupa, Corrosion of glazes with functional films in detergent solutions, Adv. Sci. Technol. **45** (2006), 156-161, Trans Tech Publications, Switzerland.

M. Piispanen, J. Määttä, T. Kronberg, S. Areva, A-M. Sjöberg, L. Hupa, Effect of mechanical and chemical wear on cleanability of functional and traditional glazed surfaces, Proc. 10th ECerS 2007, Berlin, Germany, ISBN-3-87264-022-4 (CD-Rom), 2008.

Contribution of the author

The following describes the author's contribution to the papers on which this thesis is based

I. The author was responsible for the experimental design of the work and mathematical modelling, the interpretation of all data from the HSM, SEM, XRD, PEI and gloss analyses. The author arranged and participated in the industrial firings. The author was the main author of the publication.

II. The author participated in the experimental design of the study and in the interpretation of the results. The author participated in writing the publication.

III. The author was responsible for the experimental design of the work, the interpretation of all data from the SEM, XRD, and gloss analysis. The author arranged and participated in the industrial firings. The author was the main author of the publication.

IV. The author was responsible for the experimental design of the work, the interpretation of all data from the HSM, SEM, XRD, ICP-AES, gloss, chemical durability and surface topography analyses. The author arranged and participated in the industrial firings. The author was the main author of the publication.

V. The author was responsible for the experimental design of the study and the application of the fluoropolymers and double glazed surfaces as well as the interpretation of the SEM and COM analysis. The author was the main author of the publication

VI. The author participated in the experimental design of the study and in the interpretation of the results. The author also participated in writing the publication.

List of abbreviations and symbols

Abbreviations:

AES	Atomic Emission Spectroscopy
AFM	Atomic Force Microscopy
ASTM	American Society of Testing Materials
BSS	British Standard Society
CC	China Clay
Co	Corundum
COM	Confocal Optical Microscope
DIN	German Institute for Standardization
Do	Dolomite
EDXA	Energy Dispersive X-ray Analysis
EN	European Norm
FP	Floating Point
FS	Feldspar
FTIR	Fourier Transform Infrared Spectroscopy
HCP	Half-Cone Point
HSM	Hot-Stage Microscopy
ICP	Inductively Coupled Plasma
ISO	International Standard Organization
PEI	Porcelain Enamel Institute
MBL	Minimum Base Line
Q	Quartz
SEM	Scanning Electron Microscope
Softening	Softening Point

SP	Sintering Point
VSI	Vertical Scanning Interferometry
VFT	Vogel-Fulcher-Tamman
VTT	Technical Research Centre of Finland
Wo	Wollastonite
Wt%	Weight percent
XRD	X-ray diffraction
Zr	Zirconium silicate

Symbols

°C	degree Celcius
R^2	mean square error
T_f	melting temperature
T_g	glass transition temperature
η	viscosity
T_1	onset of sintering temperature
T_2	onset of melting range temperature
T_3	onset of main melting temperature
Sa	arithmetic average of the surface roughness
Ra	arithmetic average of profile height
ΔE_s	soil amount attached to the surface
ΔE_{rem}	soil amount removed from the surface
ΔE_{res}	soil residue
ρ_i	amount of element *i*

Table of content

1. Introduction

New demands like replacing raw materials used today in glazes to more environmentally friendly ones, lowering peak firing temperatures, or going to shorter firing cycles all require adjustment of the overall glaze compositions. For achieving a high-quality surface, a thorough understanding of the influence of different raw materials on the sintering, the melting, as well as on the crystallization behaviour of the glaze is essential. Although ceramics are considered to provide easy-to-clean surfaces, considerable effort and money are spent on cleaning the soiled surfaces. Functional surfaces have been developed to increase the anti-soiling and cleanability properties of traditionally glazed surfaces. These new requirements and changes have led to the need for a better understanding of the properties needed for achieving glazed surfaces with desired appearance and performance.

Raw glazes are made from mixtures of minerals and oxides instead of pre-melted glasses, the so-called frits. Raw glazes are cost-effective alternatives for ceramics fired at a high peak temperature (> 1150 °C) to low porosity. Raw glazes are mainly used for sanitary ware, stoneware and porcelain, but also e.g. for dense floor tiles. Typically, many of the raw materials come from local mining plants and thus are cost-efficient alternatives. During the past decades, the utilization of fritted formulations has steadily increased, especially in the ceramic tile industry. Homogeneous, fritted glazes are indispensable for obtaining desired and controlled surface textures on ceramics fired in a fast-firing cycle (30-50 min). On the other hand, elimination of the glaze melt fritting process by using raw glazes leads to substantial savings in the total energy consumption. In general, the reaction kinetics during the firing depends on the overall glaze formulation, the chemical and mineralogical composition as well as the particle size of the raw materials. When using raw glazes in fast-firing, the glaze composition must be carefully tailored for a desired and controlled reactions. Future utilization of raw glazes depends on whether the formulations can be adapted for changes in the manufacturing conditions such as shorter firing schedules and lower peak firing temperatures, or changes in the requirements for the final glaze properties.

Phase composition, crystalline phases present, and surface topography all influence the properties of the fired glaze surface. The phase composition is controlled by the reaction kinetics of the raw materials during the heating step and the soaking time at the peak temperature. In addition, the crystallization tendency during the cooling also affects the final surface phase composition. The crystalline phases which are found in traditionally fired glazes after the long firing cycle correspond to the

phases found in relevant phase diagrams, whereas in fast-firing the final phases often are those that are formed already during the first raw material reactions.

Glazed surfaces are typically used in applications where the protection against soil attachment to the substrate is required and where easy cleaning is desired. The cleanability and the adhesion of soils depend on surface properties such as the chemical composition, phase composition and roughness of the surface. However, if the surface is exposed to corrosive environments or mechanical wear, surface pitting and degradation can alter the surface structure and thereby diminish the cleanability during the life cycle. Chemical durability of glazes is often discussed as the durability of the amorphous phase present in accordance with homogeneous amorphous glasses. However, the glaze appearance can vary from glossy and homogeneous surfaces to matte surfaces containing several different crystalline phases embedded in an amorphous phase and further to compositions which mainly consist of crystalline phases with some residual amorphous phase. Thus, the chemical durability of glazes is a complex phenomenon and should be discussed as the resistance of the amorphous and the crystalline phases. In addition, the chemical durability of the interfacial thin layer between the phases may have an impact on the overall durability.

Special functional coatings have been applied on ceramic glazes to enhance their soil-repelling and cleanability properties. However, the effects of many of the coatings are still not fully understood, partly due to the fact that no standard method to measure the cleanability is available. In addition, the cleanability also depends on several parameters such as the composition of the soil, the cleaning method and the overall surface characteristics. Also, the effect of mechanical and chemical wear of the coating and their influence on the overall cleanability are not thoroughly understood.

Purpose of the work

The purpose of this work was to increase the overall understanding of surface properties of raw glazes by studying the influence of the glaze composition on the melting behaviour as well as on the phase composition of the final glaze after different firing schedules in industrial kilns and laboratory furnaces. Additionally, the purpose was to gain better knowledge about the cleanability and chemical and mechanical durability of glazed surfaces with and without additional functional coatings.

This work is based on experiments done over a long time span in ceramic tile and sanitary ware industries using raw glazes in production. Most of the experimental work was done and reported during the period 2001 to 2010. Some unpublished results were revisited and summarized in two publications in 2019-2020.

This work is divided into three parts as follows:

1) Influence of raw glaze composition on melting behaviour and surface properties
2) Surface appearance and chemical durability of raw glazes containing dolomite and wollastonite
3) Cleanability and durability of soil-resistant surfaces on traditional ceramics

The key factors studied in this work are summarized in Fig. 1.

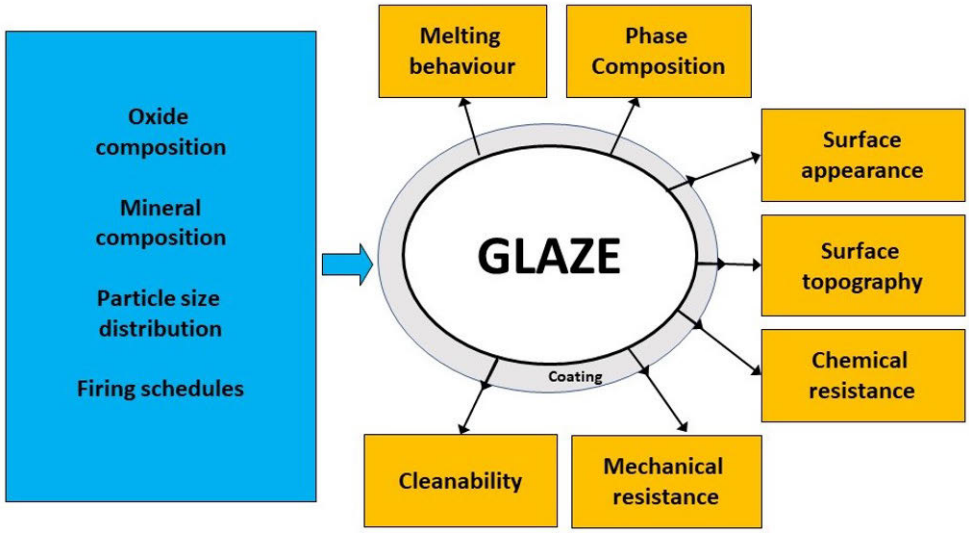

Fig 1. Factors affecting the quality of raw glazed ceramic surfaces.

The goals of this work were:

- To explore whether the typical sample shapes and sintering curves measured with hot-stage microscopy can be used to describe and model the melting behaviour of raw glazes.

- To gain detailed information about the influence of glaze composition and firing schedule on phase composition and surface roughness

- To understand the impact of wollastonite and dolomite on the melting behaviour and the development of matte raw glazed surfaces. An additional goal was to explore the effect of phase composition on the chemical durability of the matte raw glazes.

- To assess the impact of additional coatings on the cleanability of glazed surfaces. To estimate the effect of mechanical and chemical wear on the surface properties.

2. Literature review

2.1 Glaze history

Glazes are thin (75-500 μm), usually smooth and essentially amorphous coatings on ceramic ware [1]. Glazes mainly consist of an amorphous phase, but in opaque or matte glazes, the amorphous matrix also contains crystalline phases. The composition of the glaze is chosen to ensure certain properties, such as adhesion to the ceramic substrate, desired melting behaviour, suitable thermal expansion, transparency or opacity, surface texture, chemical and mechanical resistance.

The earliest glazes were made from aqueous suspensions of quartz sand mixed with an added flux of sodium salts or plant ash [2]. The suspension was applied on a fired ware and during the refiring, the particles fused into a glassy layer. The first opaque goods, i.e. glaze beads and amphoras, were produced in Egypt and are dated to around 4000 to 3100 BC [3]. In China, stoneware glazes containing calcium oxide and wood ash appeared around 1600 to 1500 BC, and a few centuries later also high-firing feldspathic glazes were applied [3]. The first lead glazes were introduced during the Warring States period in China (475-221 BC) [4]. The lead content in the glazes was about 20 %. During the Han dynasty in China (206 BC – 200 AD), a typical lead content of 50-60 wt% was used. Lead was used because it reduces the melting point of the glaze. However, lead from the glaze may be leached out by food and liquids, and today, the use of lead is no longer acceptable. Already around 2000 BC, tin was used in glazes in Mesopotamia but fell later into disuse. It was first around 900 AD when white opaque glazes containing tin oxide as opacifier were rediscovered by Islamic potters [4]. Tin glazes were spread into Europe via the island Mallorca. Later, the ceramics with this kind of white glaze were called Majolica, i.e. the name derived from the word Mallorca. Majolica manufacture developed further in Faenza in Italy (the so-called Faience) and in Delft in the Netherlands (the so-called Delftware). Tin glazing became industrially important at the end of the 19th century with the growth of sanitary ware industry [4].

The science of ceramic glazes was poorly understood until the pioneering work by Hermann Seger in the late 19th century [5]. After his work of introducing the Seger formula, the knowledge of glazes took a major step forward. The work that describes the composition of a glaze according to the mole fractions of its oxides was a valuable step ahead. The method of describing the composition through mole fraction is still today widely used when formulating glaze compositions. Since then, the progress has

continued so that the practice of ceramic glazes is well understood in many aspects [3]. The research on the formulation of lead-free glazes was intensive in the 1990s [3]. During the last decades, much effort has been put on the development of glass-ceramic glaze surfaces with improved mechanical, thermal and chemical properties [6]. The improved functionality of the surface, e.g. cleanability and self-cleaning, has been a topic for intensive studies in the past decades [7].

2.2 The glassy state and glass structure

Vitreous glaze coatings are essentially glasses, which are bonded to a ceramic substrate. While they have additional requirements as coatings on more or less porous ceramics, they also have some of the advantages and disadvantages of glasses [3]. Therefore, it is important to understand the basics of the nature of glass.

The characteristic random network structure for glass presented by Zachariasen [8] and Warren [9] suggested that the same disordered structure as observed in melt is also found in glass. Zachariasen noted that the mechanical properties and density of glass were similar to the corresponding crystal. Therefore, the same structural units, SiO_4 tetrahedra, are found in the melt, the glass and the crystalline phase. A schematic presentation of the ordered form of crystal structure in contrast to the disordered structure of glass is illustrated in Fig. 2. With this concept, a set of empirical rules that an oxide must satisfy to form glass can be defined as:

1. Oxygen atoms are bonded to no more than two cations
2. The coordination number of the cation to the oxygen is low; usually four or less.
3. Oxygen polyhedra share corners, not edges or faces.
4. At least three corners of each polyhedron must be shared. In practice, this rule gives triangles or tetrahedra.

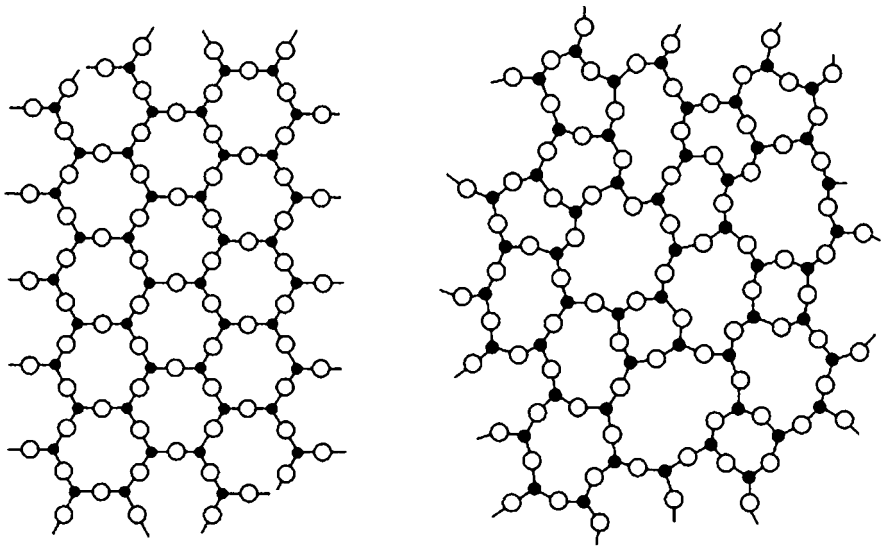

Fig. 2. Schematic two-dimensional representation of the structure of a) an ordered form of crystal structure and b) a random network structure of a glass of the same composition [3].

The oxides that meet these criteria for glass formation are called network formers (e.g. SiO_2, B_2O_3). Oxides that cannot form glasses alone but will do it when melted with a second oxide are called intermediates (e.g. Al_2O_3, TiO_2). The other ions in the glass are supposed to occupy random positions in the network. Their major function is to contribute additional oxygen ions, which modify the network structure. Hence, they are called network modifiers (e.g. Na_2O, K_2O, CaO, MgO, ZnO, and PbO).

Glass is often defined as an inorganic solid that has cooled without crystallization. However, glazes often consist of both a glassy phase and one or more crystalline phases and therefore the relationships between the different phases glass, crystals, and liquid at different temperatures become important. A volume-temperature diagram can be used to describe these relationships (Fig. 3). If a liquid of low viscosity is cooled slowly from A to B, then crystallization at T_f will occur. By contrast, if a liquid of high viscosity is cooled rapidly, crystallization at temperature T_f will not occur. Instead, the supercooled liquid continues to exist at decreasing temperature along the line BE to point E, which is the glass transition temperature T_g. At the glass transition temperature T_g, several properties change from liquid-like to solid-like properties.

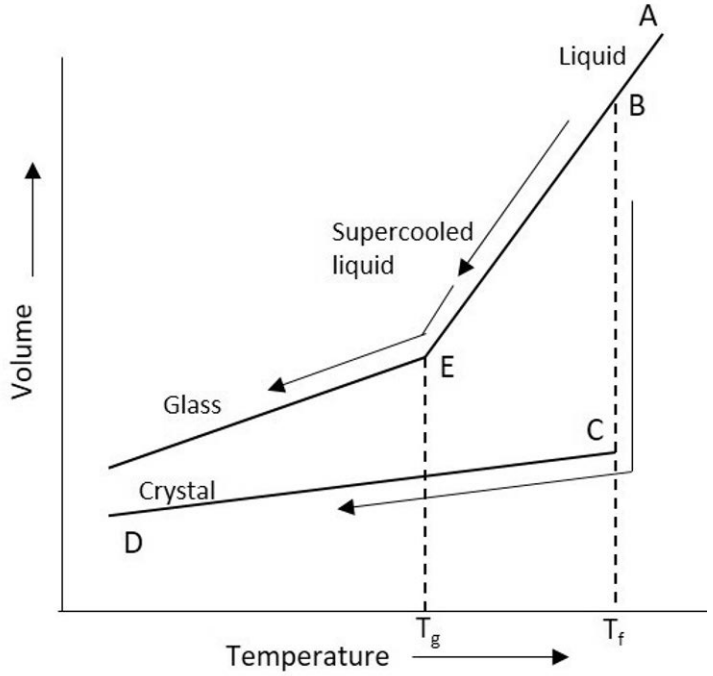

Fig 3. Volume-temperature curves for crystallization and for glass formation from liquid. T_f = melting temperature, T_g = glass transformation temperature. Redrawn according to [1].

2.3 Glaze formulation

Glazes can be classified according to characteristics of the glaze itself, the substrate, the final product, some features of the glaze application or the firing process. An example of classifications according to Taylor and Bull [1] is given below:

1. Lead or leadless
2. Raw or fritted
3. Once-fired or twice-fired
4. Tile, tableware, sanitary ware, electrical porcelain, etc.
5. Hollow-ware or flatware
6. Earthenware, hard porcelain, bone china, vitreous china, alumina, etc.
7. Dipping, spraying, waterfall, etc.
8. Fast-fire or conventional fire
9. High temperature or low temperature

10. High expansion or low expansion
11. Oxidising, neutral or reducing firing
12. Coloured or colourless
13. Transparent or opaque
14. Glossy, matte, vellum or textured, etc.
15. Electrically conducting, scratch-resistant, etc.

The list above shows the complexity and interrelationships of glazes. Usually, a glaze can be classified according to several of the above-mentioned classes. In this study, the primary effort has been to study leadless raw glazes that have been once fired in a fast-firing cycle for ceramic tiles, or in a longer, traditional firing schedule typical for sanitary ware glazes.

Raw glazes, i.e. glazes made from oxides and minerals, are typically used on ceramics fired at 1150 °C or higher temperatures [1]. High firing temperatures are needed to dissolve the high-melting raw materials, i.e. quartz and corundum. Fritted glazes consist of a portion of a pre-melted glass (frit). Frits are produced by melting the raw material batch at high temperatures (1400 – 1600 °C) followed by quenching into water. The mixture is then ground into a fine powder. Fritted glazes are needed if the peak firing temperature is less than 1150 °C. Complex formulations usually contain several different frits and may contain a range of minerals. The increased interest in fast-firing for production of ceramic tiles has led to increased use of fritted glazes. Frits soften over a wider range of temperatures in contrast to raw materials that melt at a certain temperature or within a narrow temperature range. Furthermore, when using frits, the overall content of lower melting compounds, i.e. alkali oxides can be higher without causing problems for the final glaze quality. Raw materials providing only alkali oxides are water-soluble and thus not suitable for the fine-grained suspensions used as raw glazes. Also, the homogeneity of the frit enhances its melting behaviour. Compared to fritted glazes, the less expensive raw glazes are typically preferred on ceramics fired to near-zero porosity, i.e. stoneware, sanitary ware, porcelain, etc. For these, the soaking period at the top firing temperature is usually long enough for the raw material reactions to proceed to the desired degree needed for a desired surface finish of the final glaze. The phase composition of the fired raw glaze depends on the kinetics of the various reactions between the raw materials during the heating and soaking periods at the peak firing temperature, as well as on the phase changes in the glaze during the cooling period [10]. In general, the reaction kinetics during the firing schedule depends on the overall raw glaze batch formulation, the chemical and mineralogical composition as well as the grain size of

the raw materials [3]. When using raw glazes on ceramics fired at lower peak temperatures and/or shorter firing cycles, such as glazed tiles, the glaze batch must be carefully tailored for a desired and controlled reaction degree. During the past decades, the utilization of fritted formulations has steadily increased, although raw glazes would be a cost-effective alternative also in fast-firing of fully densified ceramics like frost-resistant floor or swimming pool tiles [10]. The recipe of glazes can be presented in several different ways. Raw material composition shows the percentage of each raw material in the mixture while the oxide formula shows the percentage of each oxide in the final glaze. The molecular formula is used to give the relative proportion of fluxes (alkalis and alkaline earth oxides), alumina, and silica in the recipe. Traditionally, glaze compositions are given by the so-called Seger formula, a special molecular formula, which makes it easier to compare glazes. The Seger formula is also referred to as empirical or unity molecular formula [11]. In the Seger formula, the oxides are divided into three categories: monovalent and divalent basic oxides in one category (flux), amphoteric or trivalent basic oxides in the second category, and tetravalent or pentavalent acidic oxides in the third category. Then, the total molar amounts in each category are normalized to the sum of the fluxes. In this way, the content of the second and third category components are related with the unity 1 of fluxes, e.g. $MO+M_2O$: M_3O_3: MO_2 = 1: 0.5: 3.5 for a typical sanitary ware glaze.

Seger formula works well for glazes fired at higher temperatures but is less suitable for glazes fired at lower temperatures, since some of the category one oxides (e.g. MgO, CaO) are powerful fluxes at higher temperatures but refractory at lower temperatures [3]. For matte or crystalline glazes, the Seger or unity molecular formulas are also regarded too simple. In the experimental part of this thesis, the oxide and the raw material compositions, not Seger formula, are used for expressing the glaze compositions.

2.4 Raw materials and oxides

Raw materials for raw glazes are selected from processed and beneficiated minerals. The relatively low cost of a raw glaze is based on the fact that raw materials used in them are plentiful, easy to obtain, consistent and economically priced [1,3]. Many of the minerals consist of more than one of the oxides needed for the final composition. For cost reasons, the utilization of only such raw materials that contain only one oxide is not common. Table 1 shows the most common raw materials and the oxides introduced by them into traditional glazes [3]. Most ceramic glazes are applied as an aqueous slip on the substrate. For this reason, water-soluble raw materials are not

considered in raw glazes. In contrast, water-soluble raw materials such as high-alkali and boron compounds can be used in frit preparation. A high content of alkali oxides and boron oxide are needed in formulations of glazes for ceramics fired at lower temperatures.

Generally, traditional glazes are composed of the components; silica, alumina and flux. Below is given a short description of the impact of main constituents, i.e. oxides, and the most common raw materials used to introduce these oxides in traditional glazes. The information is gathered from relevant literature [1, 3, 12-15].

Silica (SiO_2) is the main component of glazes. Silica can be added as a natural raw material, e.g. quartz sand or flint. It is often introduced as a component of raw materials for other oxides, too. Minerals such as feldspar and nepheline are commonly used to contribute some alumina and alkali metal oxides in an economical form. The silica content of commercial glazes varies from 45-80 wt%. Silica is the major glass former and occasionally the only network-former used in glazes. The higher the proportion of silica in the glaze, the higher the firing peak temperature. In one hand, a high silica content provides a good resistance towards mechanical and chemical attack; on the other hand, the peak firing temperature of the glaze increases with the silica content. The melting point of silica is around 1700 °C. Since the firing temperature of all commercial ceramics and glazes is lower, additional raw materials, fluxes, are needed. Together with the fluxes, the high-melting oxides silica and alumina form lower-melting mixtures, thus forming melts that are powerful enough to dissolve the residuals of these refractory oxides during the firing.

Alumina (Al_2O_3) is an intermediate oxide that can take part in the network formation, depending on its content in the glaze. Alumina is added into raw glazes as a pure oxide, i.e. corundum, or introduced by e.g. feldspathic minerals and clays. As an intermediate oxide, alumina increases the viscosity and surface tension of the molten glaze, and thus makes the melt stiffer, thus preventing it from running off the piece during firing. Alumina decreases the thermal expansion and thus affects the attachment of the glaze to the substrate. Finally, alumina increases the chemical and mechanical durability of the fired surface.

The alkali metal oxides *Na_2O and K_2O* are the most powerful fluxes used in commercial glazes. Compounds of alkalis are widely distributed in nature as water-soluble minerals and therefore cannot be used in high amounts in raw glazes. The main source for alkalis in raw glazes is various feldspars. All feldspathic materials act as fluxes in ceramic glazes and bodies. Most common feldspar minerals used in ceramic manufacture are potassium feldspar, or microcline ($K_2O \cdot Al_2O_3 \cdot 6SiO_2$), and

soda feldspar, or albite ($Na_2O \cdot Al_2O_3 \cdot 6SiO_2$). These minerals are usually found as mixtures of both potassium and soda feldspars. The ratio Na/K influences several properties. The ratio controls the melting behaviour by forming low-melting mixtures together with other oxides. The ratio also affects the thermal expansion, the chemical resistance and the gloss, etc. The alkali content in glazes is preferably kept low, typically < 6 wt%, to maintain good chemical durability and to control the thermal expansion of the glaze.

Calcium oxide (CaO), a fluxing oxide, is added to the glaze to enhance the melt formation during firing and to decrease the viscosity of the molten glaze. Typical raw material sources for CaO are limestone ($CaCO_3$) and wollastonite ($CaSiO_3$). These minerals are usually classified as fluxes because they lower the viscosity of the melt formed during the firing reactions. In the reaction of limestone and quartz to calcium silicate, CO_2 is evolved. However, when using wollastonite as the lime source, no gases are evolved during the firing. Wollastonite melts and dissolves readily and thereby aids the glaze to smooth out rapidly and completely. The other raw materials in the glaze recipe partly dissolve in the melt formed by the fluxes and their reactions. CaO increases the mechanical strength and hardness of the glaze and it improves the durability against acids and water. However, an excess of calcium oxide increases the tendency of the glaze to devitrify. Depending on the glaze composition, precipitation of anorthite ($CaO \cdot Al_2O_3 \cdot 2SiO_2$) or wollastonite ($CaSiO_3$) crystals will produce glazes with varying degree of matteness.

Magnesium oxide (MgO) is an effective fluxing component at high temperatures and it also reduces the melt viscosity, being most effective at around 1200 °C. MgO is usually added as dolomite ($CaCO_3 \cdot MgCO_3$) or talc ($3MgO \cdot 4SiO_2 \cdot H_2O$). Small amounts of dolomite are reported to enhance the melting of the glaze while amounts higher than 8 wt% lead to the precipitation of diopside crystals giving a mat, almost satin mat surface. Dolomite also adds CaO to the glaze composition. Talc yields water of crystallization at 1100 °C, evolving gases. Thus, addition of talc is not recommended as a raw material in glaze compositions.

Table 1. Raw materials and added oxides [3].

To add	Raw materials	Other oxides introduced
Li_2O	Spodumene	Al_2O_3, SiO_2
Na_2O	Na-Feldspars	(K_2O), Al_2O_3, SiO_2
	Nepheline syenite	(K_2O), Al_2O_3, SiO_2
K_2O	K-Feldspars	(Na_2O), Al_2O_3, SiO_2
	Nepheline syenite	(Na_2O), Al_2O_3, SiO_2
	Muscovite mica	Al_2O_3, SiO_2
CaO	Wollastonite	SiO_2
	Limestone	
	Dolomite	MgO
MgO	Magnesium carbonate	
	Dolomite	CaO
	Talc	CaO, SiO_2
SrO	Strontium carbonate	
BaO	Barium carbonate	
ZnO	Zinc oxide	
PbO	Lead bisilicate	SiO_2
Al_2O_3	Corundum	
	Feldspars	Na_2O, K_2O, SiO_2
	Nepheline syenite	Na_2O, K_2O, SiO_2
	Kaolin clay	SiO_2
	Ball clay	SiO_2
	Muscovite mica	K_2O, SiO_2
	Pyrophyllite	SiO_2
SiO_2	Quartz sand, Flint	
	Feldspars	Na_2O, K_2O, Al_2O_3
	Nepheline syenite	Na_2O, K_2O, Al_2O_3
	Wollastonite	CaO
	Kaolin clay	Al_2O_3
	Ball clay	Al_2O_3
	Muscovite mica	K_2O, Al_2O_3
	Pyrophyllite	Al_2O_3
	Talc	CaO, MgO
	Zircon	ZrO_2
ZrO2	Zircon	SiO_2
TiO2	Anatase	

Zinc oxide (ZnO) is a valuable flux in glazes at firing up at about 1050 °C. At higher temperatures, ZnO has a large viscosity reducing effect; thus, its amount has to be adjusted according to the firing temperature. Correspondingly, ZnO extends the firing range of high-temperature glazes. It reduces the thermal expansion and improves the gloss and whiteness of the glaze. Higher amounts of ZnO, exceeding 20 wt% can lead to crystallization of willemite (Zn_2SiO_4) and gahnite ($ZnAl_2O_4$). The raw material for ZnO in the glazes is zinc oxide powder.

In addition to the fluxes used in this study, also other fluxes are used in commercial glazes. *Boron oxide (B_2O_3)* is an effective fluxing agent at all firing temperatures. Boron oxide is the second most important network former after silica in glazes. Boron compounds are rarely used in raw glazes, because of their water solubility. In contrast, they are essential ingredients in fritted formulations. Boron oxide also effectively lowers the thermal expansion. *Lead oxide (PbO)* was for a long time a very important oxide in glaze formulations. Lead oxide is a network modifier and an effective flux up to about 1150 °C. Glazes containing lead are characterized by their low surface tension, low viscosity, wide firing range and high index of refraction. However, the toxicity of lead has led to strict limitations of its use today.

Opaque glazes are usually white. The colour is obtained through the addition of e.g. ZrO_2 containing frits, zirconium silicate ($ZrSiO_4$) pigments or tin oxide (SnO_2).

In addition, a clay such as kaolin is usually also added as a suspending agent in glaze slips to prevent sedimentation. Kaolin also serves as a source of alumina and silica in the recipe.

Finally, small amounts of different additives such as colour pigments, crystallization agents, adhesive binders, deflocculants etc. are needed to adjust the rheology or final properties of the glaze.

The successful formulation of a glaze is not just a matter of achieving the proper final oxide formula. The raw materials providing the desired glaze oxide composition must be chosen according to their melting or dissolution behaviour during the firing schedule. For achieving a defect-free glaze, the melting must not begin before the gas produced by the maturing of both the glaze and the substrate has escaped.

2.5 Firing

Reactions in raw glazes start with driving off mechanically bound water at 100-200°C, chemically bound water up to around 600°C and decomposition of carbonates at around 800°C [1]. However, the sintering of the glaze, i.e. formation of intermediate compounds and neck-growth between the raw material particles, starts typically at

around 1000°C. At these temperatures, the sintering is mainly affected by melting of feldspars and other fluxing materials. The firing reactions continue with the dissolution of quartz and other refractory raw materials in the melt formed. The extent and kinetics of these reaction stages are relevant for the final appearance of the glaze. Thus, the final properties and appearance of the same glaze composition fired at different firing cycles depend on each particular cycle.

The firing cycle applied depends on the manufacturing technology, the shape and the size of the ceramic ware, body and glaze composition, porosity demand in the fired product, and the desired final surface appearance. The total amount of heat applied to the ceramic ware is significant. This is affected by the heating rate, the peak firing temperature, the length of the soaking period, and the cooling rate. Ceramics are usually fired once or twice. Twice-firing or biscuit firing is still used for e.g. porous earthenware or other small pieces to prevent distortion of the pieces or when using artistic pottery glazes [16]. The second firing is usually carried out at a lower temperature to prevent contraction of the body but to give desired glaze appearance. Once-firing is favoured when firing large, complex-shaped articles of high value, e.g. sanitary ware. These large articles are not completely covered with glaze and they can support themselves without distortion during the once firing. However, the main reason for once firing is the economic benefit from reduced energy costs. Today, most tiles are fired in a single fast-firing process. The modern roller kilns have contributed to reducing the firing schedules to as fast as 30-50 minutes from cold-to-cold, depending on the tile type fired. The firing peak temperatures vary with the glaze composition and the desired porosity of the fired ware. Typically, porous wall tiles glazed with fritted glaze formulations are fired at 900 to 1150 °C, while dense frost resistant floor tiles with raw glaze require temperatures around 1200 °C. For larger shapes of sanitary ware, the fastest firing schedules are 12 to 15 hours from cold-to-cold at the peak temperature of around 1200 °C. The main limiting factor for the firing schedule of the complex body shape of a typical sanitary ware is the requirement of uniform sintering without stresses and deformation.

The ceramic ware is also subject to stresses generated by the quartz inversion at 573 °C. At this temperature, quartz - the most common room temperature crystal form of SiO_2 in the raw materials - changes from the alpha to the beta form, which means that the molecules rearrange themselves and expand 1–2 % during the heating, and contract the same amount during cooling [17]. Though quartz inversion affects the porous, mainly non-sintered ware during heating, quartz inversion has a much greater impact on the glazed ware that has reached a point of maturation. Thus, when

cooling the kiln through the quartz inversion temperature, or when re-heating an already fired ware, the residual unreacted quartz may lead to failure due to local stresses. Larger and complex pieces are especially sensitive to the quartz inversion temperature. Thus, their firing schedules are longer due to slower cooling rates in single firing through the critical inversion temperature range. Sanitary ware is usually fired in continuous tunnel kilns. In continuous production, the use of tunnel kilns can be more economical than firing in intermittent or batch kiln. The kilns are also more effective today as they are insulated with fibres instead of bricks. The fibre insulation allows more rapid heat transfer from the furnace and thus allows faster total firing cycle.

2.6 Melting behaviour of ceramic glazes

Melting behaviour of fritted formulations can be expressed mainly by their viscosity-temperature relationships and crystallization tendencies specified by their oxide composition. Fritted formulations start to soften above their glass transformation temperatures. If the crystallization tendency of the frit is low, the viscosity of the melt decreases smoothly with increasing temperature. In literature, typical hot-working properties of homogeneous glass melts are described as simple additive functions of their oxide composition [18-20]. Such calculation models are useful also when estimating the firing behaviour of fritted glazes. Similar models can also be useful when estimating the viscosity of raw glazes at or close to their top firing temperatures. In addition to describing the properties of a certain composition, the models enable computing the glass or glaze composition satisfying a set of desired property values by using different optimization techniques [21, 22]. However, as raw glazes are never entirely homogeneous, not even at their highest firing temperatures, the measured property values are likely to deviate from the values calculated using models based on homogeneous melts.

2.6.1 Hot-stage microscopy

Hot-stage microscopy has been used to characterize the melting behaviour of raw materials, glasses and glazes [23]. The first hot-stage microscope studies of ceramics were carried out already in the 1950s and 1960s [24-29]. Since the mid-1990s, the technique has again been widely applied within the research of glasses and ceramics [30-39]. Hot-stage microscopy gives several characteristic sample shapes, which can be used to describe the processes taking place during the heating of the sample. Typical changes in the sample shapes recorded during heating of a glaze are shown in Fig.4.

Also, sintering and melting curves based on either the sample height or the sample area as functions of temperature have been used to characterize the melting behaviour. In some early studies, hot-stage microscopy has been used to analyse the processes taking place in silicate materials during heating based on standards developed for ash melts [24, 26, 40-41]. The standard DIN 51 730 [42], originally based on hot-stage microscopy of ashes and slags, was applied to ceramics due to the similar nature of these materials. Also, in the standards, British Norm BSS 453 [43] and the American Norm ASTM D 271 [44], the melting behaviour was defined through several shapes the sample displays at different temperatures during heating in hot-stage microscopy. In these standards, the temperatures at which the sample reaches a typical shape are used to characterize the sintering and melting behaviour in detail.

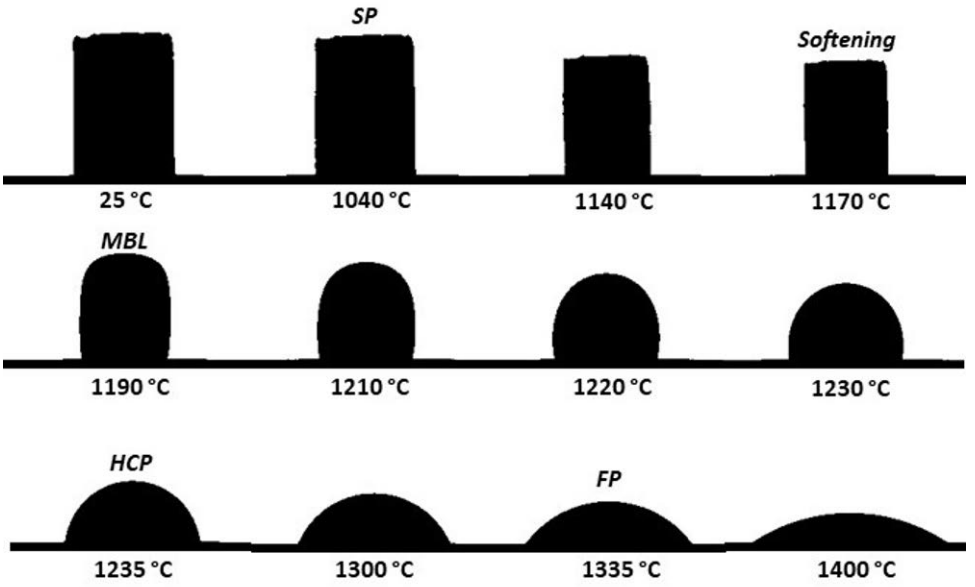

Fig. 4. A typical change in sample shapes of a glaze sample during heating in a hot-stage microscope. Sintering point (SP), Softening point (Softening), Minimum baseline point (MBL), Half-cone point (HCP) and Floating point (FP) are shown. The images were recorded for glaze 8 (Appendix 1).

Scholze [28] developed the interpretation of the characteristic points from hot-stage microscopy further to measure the viscosity of glass melts. He used two more points besides those described in DIN 51 730 to characterize the viscosity. The first

point was defined as the *sintering point*, given by the temperature at which the sample started to shrink (SP in Fig. 4). The other new point was the *minimum baseline point* (MBL in Fig. 4), given by the temperature at which the contact line between the sample and the sample holder was shortest. The temperatures for these typical sample shapes were then calibrated with the calculated viscosity values based on Vogel-Fulcher-Tamman (VFT) equation. Scholze's study showed that hot-stage microscope can be used to measure the viscosity of glass melts within the range 10^{10}- $10^{4.2}$ dPa·s, i.e. roughly between the deformation ($10^{11.4}$ dPa·s) and working points (10^{4} dPa·s) of glass-forming melts. According to Scholze, the surface tension of the glass melt did not affect the measured viscosity values. Pascual et al [34] reported that the viscosity values from hot-stage microscopy could be combined with viscosities from rotational viscometer (10^{5} – 10 dPa·s) and fibre elongation method (10^{13} – 10^{8} dPa·s) to give the total viscosity range of interest for silicate melts. In a later work [35], they obtained more precise viscosity values of the same geometries by considering various physical parameters affecting (glass surface energy, particle size distribution, heating rate) and analysing the different sources of errors. However, Vedel et al [45] observed that for glasses crystallizing easily during heating, hot-stage microscopy could be used to describe only the low-temperature viscosity values. They used the shape of the sintering curve to estimate whether the HSM values can be used to describe the glass viscosity or not. After the initial sintering, any hold or swelling in the sintering curve was found to correlate with the crystallization of the amorphous melt, thus preventing the characterization of the viscosity values at higher temperatures.

Ahmed and Earl [36] combined hot-stage microscopy with dilatometry to characterize the melting behaviour of porcelain glazes. The melting behaviour was estimated from the melt viscosity described by three temperature points: the dilatometric glass transition temperature, Tg ($\eta = 10^{13}$ dPa·s), the dilatometric softening point, Ts ($\eta = 10^{10.25}$ dPa·s) and the half-cone point from hot-stage microscopy ($\eta = 10^{4.55}$ dPa·s). These three points were used to solve the three unknown constants A, B and T_0 in the VFT equation. The calculated viscosity values were suggested useful when estimating the effect of changes in the glaze recipe on its melting behaviour.

Amoros et al [46] developed a non-isothermal multi-step kinetic model that describes the progress of sintering degree with temperature for floor and porcelain tile raw glazes. The sintering process and sintering kinetics were determined for the glazes using constant-rate heating in hot-stage microscopy. When combined with analysis of the microstructure and phase content, the sintering could be divided into one to

three partly overlapping stages and the sintering mechanisms and kinetic models in each step were identified. In a recent study, Amoros et al introduced a model that describes the non-isothermal sinter-crystallization of formulations with high frit contents to give satin glazes containing several phases [47]. The kinetic model describes the phase evolution in systems which exhibit three-stage sintering, i.e. sintering with concurrent crystallization (stages I and II) and sintering with partial melting of the crystalline phases (stage III). The effective sintering viscosity values of the glaze melt calculated with the kinetic model were in good agreement with the experimental values based on data obtained by hot-stage microscopy using different heating rates. The new kinetic model giving the effective sintering viscosity was assumed to give a better understanding of the sintering behaviour of complex glaze compositions.

The early theories and characteristic points of hot-stage microscopy have been combined into a routine in which five sample shapes during heating are measured [31], cf. Fig 4. Today, these temperatures and corresponding characteristic shapes are defined as:

1) Sintering point (SP), the temperature where the sample height has decreased by one %,
2) Softening point (Softening), the temperature of the first rounding of the edges of the sample,
3) Minimum baseline point (MBL), the temperature where the sample has the shape of a sphere,
4) Half-cone point (HCP), the temperature where the sample forms a hemisphere, and
5) Floating point (FP), the temperature where the sample height is 33 % of its initial height.

2.7. Properties of the fired glaze surface

2.7.1 Surface appearance

Glazes are classified according to their optical characteristics into transparent versus opaque or glossy versus matte surface finish (Fig. 5.). Transparent glazes have a uniform refractive index so that most of the light incident at the air/glaze interface is transmitted through the glaze before being reflected or scattered from or partially absorbed by the substrate [1]. Opaque glazes are the result of diffusion, reflection and refraction of incident light from particles or bubbles in the glaze layer. This scattering occurs when the particles have a different refractive index compared to that of the surrounding amorphous phase. The opacity depends on the concentration and size of the opacifying particles, the refractive index difference between the amorphous and opacifying particles and the glaze thickness. The dispersed phase does not have to be crystalline. Gas bubbles or amorphous phase separations can also give opacity in the glaze.

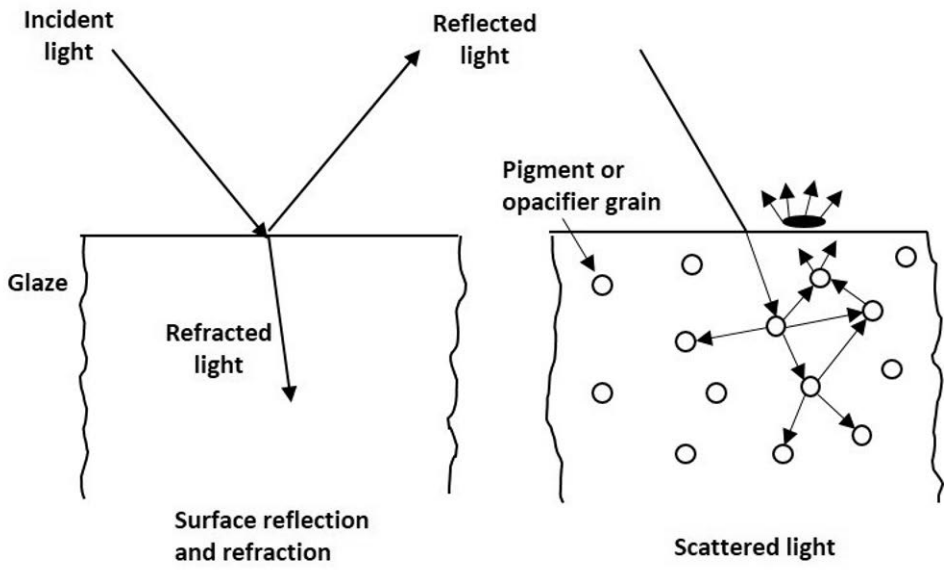

Fig. 5. The optical characteristics of a transparent glaze (left) and an opaque glaze (right). Redrawn from Taylor and Bull [1].

The gloss of a surface is difficult to define exactly, but it is related to the relative amounts of specular and diffuse reflection [48]. It has been found to be most closely related to the sharpness and perfection of the reflected image, and thus to the intensity of the specular reflection. Fig. 6 shows the difference in the reflective response of surfaces with a different surface appearance [3]. A high-gloss surface shows a high percentage of specular reflection compared to diffuse reflection. A satin matte surface has only a little specular reflection and more diffuse reflection and in a matte surface, all the reflectance is diffuse with no specular reflection.

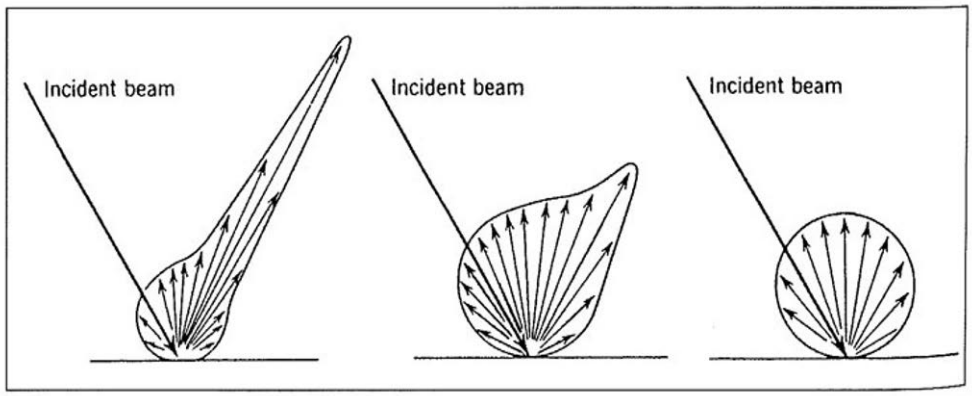

Fig. 6. Light reflection from (left to right) a high gloss, satin-matte, and a matte glaze [3].

Matte and crystalline glazes are partially or fully opaque. The presence of crystalline phases with different refractive indices compared to the glossy glass matrix leads to the overall appearance. Matte glazes can be produced by adding to the recipe tiny crystals, which then grow in size during the firing cycle. Alternatively, the glaze recipe can contain crystals which do not melt during the firing. The glaze composition can also be adjusted so that certain crystals precipitate during the firing, i.e. the glaze partially devitrifies. In general, the matte appearance depends on the amount of the crystalline phase(s) in the glaze. If the matte glaze is produced by crystallization from the melt during the cooling cycle, the cooling rate is carefully controlled to provide the desired degree of crystallization. In addition, gloss vs. matteness is also affected by surface roughness [48]. Light reflection is specular, i.e. at a certain angle from the smooth surface. In contrast, when the surface is rough, the incident light undergoes

diffuse reflection and is partly reflected in every direction (Fig. 7). Thus, the fraction of light reflected in diffuse and specular form depends on the roughness of the surface.

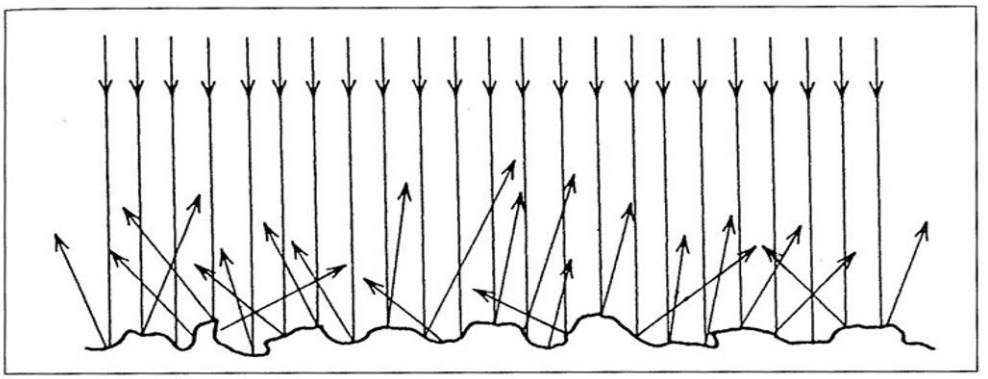

Fig. 7. Light reflection from a rough surface [48].

The surface quality can be reduced by faults arising from e.g. unwanted glaze reactions, incomplete glass-forming reactions, kiln conditions, stresses in the glaze, impurities, etc. [1]. Controlling the surface roughness plays an important role when enhancing the surface quality. The topography is influenced by the melting of the glaze, crystals at the surface, and glaze defects such as crazing and bubbles. Apart from the aesthetic point of view, the topography will also affect the cleanability of the surface. Matte glazes have usually a high surface roughness which depends both on the crystallinity of the glaze and the morphology of the crystals precipitated at the surface [49]. The particle size of the raw materials directly influences the surface quality of the glazes [50-53]. By suitable grain size selections, improved surface roughness can be achieved. Optimization of quartz and feldspar grain size has the most advantageous effect [54-56]. A decrease of the zirconium silicate grain size improves the whiteness and gloss but increases the surface roughness [54]. All glazes contain gas bubbles. Many bubbles have little or no effect on the glaze quality but if they rise to the surface and form open bubbles during the firing process the surface roughness and thus the cleanability are affected [57, 58]. In a single-firing process, the glaze must not melt and seal the surface before the gases from the green body have escaped. When using e.g. carbonates in the glaze composition, the firing schedule must be suited so that the gases can escape and not be trapped at the surface.

2.7.2 Phase composition

The phase composition of the final glaze depends on the reaction kinetics of the raw materials during the heating and the soaking period at the peak firing temperature, as well as on the phase changes taking place during the cooling period [10]. The firing parameters are selected to achieve glossy versus matte, or transparent versus opaque surface appearance. Fundamentally, the requirements for the final surface appearance depend on the application of the fired ware. In addition, the aesthetic considerations of the customers also affect the firing conditions of a particular glaze. In several cases, crystallization is considered as an undesirable phenomenon in industrial production of glazes. In sanitary ware, white opaque raw glazes are commonly used, while transparent glazes are widely used in tableware glazes that are in contact with food products. Further, in floor tiles, a hard, often glass-ceramic surface is needed to withstand the abrasion in harsh environments. Crystalline glazes are also widely used to improve the decorative properties of ceramic art products.

In a transparent, high-glossy glaze the glass phase has no dispersed particles or porosity, and the surface is ideally perfectly smooth [48]. The gloss is reduced by gas bubbles that rise and burst at the surface, forming small visible pinholes. During the firing, air introduced into the glaze between the raw material particles or CO_2 released from carbonate raw materials forms gas bubbles which penetrate through the glaze layer and can sometimes be trapped at the surface. Also, an overfiring of the glaze can cause bubbles at the surface [3]. Basically, overfiring means that the glaze has been fired at too high a temperature so that some of the glaze constituents have volatilised. Precipitation of fine-grained crystals gives the typical surface texture and lower gloss of matte glazes. The composition of the crystals varies with the composition and heat treatment, but anorthite is the most common type, followed by mullite and wollastonite [47]. For matte glazes, the crystals should be uniform and relatively small. For other effects, large crystals are favourable. For a fixed alkali and alkaline earth content, the ratio Al_2O_3 to SiO_2 determines the appearance of a ceramic glaze. Underfired glazes, i.e. glazes which have not reacted to the desired degree due to a too low peak firing temperature or too short firing cycle, also have a matte surface. However, they do not qualify as matte glazes as the rough, uneven surface gives them an unaesthetic appearance and make them unsuitable for practical use [3, 12].

2.7.2.1. Ceramic phase equilibrium diagrams

At equilibrium, a system is in its lowest free energy state for the composition, temperature, pressure, and other imposed conditions [48]. When a given set of system parameters is fixed, there is only one mixture of phases that can be present, and the composition of each of these phases is determined. Phase equilibrium diagrams provide a clear and concise method of graphically representing this equilibrium situation and are an invaluable tool for characterizing ceramic systems. However, in many processes, the time for the reactions is limited, and ceramic systems seldom achieve equilibrium conditions described by the diagrams [48]. Particularly for systems rich in silica, the high viscosity of the liquid phase leads to slow reactions rates and very long times before equilibrium is established. In fact, equilibrium is rarely achieved. However, equilibrium diagrams can be used for finding the limits for different combinations of oxides. For fast-fired glazes, equilibrium conditions are rarely achieved. For glazes fired in a longer firing schedule, the phases present in the final product can be estimated based on the starting oxide composition and their corresponding phase diagrams [59-60]. In similar compositional ranges as used in this thesis, the crystalline phases developed in glazes fired in a traditional, long firing schedule was found to correspond to those found in relevant phase diagrams. For the same glazes in fast firing, the phases could better be described by the first raw material reactions.

The phase diagram for the system CaO-Al_2O_3-SiO_2 that is of relevance for the glaze compositions used in the experimental part of this thesis is shown in Fig. 8 [61]. The composition range for the experimental glazes is marked with a red oval in the diagram. However, the presentation of the compositions was simplified by considering all the fluxes ($CaO + MgO + K_2O + Na_2O$) to be equivalent to CaO. The marked area includes three compatibility triangles: pseudowollastonite-anorthite-silica, anorthite-mullite-silica, and pseudowollastonite-anorthite-gehlenite. Basically, the crystalline phases given by the compatibility areas are possible in the experimental glazes which have been fired so that they have achieved their equilibrium conditions. In the triangle pseudowollastonite-anorthite-silica, the lowest melting temperature is the ternary eutectic at 1170 °C. The ternary eutectic temperatures for the other two systems are 1368 and 1265 °C. For the compositions within the compatibility triangle of the lowest ternary eutectic, melt formation starts at 1170 °C, i.e. at a lower temperature than the firing peak temperature of 1215 °C used in this work. The alkaline oxides present in the glazes are likely to decrease this melt formation

temperature. Possible crystalline phases in the fired ware would be anorthite, pseudowollastonite or SiO_2 (quartz) crystals.

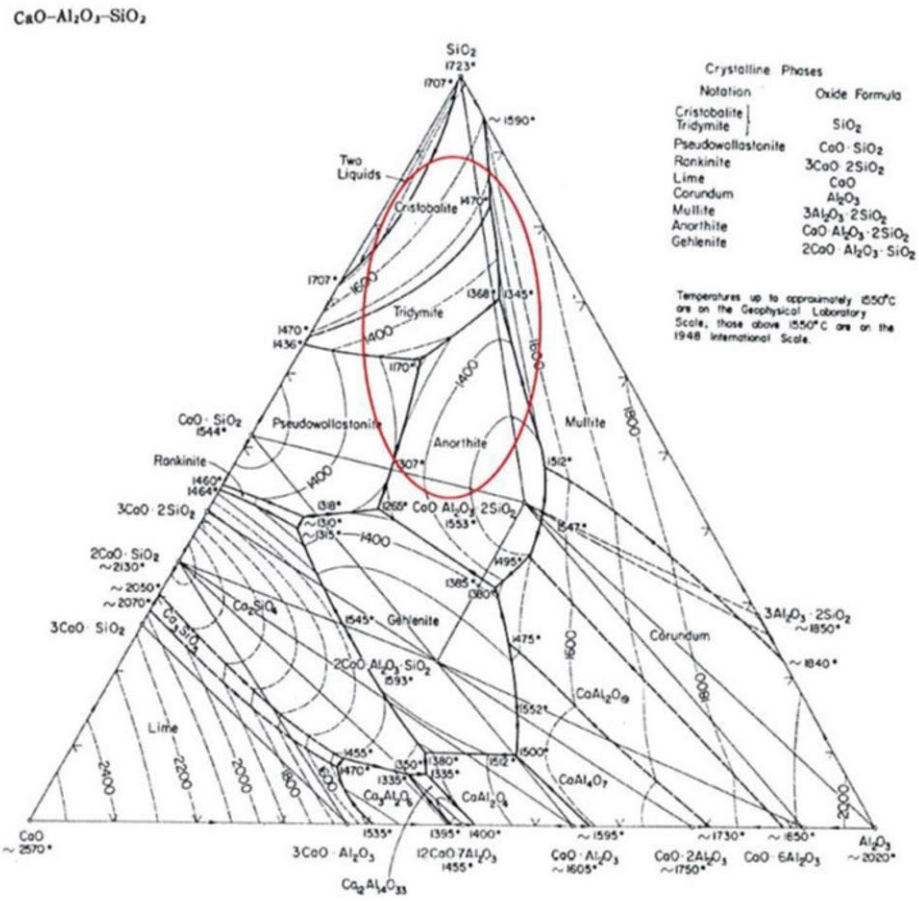

Fig. 8. Phase equilibrium diagram for the system CaO-Al_2O_3-SiO_2 [61]. The area inside the oval shows roughly the compositional range of the experimental glazes used in this study (Publication II).

Another phase diagram of interest of the experimental glazes in this study is the phase diagram for albite and anorthite (Fig. 9). The diagram shows that anorthite and albite form a continuous series of solid solutions, plagioclase feldspar [61]. This means that the chemical composition of the crystals varies within certain limits without forming two different crystal types.

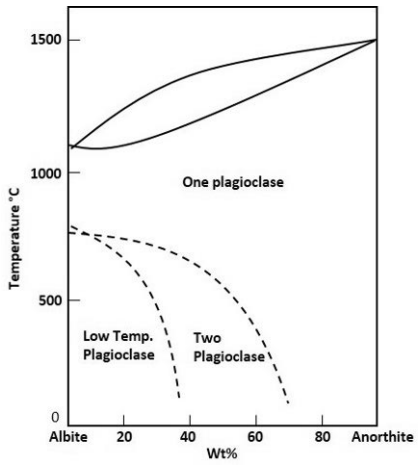

Fig 9. Phase equilibrium diagram for the plagioclase solid solution albite-anorthite. Redrawn from Levin at al. [61].

2.7.2.2. Crystalline phases in glazes

Matte or crystalline glazes obtain their appearance from crystalline phases present in the glaze layer. The most common types are lime matte, containing wollastonite ($CaSiO_3$) crystals and zinc matte, containing willemite (Zn_2SiO_4) crystals [1]. Lime matte can be produced by adding a high amount of limestone ($CaCO_3$) or whiting ($CaCO_3$) to the recipe that decompose and react with silica to form wollastonite crystals. Additionally, an addition of the mineral wollastonite will give the same effect. Wollastonite content, as the mineral, in glossy raw glazes is typically 16…22 wt% whereas higher wollastonite contents, up to 30 %, give matte glazes [1]. Incorporation of MgO as dolomite ($CaCO_3{\cdot}MgCO_3$) or talc ($3MgO{\cdot}4SiO_2{\cdot}H_2O$) can also give a matte surface by crystallization of diopside ($CaO{\cdot}MgO{\cdot}2SiO_2$) crystals. Incorporation of e.g. BaO, SrO or TiO_2 in the glaze recipe has also been used to develop crystalline phases with a matte surface appearance [3]. Increasing the alumina content - and thus decreasing the SiO_2/Al_2O_3 ratio - also favours the development of a matte appearance [12]. Incomplete melting of the raw materials will also result in a matte surface appearance. However, these surfaces have usually uncontrolled roughness and several of their other surface properties are also poor [3, 12]. The precise amount of raw materials or oxides needed for achieving a matte surface appearance also depends on the overall composition of the glaze as well as the firing schedule and the peak

temperature. Especially when the crystalline phases are crystallized from the molten glaze during the cooling, the control of this step is crucial.

Much effort has been put into developing glass-ceramic glaze surfaces with improved mechanical, thermal and chemical properties compared to traditional glazes surfaces [6]. The glass-ceramic surface consists of a residual amorphous phase and polycrystals [62]. The polycrystalline microstructure, which gives the desired surfaces properties, is obtained by using glass frits which crystallize and sinter during firing [63]. High melting temperatures between 1450 to 1600 °C are used to prepare the homogenous frits for glass-ceramic coatings. During the ceramic firing cycle, the frits first melt, and then nucleate and crystallize into a glass-ceramic. On ceramic tiles, the crystallization typically takes place at 1100…1200 °C. The main crystal types in glass-ceramic coatings vary with the composition, but zircon ($ZrO_2 \cdot SiO_2$), anorthite ($CaO \cdot Al_2O_3 \cdot 2SiO_2$), mullite ($3Al_2O_3 \cdot 2SiO_2$), cordierite ($2MgO \cdot 2Al_2O_3 \cdot 5SiO_2$), diopside ($CaO \cdot MgO \cdot 2SiO_2$) and wollastonite ($CaO \cdot SiO_2$) are frequently reported [6]. Ceramic tiles with improved surface properties have been achieved when using glass-ceramic coatings within the quaternary system CaO – MgO – Al_2O_3 – SiO_2 together with different additives enhancing the fusibility or controlled crystallization of the melt. In this system, the compositions within the cordierite ($2MgO \cdot 2Al_2O_3 \cdot 5SiO_2$) primary field and the diopside/pyroxene ($Ca,Mg(Si,Al)_2O_6$) primary fields have been studied [64-75]. In principle, the glass-ceramic glazes have higher MgO/CaO ratio and higher alumina and lower silica contents than traditional raw glazes.

Below is given a short description of the crystalline phases that formed in the experimental glazes in this study, based on the relevant literature [48, 76-79].

Wollastonite (β-$CaSiO_3$) is a white mineral with a chain structure and theoretical content of 48.25 wt% CaO and 51.75 wt% SiO_2. Wollastonite is formed after decomposition of limestone to calcium oxide and carbon dioxide at around 800-900 °C, followed by a reaction with silica to form wollastonite

$$CaCO_3\ (s) \rightarrow CaO\ (s) + CO_2\ (g)$$

$$CaO\ (s) + SiO_2\ (s) \rightarrow CaSiO_3\ (s)$$

Wollastonite crystals have an acicular structure and when such crystal is broken, the fragment usually also have an acicular shape. The structure of wollastonite crystals originated from the mineral wollastonite can vary, depending on origin and composition.

Pseudowollastonite (α-$CaSiO_3$) is the high-temperature form of wollastonite. At a temperature of 1125 °C, wollastonite is irreversibly transformed into pseudowollastonite with an insignificant change in the volume. Pseudowollastonite crystals have a hexagonal plate structure. The crystals melt at 1540 °C. For the mineral wollastonite, the temperature when the structure changes from β to α varies depending on the impurities in the mineral. The impurities increase the structure change temperature as the change occurs only after the impurities have dissolved at temperatures usually higher than 1200 °C.

Diopside ($CaO{\cdot}MgO{\cdot}2SiO_2$) is a monoclinic pyroxene mineral with theoretical content of 25.90 wt% CaO, 18.61wt % MgO and 55.49 wt% SiO_2. Diopside crystals have usually a single, short, prismatic shape. Diopside typically forms when dolomite decomposes and reacts with quartz or other silica raw material. Dolomite decomposition starts already at 400-500 °C and is complete at about 700°C after which diopside forms as a result with a reaction with silica. This reaction starts at about 800°C and is finished at about 1000-1100°C.

$$CaCO_3{\cdot}MgCO_3\ (s) \rightarrow CaO{\cdot}MgO\ (s) + 2\ CO_2\ (g)$$

$$CaO{\cdot}MgO\ (s) + 2\ SiO_2\ (s) \rightarrow CaO{\cdot}MgO{\cdot}2SiO_2$$

Anorthite ($CaO{\cdot}Al_2O_3{\cdot}2SiO_2$*)* is the calcium-rich end member of the plagioclase feldspar mineral series. Anorthite forms when Ca-rich compounds react with alumina and silica-rich compounds. In ceramics, Ca-containing sources are usually wollastonite, limestone or dolomite whereas feldspar, clay and quartz are typical ~~as~~ alumina and/or silica sources. Temperatures at around 1200-1230 °C are needed for crystallization of anorthite in ceramics. Anorthite is usually observed in glazes containing lime after a longer firing schedule. Anorthite seldom appears as a single-phase but it often forms a continuous series of a solid solution with albite.

2.7.3. Mechanical durability

Glazes are used in several applications where they are exposed to harsh treatments. Mechanical durability, i.e. resistance to scratch and abrasion, is an important property of especially glazes used as floor tiles. Additionally, they must exhibit slip resistance to prevent personal injury. Similarly, glazed tableware needs a good resistance against metal-marking from cutlery and conversely also does not scratch the metal in the cutlery. Floor tiles can be made scratch-resistant by incorporating a high degree of hardness into the surface. The can be achieved by adding coarse particles of high hardness such as corundum or zircon into the glaze giving a textured surface finish.

Alternatively, a smooth matte surface can be obtained with crystalline phases having a high degree of hardness [1]. Today, controlled crystallization of glazes is the most efficient and economical solution to obtain high quality, mechanically resistant coatings on floor tiles [80]. During the last decade, the use of glass-ceramic glazes containing different crystalline phases has been reported. Glass-ceramics in the Li_2O-Al_2O_3-SiO_2, CaO-MgO-SiO_2-Al_2O_3, ZnO-Al_2O_3-SiO_2-ZrO_2 and ZnO-MgO-Al_2O_3-SiO_2 systems have been reported for the application of floor tiles with high resistant to wear and high surface hardness [74].

2.7.4. Chemical durability

In general, the chemical durability of glazes is good in aqueous solutions. However, depending on the compositions of the glaze and the solution, the temperature etc. the glaze surface can undergo ion exchange, dissolution or absorption reactions [1]. Visually, corrosion of the glaze can be seen as a decrease in gloss, change in colour or even surface pitting and degradation. The chemical durability of glazes is often discussed as the durability of the amorphous phase in accordance with silicate glasses. The effect of the oxide composition on the chemical durability of glasses is well reported in the literature [81-83]. The durability of glasses in aqueous solutions is classified into three categories of acid, alkaline or hydrolytic durability. At silicate glasses, the principal mode of acid attack is an ion exchange reaction of the modifying ions in the glass structure by the H^+ ions in the acid. This reaction leaches out the modifying ions from the surface and leads to the formation of a silica gel layer which might act as a barrier to further reactions [82]. In general, the good acid durability of quartz glass is decreased by incorporation of network modifiers, i.e. alkalis and alkaline earths. Further, in silicate glasses, the acid durability is increased when replacing alkalis by alkaline earths. Also, adding Al_2O_3, ZrO_2, TiO_2 and B_2O_3 improve the acid durability of amorphous silicates. In contrast, the hydroxide ions in alkaline solutions destroy the network structure of silicate glasses. The hydroxyl ions in the solution will attack the siloxane bonds, i.e. the oxygen bridges between two silicon, resulting in a gradual dissolution of the silicate network and extraction of silica. The reaction rate is typically linear with time. All the glass components are released into the solution in uniform concentrations if there is no build-up of insoluble reaction products on the sample surface. The hydrolytic attack by water has a similar mode of attack as the acid attack. However, if the solution in contact with glass becomes very alkaline after the acid attack, e.g. due to low solution volume, the hydrolytic reactions continue with a typical alkali attack.

Chemical durability of glazes cannot directly be compared to the durability of homogeneous glasses. In general, the high contents of alumina and silica and the low contents of alkali oxides make the durability of amorphous silicate phases in glazes superior to conventional soda-lime glasses. The glaze appearance can vary from glossy, homogeneous amorphous surfaces to matte surfaces consisting of several different crystalline phases embedded in an amorphous matrix. Therefore, the corrosion behaviour of a glaze should be described by several mechanisms depending on the surface phase composition [84]. In general, the chemical durability of ceramic glazes is a combination of the resistance of the amorphous and the crystalline phases and the interfacial layer between them. In matte glazes, both the composition and the origin of the crystalline phases affect the durability. The firing of the glaze will also influence the final surface structure, thus complicating the prediction of chemical durability directly from the chemical composition calculated from the starting raw materials. In glass-ceramic glazes, zircon, diopside, anorthite and cordierite crystals have been found to have excellent durability in alkaline and acidic solutions while wollastonite crystals are attacked by acidic solutions [85-91]. Similarly, in raw glazes, the diopside crystals present have been found to have a good durability in acidic and alkaline solutions while wollastonite crystals are attacked by acidic solutions [92-96]. In acidic solutions, the dissolution of wollastonite was reported to be incongruent, i.e. to have different dissolution rates for calcium and silicon species and thus lead to a silica-rich crystal remnant at the surface. Diopside crystals showed, however, no differences in the dissolution rate between the different components. Three different corrosion mechanisms depending on the pH of the attacking solution were reported for glass-ceramics containing 20 vol% of crystals [97]. In acidic solutions, the corrosion was described by ion exchange of the amorphous phase. In neutral and alkaline solutions, the network of the amorphous phase and the corrosion of the grain boundaries between the amorphous and crystalline phases are attacked. The phase boundary attack was assumed to depend on stresses or minor compositional differences in the grain boundary compared to the bulk phases [97]. For raw glazes, the surface quality and the chemical durability were also affected by the selection of the grain sizes of the raw materials [98]. The hard raw material $ZrSiO_4$ often used to opacify the glazes, has been reported to give not only the desired surface appearance but also to improve the chemical durability of the surface [99].

Dissolution kinetics of silicate minerals has been studied in detail by the geochemical community [100, 101]. In general, the dissolution of silicate crystals was found linear and had a strong pH dependence [102]. The reactions were initiated at

grain boundaries or imperfections and impurities in the crystal structure and grain surfaces. Silicates dissolve incongruently at acidic pH and form altered layers enriched in silica [103]. The incongruent dissolution takes place as an exchange of protons with cations such as Ca, Mg, K, etc. that exhibit more ionic and weaker bonding to neighbouring oxygen atoms than the network former silicon [104]. As a result, silica forms a proton-enriched leached layer that dissolves slower than the pristine mineral. The protonated leached layer was assumed to undergo reconstruction/polymerization reactions that increase the connectivity of the silica network and thus can reduce the rate of silica release in solution [101]. This kind of behaviour has been observed not only for crystals such as wollastonite but is in principle similar to the mechanisms discussed above for silicate glasses [105-107]. Wollastonite dissolution rates measured over the pH range 0.9-12 were stoichiometric at pH > 4 but highly non-stoichiometric at pH < 4 with preferential Ca release [108]. Dissolution rates as deduced from Si release continuously decreased with increasing pH. Dissolution of wollastonite and other Ca/Mg silicates was controlled by a Ca-proton exchange reaction in acidic solutions. This reaction resulted in a collapse of the mineral structure at pH < 4. In contrast, the hydrolysis of Ca-O bonds in accordance with the faster breaking rates of Si-O bonds controlled the dissolution of wollastonite in moderately acidic to alkaline solutions. The Ca-H exchange reaction in acidic solution leads to the formation of a highly microporous and thick amorphous silica-rich layer that continuously grew until total Ca removal from the original wollastonite lattice. Simultaneously, as a result of the highly connected porosity, strains that developed in the structure and the intense hydration generated by Ca leaching were assumed to contribute to the collapse of the residual silica polymer to give a more condensed structure likely via bond reorientation and dissolution-precipitation reactions.

The chemical durability of ceramic tile surfaces is classified according to the standard ISO 10545-13 [109]. In this standard, the chemical durability is divided into different classes based on a visual inspection of the surface appearance after exposures to several test solutions. As this visual method does not require any special equipment, it is well suited for everyday product and quality control as well as for overall estimation and comparison of the chemical durability of glazes with different compositions. The standard method has been criticized for being too simple and giving only qualitative information on whether the surface is affected or not by the solutions [93, 110]. The method does not give any detailed information on the extent or mechanism of the surface damage. When developing new better glaze compositions or exploring the corrosion mechanisms in detail, more refined analysis methods must

be employed. Surface-sensitive methods such as scanning electron microscopy, atomic force microscopy and X-ray diffractometry have been used for gaining more detailed knowledge of the corrosion mechanisms of glazes [111]. In general, the highest chemical durability is required in applications where the surface is in continuous contact with a solution containing corrosive species, e.g. tiles used in swimming pools.

2.7.5. Soiling and cleaning of glaze surfaces

Glazes are often used when an easy-to-clean surface is needed and in applications where it is important to enhance the soil and deposit repelling properties of the surface. Such environments are e.g. hospitals, bathrooms and kitchens. However, surface pitting and degradation in service can diminish cleanability [112]. Surface degradation might also lead to the opening of closed porosity in the glaze thus leading to micro-scale holes which are often hard to clean by conventional cleaning techniques.

Cleanability of a glazed surface is difficult to measure and define due to complex chemical and physical interactions between the soiling components and the glaze surface. A wide range of substances may soil the surface through several different mechanisms. Also, the surface properties of the glaze might change during the soiling or the cleaning procedure. To determine the cleanability of surfaces, a number of different methods, ranging from visual inspections to molecular scale techniques, are used. Cleanability is associated with stain resistance which is measured for ceramic tiles according to the ISO 10545-14 standard [113]. In the standard, the surface is stained with different test solutions and after a period of time washed using different cleaning routes. The classification of the cleanability is performed visually to determine if the stain is removed or not. However, more accurate methods are needed to gain more detailed information about the soiling and cleaning mechanisms. For ceramic glazes, cleanability has mainly been studied by colourimetry or spectrophotometry to measure the removal of a coloured soil (e.g. ferric oxide, model soils coloured with soot) from the surface [114-116]. Fourier transform infrared spectroscopy (FTIR) has been used to measure the cleanability of organic soil (e.g. stearic acid, oleic acid) from the surface [117]. Radiochemistry has also been applied to determine the cleanability of ceramic surfaces [118]. Contact angel measurements have also been used to gain information on various hydrophobic-hydrophilic characteristics of the soil and the surface. During the last decade, most cleanability studies of glazes deal with assessing the effect of additional photocatalytic coatings on

the surfaces. The photo-degradation of dyes, especially methylene blue, has been used to determine the effect [119].

The interaction of the glazes with soiling components depends on topography, phase composition and chemical composition of the surface [112, 120]. Thus, improvements in the properties of the outmost surface of the glaze layer have a great influence on the performance of the final ceramic products. The topography affects the soil resistance and cleanability of the surface in different ways. On one hand, a well-controlled nano-scaled roughness increases the contact angle of liquids on the surface and thereby makes the surface soil-repelling. On the other hand, an increased smoothness of the surface benefits the mechanical cleaning processes. Pinholes often seen on glaze surfaces affect the surface roughness. The polishing process used for some ceramic tile surfaces can also open up pores at the surface and thus reduce the cleanability [115]. Thus, minimising the porosity and pinholes in glazes increases the cleanability of the surface.

In bathroom environments, the hardness of water, e.g. lime, magnesia and dissolved silicate species often lead to the formation of deposits [121, 122]. Their removal from the surface is affected not only by the composition of the deposit but also by the surface nano- and microstructure. Deposits containing lime and magnesia are effectively removed with acidic cleaning agents. However, the silicates in the spots bond chemically to the hydrated silicate layer, and consequently, they are very hard to remove [122]. As the deposited layer is likely to act as a site for soil and bacterial attachment, avoiding their formation or enhancing their removal is essential.

The attempts to improve the cleanability of ceramic surfaces can be categorized into two different groups [49]. (1) Methods focusing on applying an additional functional coating or the application of a transparent amorphous layer or (2) modification of the glaze layer mainly by producing a surface as smooth as possible.

2.8. Improved surface properties through surface modification

During the 2000s, different surface coatings on glazed surfaces were introduced on the market to achieve soil-repelling properties and to improve the cleanability. Functional coatings with antibacterial, water repellent and self-cleaning properties were applied on products to give added value to the customer [7]. Passive self-cleaning surfaces only repel soil, while an active self-cleaning surface also decomposes soil. The cleanability is improved by implementing either a hydrophobic or a hydrophilic coating at the surface (Fig. 10). The coatings control the wettability of the surface. Wettability depends on surface energy, surface roughness and chemical heterogeneity

[123]. Hydrophobic coatings based on fluoropolymers are commercially utilized on some sanitary ware. On ceramic tiles, most effort has been put to introduce surfaces with the photocatalytic effect of TiO_2. Glaze surfaces are often used in mechanically and chemically demanding environments, thus the applied coatings should also fill the requirements in these environments.

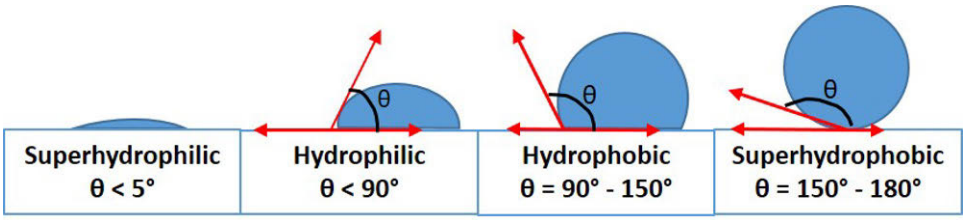

Fig 10. Schematic views of different superhydrophilic, hydrophilic, hydrophobic and superhydrophobic surfaces.

2.8.1. Photocatalytic and hydrophilic coatings

Perhaps the most studied self-cleaning surfaces are those based on TiO_2. The self-cleaning character of TiO_2 surface is based on two separate phenomena: the photocatalytic action and the superhydrophilic nature of the surface. The photocatalytic effect of TiO_2 is based on semiconductor photochemistry and was first reported by Fujishima and Honda in 1972 [124]. Since then, the technology has been adapted to several different substrates and has been the topic of numerous patents and a high number of scientific papers [125-130]. A photocatalyst is generally defined as a semi-conducting metal that produces charged free radicals from water and oxygen in the presence of UV-light. The charge of these free radicals makes them extreme biological and chemical reactants. A TiO_2-based coating on the surface, when exposed to UV-illumination, decreases the water contact angle close to 0°, i.e. the surface becomes superhydrophilic. The UV-light activated photocatalytic active coating causes reactions at the surface, breaking down organic material to H_2O and CO_2 and can thus is called an active self-cleaning surface.

The utilization of photocatalytic TiO_2 coatings on ceramic glazes has been widely reported [131-135]. da Silva et al [119] recently summarized the research work done on photocatalytic tiles in a review article. The critical aspects for the interactions of TiO_2 coatings with ceramic tiles include high sintering temperature, reactions between titania and substrate, adhesion of the TiO_2 film/particles to the substrate, and changes in the appearance of the tile surface. A failure in one or more of these aspects will lead

to products that do not work properly in their target application. Ceramic tiles are usually sintered at 1150 to 1240 °C. If TiO_2 is heated to these temperatures, the much more active form of TiO_2, anatase is transformed to the less active rutile form. Thus, the surface will not be photoactive anymore. To avoid this a second firing step at temperatures varying from 600 to 900 °C can be implemented, causing higher production costs.

Doping or coupled photocatalyst have been reported as alternative methods to increase the photocatalytic performance. The doping has been used e.g. to shift the anatase to rutile transformation to higher temperatures to allow a higher firing temperature or to increase the photocatalytic activity compared to pure TiO_2. Titania has a relatively high band gap value of 3.2 eV, which means it can be activated only with UV-light. Doping is also used to extend the band gap excitations towards the visible region. For ceramic glazed tiles, $ZnTiO_3$ [136], Nb_2O_5 [137, 138] and W-doped TiO_2 [139] have been suggested. In addition, ZnO has been found to be a promising additive as a photocatalytically active oxide in glazes [140].

Photocatalytic tiles have been manufactured and commercialized since 2003. However, their utilization is still limited, mainly due to uncertainties of the photocatalytic efficiency. da Silva et al [119] suggested the following parameters for production of photocatalytic ceramic tiles:

- Deposit method: spraying
- Synthesis method: sol-gel
- Titanium precursors: titanium (IV) tetra isopropoxide, diethanolamine and absolute ethanol
- Sintering temperature: 600 – 800 °C; if higher temperature, 900 °C, is required, the sol-gel should be doped with e.g., Nb_2O_5

2.8.2. Hydrophobic Coatings

Hydrophobic coatings (e.g. fluorocarbon polymers, silicons) give surfaces with high water contact angles (70- 90°) and thus improve the water flow and cleanability. A hydrophobic surface/coating with low surface energy makes the surface repellent to water and oil compounds, thus improving the stain resistance of the surface. Superhydrophobic surfaces have water contact angles higher than 150°. Contact angles up to 180° can be obtained on e.g. fluorinated surfaces that also have a specific nano-scale patterned structure [141,142]. The basic ideas for self-cleaning surfaces were found in nature. The structure of lotus plant leaves and the wings of insects are

superhydrophobic because of their surface structure and chemistry. These surfaces have been used as inspiration when designing new self-cleaning surfaces [143]. The self-cleaning effect of the superhydrophobic surface is based on spherical water droplets rolling off the surface and at the same time picking up the dirt coming on their way (Fig. 11). This self-cleaning functionality refers to the so-called Lotus effect and requires a high contact angle and a specific surface roughness [143]. Superhydrophobic surfaces are produced by creating a rough surface and by modifying the surface with materials of low surface energy, e.g. through fluorination or addition of silicon compounds. Fluorinated compounds are most commonly used in hydrophobic coatings for ceramic glazes. Fluoropolymers are utilized because of the desired surface properties provided by fluorine and easy application procedures. Fluorine-based compounds generate surfaces with extremely low surface energies thus making the surfaces repellent to water and oil compounds [144]. The hydrophobic coatings used on glazed surfaces usually consist of a combination of organic and inorganic materials of nanometre particle size to reduce the surface tension and thus improve the cleanability [132, 145].

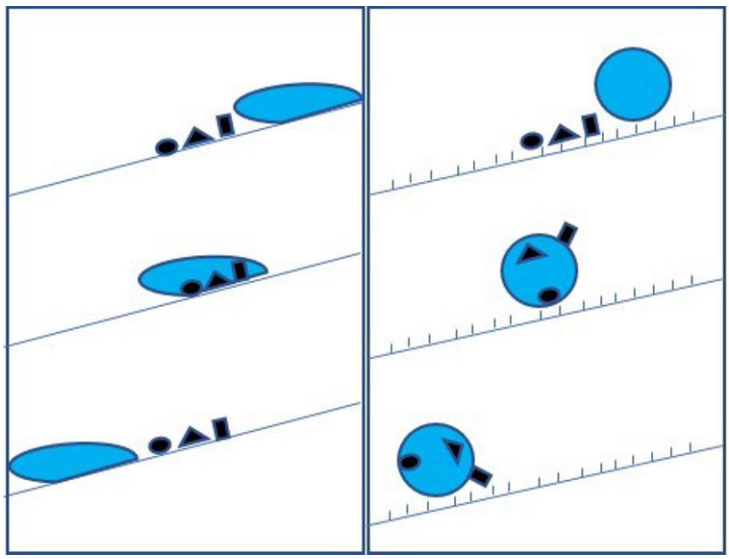

Fig 11. A summary of the connection between roughening and self-cleaning. On smooth surfaces, the particles are mainly redistributed by water (left) while on rough surfaces they adhere to the droplets and are removed when the droplets roll-off (right). Redrawn from Bartlott and Neinhuis [143].

2.8.3. Antibacterial and other functional coatings

The development of antibacterial products is increasing because the damage caused by harmful microorganism has become a serious social problem [146]. Several antibacterial agents based on the inorganic elements titanium, copper and zinc have been suggested [147]. However, silver is the best-known antibacterial agent due to its strong cytotoxic effect towards a broad range of microorganisms and its remarkably low human toxicity compared with other heavy metal ions [148]. Antibacterial glaze surfaces have mainly been produced with silver as the antibacterial agent. Silver-doped ceramics and glasses have been shown to be chemically durable and releasing silver ions for a long time thus having a good antibacterial activity [149]. In ceramic glazes, silver is often used together with TiO_2 [146-151]. This combination provides the possibility to achieve a sterilizing effect from TiO_2 under UV-light and the silver metal ion provides an antibacterial effect, even in environments not exposed to UV-light. Also, successful surfaces with Ag/SiO_2 thin films [147] and Ag_2WO_4 powders [152] have been reported.

2.8.4. Smooth, transparent glazes

Zirconium silicate ($ZrSiO_4$) added as an opacifier in traditional white, opaque raw glazes is known to affect the surface roughness. Some of the zirconium silicate crystals penetrate the upmost glassy surface layer, thus increasing the roughness on micro-scale level [54, 99, 153-155]. The smoothness aspect has been exploited in double glazed tiles where a second thin, transparent layer has been applied on the standard white glaze in order to maintain the white, opaque appearance but to enhance the cleanability by providing a smoother surface [117, 122, 156]. However, this method has not been very interesting for producers due to the additional costs arising from the second firing [49].

2.8.5. Cleanability of functional coatings on glaze surfaces

It is generally accepted that smooth surfaces are easier to keep clean than rougher surfaces [114, 115]. Cleanability and stain resistance of glazed surfaces has been reported in the literature [157]. Only a few papers have been published on the cleanability of glaze surfaces with additional coatings. Most of those studies were done in close connection with the experimental work in this thesis [112, 116, 117, 120, 122, 158, 159]. The cleanability studies showed varying results. In general, the overall surface roughness varied depending on the phase composition of the glaze, whereas

the additional functional coatings had only a minor or a negligible effect on the roughness. The cleanability of uncoated, titania, fluoropolymer, and zirconia coated glazes was found to be rather similar, likely due to their equal roughness values [116]. However, the fluoropolymer coating clearly increased the water contact angle and is thus likely to improve the cleanability of oblique surfaces. In another study [120], the coatings affected the cleanability to some extent. Soils consisting of inorganic particles were removed most efficiently from the titania and zirconia coatings. By contrast, the lowest amount of oil residues were reported on fluoropolymer coatings. The cleanability results partly depend on the model soils and cleaning methods used. Thus, only the trends reported in different studies are comparable.

The self-cleaning properties of TiO_2-based products have been intensively studied. Water contact angle measurements and degradation of dyes, mainly methylene blue, at the surface are the evaluation methods commonly used for assessing the photocatalytic effect of ceramic tiles with functional coatings. The titania surfaces have two specific characteristics: photocatalytic action and superhydrophilicity. The photocatalytic decomposition of organic contaminants on the surface is effective if the rate of contamination is lower than the rate of decontamination. For TiO_2-coated materials, organic soils on surfaces are decomposed by the photocatalytic action [160, 161]. However, the photocatalytic effect of the surface must first be activated by UV radiation. In this activation, TiO_2 reacts with the oxygen and water molecules in the air and produces free radicals leading to oxidative species. Organic particle soil and dust can be cleaned by the superhydrophilic property [126, 162]. However, the surfaces do not possess the photocatalytic effect and the superhydrophilic property simultaneously. Photocatalysts are not very effective for decomposing large volumes of soil, but they are capable of preventing the accumulation of soil layers [126, 163]. A small amount of water can be spread over the surface due to photo-induced superhydrophilicity, and soil can easily be swept away from the surface. The effect of UV-radiation of TiO_2-coated glaze surfaces has been reported to be greatest on rougher surfaces, most likely due to a higher photocatalytic activity provided by the increased surface area. UV-radiation affected the cleanability of organic particle soil but had no effect on the cleanability of oil soil [164].

2.8.6. Durability of functional coatings on glaze surfaces

The durability of functional coatings is one of the most important properties to be considered for their commercial utilization. Coated ceramic products in construction applications, e.g. in bathrooms, baths, kitchens, hospital environments must

withstand chemical and mechanical cleaning. For floor tiles, the abrasion resistance to normal everyday wear must be considered.

The durability of photocatalytic titania ceramic tiles has seldom been investigated due to the lack of specific standards and procedures [119]. However, the standard EN 1096-2 which tests the impact of weathering of coatings on glass has been applied to evaluate the durability of SiO_2-TiO_2 coatings [165]. Although some defects were found in the coating after the treatments, the defects did not affect the functionality of the overall coating. The durability of the coatings depends also on its adhesion to the glaze surface. The adhesion again depends on the processing conditions, additives, etc. used during the manufacture. Specific equipment, e.g. different scratch tests, can be used to determine the adhesion of the coating to the surface and thus give a measure of the mechanical durability of the additional coatings [119]. Overall, studies on the durability of coated ceramic glazes are very limited and most of the published results are connected to the present thesis [166-168].

3. Materials and methods

3.1. Raw materials and glaze compositions

The experimental glaze compositions were calculated using commercial grade raw materials consisting of natural minerals. These included feldspar, wollastonite, limestone, dolomite, china clay, corundum and quartz. Additionally, zinc oxide and zirconium silicate were used as opacifiers in some compositions. Oxide composition, trade name and manufacturer of the raw materials are given in Table 2. In total, 146 experimental glaze compositions and one commercial reference glaze were used to study the melting behaviour, chemical and mechanical durability as well as cleanability of raw glazes. In addition, the properties of functional coatings on some glazes were compared. A commercial raw glaze composition was used as reference support glaze for the additional coatings.

Table 2. The oxide composition of the raw materials used in this study. Oxides with content < 0.1 wt% are not shown.

Oxide	Wo[1]	FS[2]	CC[3]	Do[4]	Co[5]	ZnO[6]	Q[7]	L[8]	Zr[9]
SiO_2	52.5	67.2	47.0				98.0		35.0
Al_2O_3	<0.8	18.3	38.2		99.5		0.8		
Fe_2O_3	0.16	0.13							
CaO	43.5	0.5	0.1	30.3				52.6	
MgO	<0.6		0.2	21.7					
K_2O		7.7	1.2				0.13		
Na_2O		5.0	0.08		0.3		0.2		
ZrO_2									65.0
ZnO						100			

[1] Wollastonite, FW 325, Nordkalk Oy Ab, Finland; [2]Feldspar, FFF 300, Sibelco Nordic Oy Ab, Finland; [3]China Clay, Kaolinor IC, Imerys Ceramics, France; [4]Dolomite, Microdol Extra, Omya, Norway; [5]Corundum, Alodur 220, Treibacher, Germany; [6]Zinc oxide, Kuusakoski Oy, Finland; [7]Quartz, FFQ 200, Sibelco Nordic Oy Ab, Finland; [8]Limestone, Norweiss, Omya, Germany, [9]Zirconium silicate, Ultrox Standard, Atofina, Canada.

Glaze compositions in Series I, melting behaviour (Publication I)

Seventy-five statistically chosen recipes were used to establish the impact of the raw materials on the melting behaviour of raw glazes. The limits used for the raw materials and the corresponding oxide compositions in Series I are given in Table 3. In all batches, 10 wt% zirconium silicate was added to give the glazes roughly the same white colour and opacity. Quartz was used to fill up the batches to 100%. The raw material compositions of all glazes are given in Appendix I.

Table 3. Ranges (wt%) for the oxide composition and raw materials of the glazes in series I (Publication I).

Raw Materials	**Range**		**Oxide**	**Range**
Feldspar	20 - 50		$Na_2O + K_2O$	2.5 - 6.3
Wollastonite	10 - 30		MgO	0.1 - 2.3
China clay	5 - 15		CaO	7.6 - 22.6
Dolomite	0 - 10		Al_2O_3	6.1 - 25.2
Corundum	0 - 10		SiO_2	43.3 - 68.1
Quartz	3 - 44		ZnO	0 - 4
Zinc oxide	0 - 4			
Zirconium silicate	10		ZrSiO4	10

Glaze compositions in Series II, surface morphology development during firing (Publication II)

Fifteen statistically chosen glaze recipes were used to study the development of different phases during the firing schedules. The limits used for the oxide compositions and corresponding raw materials compositions (Series II) are given in Table 4. Neither zirconium silicate nor zinc oxide was used in this study. The raw material and oxide compositions of all glazes are given in Appendix II

Table 4. Ranges (wt%) for the oxide compositions and raw materials of the glazes in Series II (Publication II).

Oxide	Range		Raw Materials	Range
$Na_2O + K_2O$	4 - 10		Feldspar	26 - 78
MgO	0 - 4		Limestone	0 - 42.8
CaO	5 - 30		China clay	5 - 8
Al_2O_3	10 - 25		Dolomite	0 - 15.4
SiO_2	45 - 78		Corundum	0 - 14.3
			Quartz	0 - 48.8

Glaze compositions, surface characteristics in Series III (Publications III-IV)

Twenty-five glaze recipes (Series III) were used to study the impact of wollastonite and dolomite on the surface characteristics. The limits used for the oxide compositions and the corresponding raw materials compositions are given in Table 5. A low SiO_2/Al_2O_3 -ratios of 2 wt% was used to enhance the development of a matte appearance of the glaze surfaces. The raw material and oxide compositions of all glazes are given in Appendix III.

Table 5. Ranges (wt%) for the oxide compositions and raw materials of the glazes in Series III (Publications III-IV).

Oxide	Range		Raw Materials	Range
$Na_2O + K_2O$	5		Feldspar	34.5 - 37.6
MgO	0 - 4		Wollastonite	8.6 - 39.1
CaO	10 - 18		China clay	10
Al_2O_3	24 -28		Dolomite	0 - 16.4
SiO_2	48 - 56		Corundum	11.5 - 16.6
			Quartz	0 - 16.6

3.2 Manufacture of the experimental glazes

Batches of 500 g of each experimental glaze were wet-milled to an average particle size of 100% < 40 μm, 80% < 10 μm, 70% < 5 μm and 22% < 1 μm. The suspensions were either sprayed on green tiles (Publications I, III-VI) or applied in a waterfall process in laboratory scale (Publication II). The tiles were fired in three different kilns. An industrial fast-firing roller kiln was used for the production of floor tiles (Publications I-IV), industrial tunnel kilns for the production of sanitary ware (Publication III-VI) and a laboratory furnace, Carbolite RHF 16/35 for testing in the laboratory environment (Publication II). Firing schedules and peak temperatures used are shown in Table 6.

Table 6. Kilns and firing schedules used in the firing of the experimental glazes.

Kiln	Heating	Soaking time at peak temperature	Cooling	Peak temperature	Publication
Industrial kiln, fast-firing, tiles	20 min	2-5 min	20 min	1215 °C	I-IV
Industrial kiln, sanitary ware 1	12 h	30 min	12 h	1235 °C	III-IV
Industrial kiln, sanitary ware 2	5,5 h	15 min	6.5 h	1210 °C	III-IV
Industrial kiln, sanitary ware 3	8 h	20 min	9 h	1210 °C	V-VI
Laboratory furnace, cycle 1	55 min	0-1 min	6-8 h	1215 °C	II
Laboratory furnace, cycle 2	55 min	1 h	6-8 h	1215 °C	II
Laboratory furnace, cycle 3	55 min	4 h	6-8 h	1215 °C	II
Laboratory furnace, cycle 4	55 min	24 h	6-8 h	1215 °C	II

3.3. Melting behaviour with hot stage microscopy (HSM), (Publications I, III-IV)

A small sample of each batch was dried and pressed using ethanol as the binding agent with a Leitz hand press to cylinders (3 mm in height, 2 mm in diameter) for the melting behaviour studies. The samples standing on an alumina support were transformed into a hot-stage microscope (Misura 3, Expert Systems Srl, Italy). The furnace of the microscope was heated at a constant rate of 10 °C/min up to 1400 °C. The samples were automatically imaged by a video camera at every 5 °C increase in temperature. The changes in the height and the shape of the image were used to characterize the firing behaviour of the glaze.

3.4. Surface characterization techniques

Scanning Electron Microscope, SEM (Publications I-VI)

The morphology and chemical composition of the fired glazes were studied with scanning electron microscopy (LEO 1530, Zeiss) combined with energy dispersive X-ray analysis (EDXA, Vantage, Thermo Electron Corporation).

Confocal optical microscope, COM (Publications II, V-VI)

White light confocal microscopy (COM, NanoFocus μsurf®) was used to capture 3D images and to measure surface topography of the surfaces. The surfaces were imaged with lenses giving 20x and 100x magnifications.

X-ray powder Diffraction, XRD (Publications I-IV)

X-ray diffractometry (XRD, X'pert by Philips, Cu-α radiation) was used to determine the crystalline phases in the glazes. Sample preparation included cutting the ceramic glazed tiles into roughly 1.5 x 1.0 cm sized pieces.

Gloss (Publications I, III)

The gloss of the glazes was measured by a reflectometer (REFO®3) with the measuring angle 60°.

Chemical durability (Publication IV)

After the firing, the chemical durability of the glazed tile surfaces was determined using the procedure described in the ISO 10545-13 standard [109]. The tiles were exposed with test solutions belonging to the group low concentrations of acids and alkalis (L): i) hydrochloric acid (3 vol%, exposure time 4 days), ii) citric acid (100g/L, exposure time 24 hours), and iii) potassium hydroxide (30 g/L, exposure time 4 days). A glass tube was fastened with modelling clay to the glaze surface, after which 17 ml of the test solution was placed in the tube. After the specified testing times, the solution was removed and the exposed surface examined and classified. The surfaces were visually classified by observing any surface damages and then marked with a pencil. In short, a surface with no visible damages and also the pencil mark easily removed with wet cloth indicates that the glaze is chemically durable in the solution and belongs to the class GLA (Class A, resistance to low concentrations of acids and alkalis of glazed tiles). Similarly, a glaze with several visible surface damages has poor chemical durability and is classified as GLC (Class C, resistance to low concentrations of acids and alkalis of glazed tiles). Further, glazes with some damage or some pencil marks after the cleaning are classified as GLB (Class B, resistance to low concentrations of acids and alkalis of glazed tiles). Besides the standard test procedure, the impact of test time and the concentration of hydrochloric acid on durability was explored. In these measurements, the glazes were exposed to 0.1 vol% and 3 vol % HCl-solutions for 1, 3, 7 and 28 days. After the exposure, the same standard method was used to classify the surfaces. In addition to the procedure given in the standard, selected surfaces were also studied using SEM-EDXA and XRD.

Inductively coupled plasma – atomic emission spectroscopy, ICP-AES (Publication IV)

Inductively coupled plasma – atomic emission spectroscopy (ICP-AES, Thermo Jarrell Ash AtomScanTM 25 using the program ThermoSPEC version 6.20) was used to analyse the concentrations of the ion species (Ca, Mg, Al, Na and Si) leached out from the glazes into the experimental solutions, i.e. the solutions used for the chemical durability tests described above. In these tests, Teflon rings with an inner diameter of 28 mm and height 20.5 were sealed to the glazed surfaces using O-rings and spring clips [95]. Then, 10 ml of the solution was added and the ring was covered with a film. The relatively small volume of the solution was assumed to give concentrations high enough for the dissolved ions to enable the detection of also minor surface leaching.

Mechanical durability (Publication I)

The resistance to abrasion or hardness of the surfaces was measured by the PEI (Porcelain Enamel Institute) method according to the standard ISO 10545-7 [169]. In short, the surfaces are put under an abrasive load of steel balls, aluminium oxide and water. The resistance to abrasion is divided into five classes according to a visual determination whether damage of the surface can be observed after a certain number of revolutions (rev): class 0 (100 rev.), class 1 (150 rev.), class 2 (600 rev.), class 3 (750 and 1500 rev.), class 4 (2100, 6000 and 12000 rev), and class 5 (> 12000 rev).

3.5. Surface modification (Publications V-VI)

3.5.1. Applications of coatings

All coatings were applied on the reference white opaque glaze. The substrate glazes for the additional coatings were prepared by milling the raw materials and sprayed on green tiles. Then, the tiles were fired in an industrial tunnel kiln for sanitary ware for 13 hours with a peak temperature of 1235 °C.

Three different commercial fluoropolymer coatings were studied: F1, ECC-4000 by 3M (Publication V-VI); F2, ETC-140 by Clariant (Publication VI); and F3, ECC-1000 by 3M (Publications V). All coating solutions were sprayed on the glazed tiles at room temperature. Additionally, the coating F3 (ECC-1000) was cured at 100 °C after spraying.

Two silane-based experimental sol-gel coatings, PRO A and PRO B developed by VTT (VTT Technical Research Centre of Finland Ltd.) were used in Publication V. In these coatings, the ratio between the polymeric and ceramic components varied. Ethanol was used as the solvent in the sol and water was added for the hydrolysis reaction. The sol-gel coatings were applied by spill coating.

An experimental sol-gel ceramic titania coating, T, was studied in Publication VI. The sol-gel coating was prepared from a Ti-alkoxide derived sol solution. The samples were dipped in the solution, dried and matured at 500 °C for 1 hour to obtain a ceramic TiO_2 coating consisting of anatase crystals [170].

Double glazed surfaces were prepared using two different approaches. For both, a commercial transparent frit glaze was used as the second glaze layer. In the first method, the glazed tiles (D1) were single-fired. The reference glaze was first sprayed on the tile and immediately after that, the frit glaze was sprayed on the first glaze layer, after which the glaze was fired (Publication VI). In the second method, the glaze (D2)

was double fired. First, the reference glaze was applied and fired, and after that, the second frit glaze layer was applied and fired again (Publications V-VI). All double glazed tiles were fired in an industrial tunnel kiln for sanitary ware in a firing schedule of 18 hours at the peak temperature of 1210 °C.

3.5.2. Surface performance characterization

Contact angle measurements

In Publication VI, the static water contact angles on ceramic tiles were measured with a contact angle meter (CAM 100, KSV Instruments Ltd). A water drop (ultrapure water Milli-Q) was placed on the surface and imaged for 10 seconds collecting one image per second. Determination of the contact angle was based on the Young-Laplace equation and calculated as the mean value of four samples for each surface.

In Publication V, the data for the evaluation of wetting properties, surface free energy, hydrophobicity and oleophobicity of the non-coated and coated glaze samples were collected from contact angle measurements (CAM 200 Optical Contact Angle Meter, KSV Instruments Ltd, CAM 200 software). The surface free energy measurements were carried out by using a solvent sequence containing distilled water and analytical grades of formamide, ethylene glycol and di-iodomethane. The contact angles of the probe liquids were used for calculations of the surface free energies of the surfaces. The assessments of hydrophobicity and oleophobicity of the non-coated and coated glaze surfaces were carried out by measuring the contact angles of distilled water and oleic acid ($C_{18}H_{34}O_2$).

Soiling and cleaning experiments

In Publication V, the soiling and cleaning properties of the uncoated and coated glazed samples were measured with a soil-drop test developed at VTT. Each sample surface was contaminated with a spot of 0.5 µm of oleic acid. The follow-up of the shape and spreading tendency of the oleic acid spot on the uncoated and coated test material surfaces was performed visually. Prior to the cleaning test, the oleic acid spot was dispersed on the sample surface with rubber teat with a load of 62 kPa. The contaminated sample surface was wiped with a dry micro-fibre cloth with an approximate load of 0.7 kPa. The amount of oleic acid on the sample surfaces before and after the cleaning was qualitatively assessed with FTIR mapping method (BioRad FTS 6000, Shadow Pro Mapping Software). The FTIR analyses carried out are based on the reflection technique with the exploitation of microscope facility. The IR ray is

directed to the sample through the object lenses, which enables the adjusting of the measurable area with the exactness of 5 µm. The collection of IR spectra is carried out with a motorised sample board and automated software. From the sample area of 150 µm * 150 µm, 196 IR spectra were collected and the collection was imaged as intensity difference map of stretching vibration between carbon and hydrogen atoms.

In Publication VI, the soiling and cleaning properties were studied by colour marked mixture of fatty acids and particles. The surfaces were soiled by spin-coating with a model soil mixture consisting of sebum (212 mg), ethanol (50 ml), and soot (50 mg) as a colour marker. The sebum (Wfk Testgewebe GmbH, Germany), consisted of free fatty acids (18.0 %), beef tallow (32.8 %), fatty acid triglycerides (3.6 %), lanoline (18.3 %), cholesterol (3.7 %), hydrocarbon mixture (12.0 %) and cutina (11.6 %). The soiling was repeated four times with 20 µl of the soil suspension in order to get a visible discolouring of each surface. The surfaces were cleaned by moist microfiber clothes after 24 hours drying and fixing at room temperature. The cleaning cloth, moist with 100 wt% of water, was rotated once against the surface (pressure 0.5 bar, velocity 30 rpm in a laboratory-scale cleanability tester). The surfaces coated with TiO_2 were also exposed to ultraviolet (UV) light from a distance of 23 cm for two hours before both the soiling and cleaning step. The colour changes were determined with a spectrophotometer (Perkin Elmer Lambda 2 UV/VIS/NIR with Lab-sphere RSA-PE-20). The soil amount attached before cleaning, ΔE_s, the soil amount removed after cleaning, ΔE_{rem}, and the soil amount left after cleaning, ΔE_{res}, were calculated from CIE L*a*b* values measured for each step [171]. The amount of soil on the surfaces after different steps in the cleanability studies were calculated with equations (1) - (3).

$$\Delta E_s = \sqrt{\left(L^*_{unsoiled} - L^*_{soiled}\right)^2 + \left(a^*_{unsoiled} - a^*_{soiled}\right)^2 + \left(b^*_{unsoiled} - b^*_{soiled}\right)^2} \quad (1)$$

$$\Delta E_{rem} = \sqrt{\left(L^*_{cleaned} - L^*_{soiled}\right)^2 + \left(a^*_{cleaned} - a^*_{soiled}\right)^2 + \left(b^*_{cleaned} - b^*_{soiled}\right)^2} \quad (2)$$

$$\Delta E_{res} = \sqrt{\left(L^*_{unsoiled} - L^*_{cleaned}\right)^2 + \left(a^*_{unsoiled} - a^*_{cleaned}\right)^2 + \left(b^*_{unsoiled} - b^*_{cleaned}\right)^2} \quad (3)$$

Chemical durability

The chemical durability of the surfaces with functional coatings was determined in Publication VI. The durability was tested by immersing four samples of each surface (2.5 x 2.5 cm) in a cleaning agent solution (40 ml) of pH 9.1 at 37 °C for one, three and

seven days. This model detergent solution corresponds to commercial weakly alkaline cleaning agents. After immersion, the samples were rinsed with distilled water. The changes in roughness parameters, water contact angle, soil attachment and soil removal after the exposures were used as a measure of the chemical durability.

Mechanical durability

In Publication V, the normal cleaning process of coated ceramic glazes was measured with a wet abrasion test (modified standard DIN 53 778) by using the Erichsen washing apparatus designed for paint films. One sample of each coating type was exposed to 700 back and forth abrasion cycles and the respective replica samples were subjected to 1400 abrasion cycles. The abrasion was carried out with wetted microfibre cloths. The load applied to the sample was 0.7 kPa. The extent of the abrasion of the coated surfaces was assessed with contact angle measurements using water and oleic acid. The change in the specular-gloss of the coated surface was analysed with Micro-Tri-Gloss meter at 60 ° geometry.

In Publication VI, the mechanical resistance was evaluated from the cleanability of the surfaces after abrasion with nonwoven steel wool and moist microfiber cloth in a laboratory cleanability tester. The nonwoven steel wool was attached to the tester, after which it was rotated for 50, 100 and 150 revolutions with a constant load of 7.5 kPa. For the moist microfiber cloth, the number of revolutions was 10.000, 15.000 and 20.000 using the same 7.5 kPa load. The changes in roughness parameters, water contact angle, soil attachment and soil removal after the exposures were used as a measure of the mechanical durability.

4. Results and discussion

4.1 Influence of raw material composition on the melting behaviour of raw glazes

Melting behaviour of raw glazes influences the appearance and properties of the final glaze surface. The melting behaviour of seventy-five statistically chosen compositions was measured with hot-stage microscopy. All the characteristic temperatures describing the sintering and melting were modelled as functions of the raw material composition. The glazes were fast-fired in an industrial kiln to verify the melting behaviour and-to estimate the impact of the raw material composition on the surface composition and appearance of the final glaze. In addition, the gloss value of the fired glazes was modelled as a function of the glaze composition. More detailed information is given in Publication I.

4.1.1 Melting behaviour from hot-stage microscopy

The melting behaviour of the glazes in Series I was determined with hot-stage microscopy. The sintering curves of all experimental glazes showed a similar shape as displayed in Fig. 12. The locations of the characteristic sample shapes for the sintering point (SP), softening point (Softening), half-cone point (HCP) and floating point (FP) are indicated in the curve. In addition to the sample shapes, three temperature points T_1, T_2 and T_3, specified as the intersection points of four tangents of the sintering curve, were also used to characterize the melting behaviour.

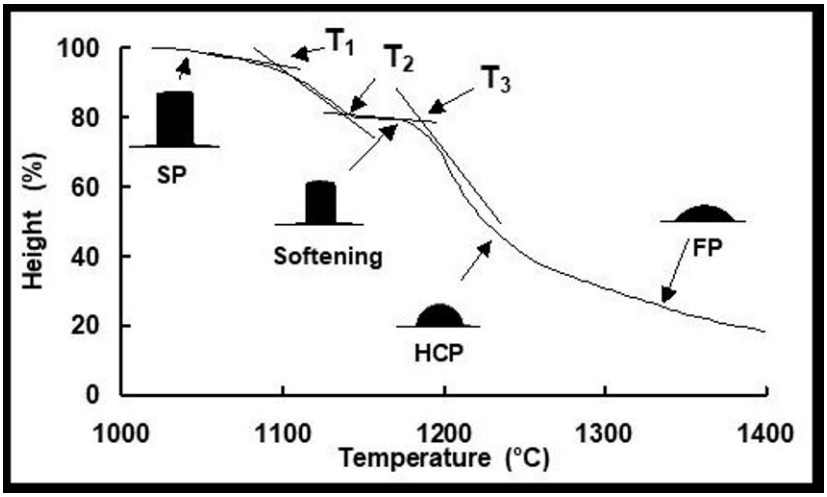

Fig 12. Sintering curve showing a typical decrease in sample height during heating in HSM. The curve is for glaze no 8 (see Appendix I). The tangent temperature points T_1, T_2 and T_3, as well as the location of the temperatures showing the typical sample shapes, are also indicated.

The first part of the sintering curve shows a rather constant sample height up to about 1000 °C. The sintering point (SP) gives the onset temperature of the first sintering. The slight decrease before T_1 suggests the commencement of solid state sintering of very finely ground particles or the melting of some raw material. The temperature, T_1 was taken as an indication of the onset of the main sintering, the start of a rapid height decrease. A small difference between the temperatures SP and T_1 was found to indicate a fast sintering process. Thus, SP and T_1 can be considered as important reference points when estimating whether the glaze is likely to allow the elimination of glaze defects caused by gases evolved from the ceramic body. The degassing of the ceramic body should be finished before the glaze seals the surface. After T_1, the sample height decreases rapidly to T_2. The slope for the line between these two points is relative to the sintering rate, the steeper the line the shorter the sintering range. At temperature T_2, the melt has driven off most of the air between the raw materials particles, as shown by the ceasing of the decrease in the height of the sample. After this temperature, the sintering process will be controlled by the viscosity of the molten phase formed and the dissolution of residual solid grains in the melt. Between T_2 and T_3, the amount of melt increases as residual raw materials continue to react with or dissolve in the melt. The last residual raw materials have dissolved at T_3. If the glaze is fired at a higher

temperature than T_3, the glaze melt likely has a low viscosity which can lead to problems with glaze flow on vertical surfaces. Again, a lower firing temperature than T_3 means that undissolved particles might be left in the glaze.

The typical sample shape indicating softening point (Softening, see page 19), is located between the temperatures T_2 and T_3. The temperatures for the shapes denoted as half-cone point (HCP) and floating point (FP) are all found at higher temperatures than T_3. HCP and FP can be used to characterize the viscosity of the molten glaze and are of utmost importance for specifying the melting behaviour of homogeneous fritted glazes.

The characteristic shape corresponding to the minimum baseline (MBL) could be observed only for a few of the glazes. It was assumed that the formation of a sphere (MBL) was prevented either by residual raw materials or by crystalline phases embedded in a highly viscous melt formed during the heating. High surface tension has also an effect on the formation of the characteristic point MBL [35].

Large differences were observed in the melting behaviour of the experimental glazes (Table 7). This was also expected because the compositions were chosen to cover a wide glaze-forming system. All the characteristic temperature points of the experimental glazes are given in Appendix IV.

Table 7. The characteristic points from HSM study and their temperature ranges (Series I).

Characteristic Point (HSM)	**Range**
Sintering point (SP)	1025 - 1140 °C
Softening point (softening)	1120 - 1310 °C
Half-cone Point (HCP)	1145 - 1400 °C
Floating Point (FP)	1165 - 1400 °C
T_1	1065 - 1175 °C
T_2	1105 - 1250 °C
T_3	1120 - 1340 °C

4.1.2 Melting behaviour from raw glaze composition

The temperatures describing the sintering and melting of the glazes were mathematically modelled with multiple regression analysis as functions of the raw

material compositions. The models describing the relation between the temperature values (°C) and the raw materials are given in Equations (4) – (10), where ρ_i, is the amount of raw material, *i,* in wt%. The raw materials were abbreviated using the following symbol: FS = feldspar, CC = china clay, Do = dolomite, ZnO = zinc oxide, Wo = wollastonite, Q = quartz and Co = corundum.

$$Sintering\ Point, SP\ (°C) = 1019.54 + 0.85\rho_{FS} + 2.67\rho_{CC} + 3.62\rho_{Do} - 29.67\rho_{ZnO} + 1.44\rho_{Co} + 0.020\rho^2{}_{Wo} + 4.77\rho^2{}_{ZnO} + 0.018\rho^2{}_{Q} \quad (4)$$

$R^2 = 86.7$

$$Softening\ Point, Softening\ (°C) = 313.31 + 3.70\rho_{Wo} + 10.22\rho_{FS} + 13.72\rho_{CC} - 5.82\rho_{ZnO} + 11.38\rho_{Co} + 11.22\rho_{Q} + 0.37\rho^2{}_{Do} + 1.13\rho^2{}_{ZnO} - 0.29\rho^2{}_{Co} + 0.1\rho^2{}_{Do+Wo} + 5.98\rho_{Wo/CC} + 75.39\rho_{Co/(Do+Wo)} \quad (5)$$

$R^2 = 94.6$

$$Half - Cone\ Point, HCP\ (°C) = 472.59 + 10.18\rho_{FS} + 11.53\rho_{CC} - 5.08\rho_{Do} + 8.74\rho_{Co} + 10.52\rho_{Q} + 0.24\rho^2{}_{Do} + 0.03\rho^2{}_{Q} + 0.15\rho^2{}_{Wo+Do} + 60.21\rho_{Co/(Do+Wo)} \quad (6)$$

$R^2 = 98.4$

$$Floating\ Point, FP\ (°C) = 157.24 + 3.17\rho_{Wo} + 16.46\rho_{FS} + 7.94\rho_{CC} + 13.29\rho_{Co} + 15.75\rho_{Q} - 0.032\rho^2{}_{FS} + 0.34\rho^2{}_{Do} + 0.14\rho^2{}_{Do+Wo} + 43.25\rho_{Co/(Do+Wo)} \quad (7)$$

$R^2 = 98.1$

$$T_1(°C) = 1131.46 - 0.50\rho_{FS} + 2.01\rho_{CC} + 1.35\rho_{Do} - 25.01\rho_{ZnO} + 4.04{\rho^2}_{ZnO} - 100.14\rho_{ZnO/Wo} + 7.57\rho_{FS/(Do+Wo)} \quad (8)$$

$R^2 = 87.4$

$$T_2(°C) = -675.72 + 21.10\rho_{Wo} + 19.48\rho_{FS} + 21.57\rho_{CC} + 18.59\rho_{Do} + 20.99\rho_{Co} + 20.96\rho_{Q} + 0.25{\rho^2}_{Do} + 1.79{\rho^2}_{ZnO} - 0.36{\rho^2}_{Co} + 10.94\rho_{FS/(Do+Wo)} + 79.40\rho_{Co/(Do+Wo)} \quad (9)$$

$R^2 = 94.2$

$$T_3(°C) = 195.31 + 4.91\rho_{wo} + 12.22\rho_{FS} + 9.71\rho_{CC} + 11.25\rho_{Co} + 13.30\rho_{Q} + 0.21{\rho^2}_{CC} + 0.37{\rho^2}_{Do} - 0.32{\rho^2}_{Co} + 0.13{\rho^2}_{Do+Wo} + 116.93\rho_{Co/(Do+Wo)} \quad (10)$$

$R^2 = 96.2$

All the characteristic temperature points could be modelled as a function of the raw material composition. The mean squared error R^2 suggested that the best fit was given for the points at the higher temperatures. At high temperatures, the amount of molten phase was large and the melting behaviour strongly depended both on the temperature and the glaze composition. At the onset of the sintering also other variables such as packing degree, grain-to-grain interactions and particle size distribution were assumed to affect the behaviour as suggested by Eppler and Eppler [3]. However, a sound estimation could also be calculated for the influence of raw glaze composition on the onset of sintering taking place at lower temperatures. It should be pointed out that the actual temperature values for the characteristics points will vary with the heating rate of the kiln [30]. However, the impact of each raw material on the calculated values is likely to follow the trend given by the Eqs. (4-10). Accordingly, the equations were assumed to be valuable tools when designing and comparing different glaze compositions. The equations can also be used for estimating the impact of a particular raw material on the melting behaviour of raw glazes.

4.1.3. Calculated impact of glaze composition on the melting behaviour

The models (4)-(9) were used to describe changes in melting behaviour when substituting different raw materials for quartz. The effect on the melting behaviour when substituting 2 wt% of each raw material for an equal amount of quartz was calculated for two starting compositions:

i)	40 % feldspar,	ii)	38 % feldspar
	18 % wollastonite,		18 % wollastonite
	5 % china clay,		5 % china clay
	27 % quartz		24 % quartz
	10 % zirconium silicate		10 % zirconium silicate
			2 % dolomite
			2 % corundum
			1 % zinc oxide

Zinc oxide is known to have a major influence on the firing behaviour as also seen in Figs. 13-14. It is the only raw material that clearly lowered the sintering point (SP) and the T_1 temperature of commercial glazes. Also, all the other characteristic point temperatures were lowered by zinc oxide. All glazes with zinc oxide showed 30 - 50 °C lower onset of sintering temperatures than the zinc oxide-free glazes.

Substituting wollastonite for silica showed only a negligible effect on the sintering range. However, a clear effect was seen for the temperature points associated with the melting of the glaze. At these temperatures, wollastonite was assumed to dissolve in the melt. This suggests that wollastonite decreases the viscosity of the silicate melt through the increased lime content.

Dolomite had roughly the same effect as wollastonite on the melting behaviour. Figs. 13 and 14 indicate that dolomite was more effective than wollastonite in decreasing the characteristic sample shape temperatures at the high temperatures.
Substituting 2 wt% of feldspar for silica showed only a small effect on the melting behaviour of the feldspar-rich glazes. The only raw material that slightly increased the calculated temperatures for the characteristic points was corundum.

The effect of mutual substitutions in the raw material composition on the melting behaviour expressed by the characteristic points in HSM analysis depended not only on the extent of the substitutions but also on the starting composition. The trends in the sintering behaviour according to Figs. 13 and 14 can easily be adapted to other

starting compositions. It should be pointed out the total effect must be calculated for each composition individually.

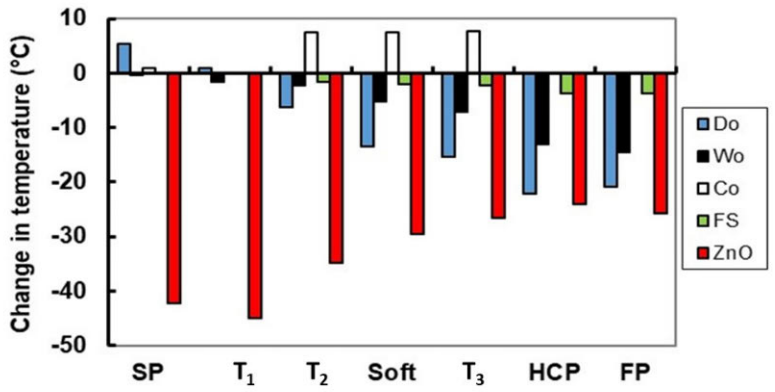

Fig. 13. The effect of substituting 2 wt% of each raw material for an equal amount of quartz on temperatures at different characteristic points for starting composition i). Do = dolomite, Wo = wollastonite, Co = corundum, FS = feldspar, ZnO = zinc oxide (Publication I).

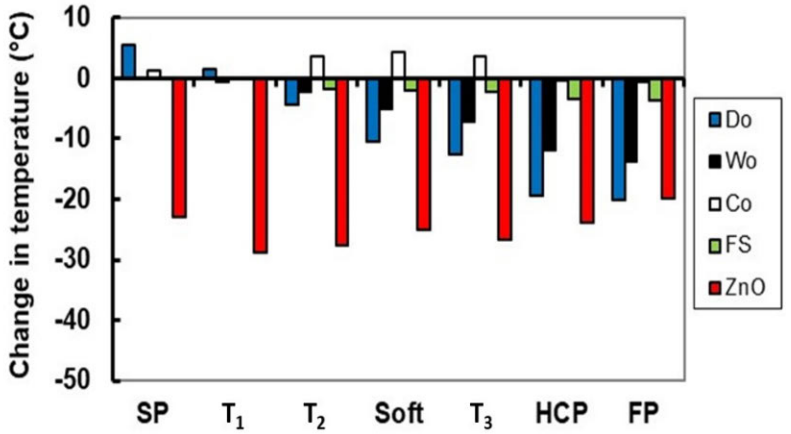

Fig. 14. The effect of substituting 2 wt% of each raw material for an equal amount of quartz on temperatures at different characteristic points for starting composition ii). Do = dolomite, Wo = wollastonite, Co = corundum, FS = feldspar, ZnO = zinc oxide (Publication I)

The models suggested that zinc oxide, dolomite and wollastonite had the greatest effects on the melting behaviour. Zinc oxide was effective in decreasing all the temperatures from the onset of sintering to fusion. Both dolomite and wollastonite decreased the temperatures with an increasing effect in the temperature range starting from the sintering range. The models give guidelines for adjusting the raw material composition for the desired melting behaviour. It should be emphasized that although the final surface morphology suggested by the equations gives the effect of the changes in the composition, the actual firing behaviour in a particular kiln but must be experimentally verified.

4.1.4. Characterization of fast-fired glazes

All seventy-five experimental glazes (Series I, see Table 3 and Appendix I) were fired in an industrial roller kiln for fast-firing of tiles. The gloss value, the crystalline phases present, and the surface hardness were determined. The measured values are given in Appendix V.

The surface appearance varied from surfaces containing some unmelted raw materials to highly glossy surfaces. The surface appearance was also displayed by the gloss values which varied from 2 to 95 gloss units (GU). According to SEM-EDX and XRD analyses, the residual raw materials consisted mainly of quartz, feldspar, wollastonite and corundum. Compared to the phase composition of the original raw materials, diopside ($CaO{\cdot}MgO{\cdot}2SiO_2$) was the only new crystalline phase found in the glaze after the fast-firing process. In the glossiest glazes, the white opacifier, zirconium silicate was the only crystalline phase present.

The dependence of the gloss value on the raw material composition was calculated with multiple regression analysis at a 95 % significance level. The model describing the relation between the gloss value and the raw material composition is given in Equation (11), where ρ_i, is the amount of raw material, *i,* used in wt%.

$$Gloss(GU) = -153.62 - 1.17\rho_{Wo} + 1.23\rho_{FS} + 5.29\rho_{ZnO} + 10.86\rho_{Do+Wo} - 0.13\rho^2{}_{Do+Wo} - 40.93\rho_{Q/(FS+CC+Co)} + 2.09\rho_{Wo/(FS+Q)} \quad (11)$$

$R^2 = 87.6$

The gloss was also calculated as a function of the theoretical oxide composition of the glazes. The model describing the relationship between the gloss value and the oxide composition in wt% is given in Equation (12), where ρ_i, is the amount of each oxide, *i,* in the glaze.

$$Gloss\ (GU) = 72.56 - 9.09\rho_{Al_2O_3} + 9.53\rho_{ZnO} - 5.84\rho_{MgO} - 4.59\rho_{Na_2O+K_2O} + 29.58\rho_{CaO+MgO} + 1564.01\rho_{CaO/SiO_2} - 10.47\rho_{SiO_2/Al_2O_3} + 35.25\rho_{CaO/(SiO_2/Al_2O_3)} \quad (12)$$

$R^2 = 90.0$

When comparing the gloss values of the fast-fired glazes with the melting behaviour, a clear correlation with the melting behaviour of the glaze was found. In the ternary phase diagram given in Fig. 15, all the compositions with a gloss value of 83 or higher are marked with red squares. The apexes of the diagram are SiO_2, Al_2O_3 and the sum of the basic oxides (Na_2O + K_2O+ MgO + CaO + ZnO). According to the HSM experiments (Chapter 4.1.1.), all the compositions marked with red squares melted to a high degree as suggested by the small or negligible amounts of residual raw materials in some of the glazes after the firing. For these glossiest glazes, the total amount of basic oxides was higher than 25wt%, SiO_2 less than 65 wt% and Al_2O_3 less than 20 wt%. For glazes with $Al_2O_3 > 20$ wt%, the gloss seemed to depend on the amount of each basic oxide present in the composition. This implies that each basic oxide affects the reactions and dissolution of corundum in different ways. As the gloss is known to correlate with the share of amorphous phases, unreacted raw materials, and new crystalline phases that form during the firing, the gloss values could be correlated with the melting behaviour. Raw materials that are known to enhance melting, e.g. zinc oxide, enhance the formation of surfaces with higher gloss values. Similarly, an increasing amounts of wollastonite and dolomite, i.e. the sum of CaO and MgO, lead to a higher gloss due to a faster melting behaviour. Since the amount of alkaline earth oxides in this work did not exceed the amount needed for crystallization of diopside, wollastonite or pseudowollastonite in a fast-firing, the glazes stayed glossy even for the highest compositions with the highest contents of these oxides that are typically known to enhance the crystallisation tendency of fast-fired glazes. It should be pointed out that the gloss models given in Eqs. 11 and 12 are

valid for fast-firing conditions only as they were based on values measured for tiles after a firing cycle of 50 minutes. A shorter firing cycle is assumed to result in a higher share of unmelted raw materials in the final glazes and thus to give lower gloss values. Any changes in the peak temperature or/and the length of the firing cycle affect the melting capacity and also the tendency of the glaze to crystallize during the cooling step [10, 59]. The particle size distribution also affects the melting behaviour and further the phase composition of the final glaze [51-55].

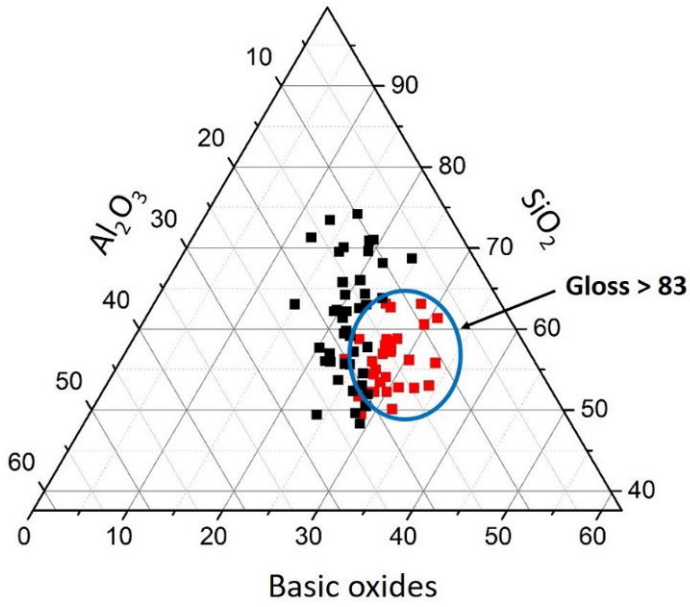

Fig. 15. The composition of the glazes with gloss values higher than 83 (red squares), expressed by their acidic, basic and intermediate oxides. Compositions are shown for the glazes in Series I fired in an industrial kiln for 50 min at 1215 °C (Publication I).

The surface abrasion resistance or hardness of the glaze surfaces were determined by the PEI method [169]. The values varied from the lowest value 1 to the highest 5 in the relative scale between the values from 0 to 5 (Appendix V). The glossiest glazes, i.e. the glazes with higher contents of amorphous phases, had the lowest resistance to abrasion (classes 1-2). Correspondingly, the hardest glazes had higher contents of crystalline phases (classes 4-5). Glazes containing residual corundum and quartz crystals were the hardest. Although these crystals are in general considered as hard, glazes with unreacted raw materials consisting of these crystals do not fulfil all the

quality requirements, especially the aesthetic requirements, for high-quality matte glazes.

Correlations between gloss values for the industrially fired glazes and the temperatures describing the sintering and melting behaviour as suggested by HSM are shown in Fig. 16. The peak temperature in the kiln was 1215 °C and all the compositions whose floating point (FP) was below this temperature (1215 °) had a gloss value of > 90. Also, the half-cone point (HCP) correlated with the gloss values roughly in a similar way. Further, the softening temperature had similar but less clear trends as FP and HCP. In contrast, the sintering point (SP) showed no correlation with the gloss value. This verified that the final fusibility or the melting behaviour of raw glazes in fast firing correlates with the gloss value. In general, the temperature points describing the raw glaze reactions at higher temperatures (HCP, FP) in the HSM analysis can be used to predict the melting behaviour in the fast-firing kiln when optimising the gloss of the glazes.

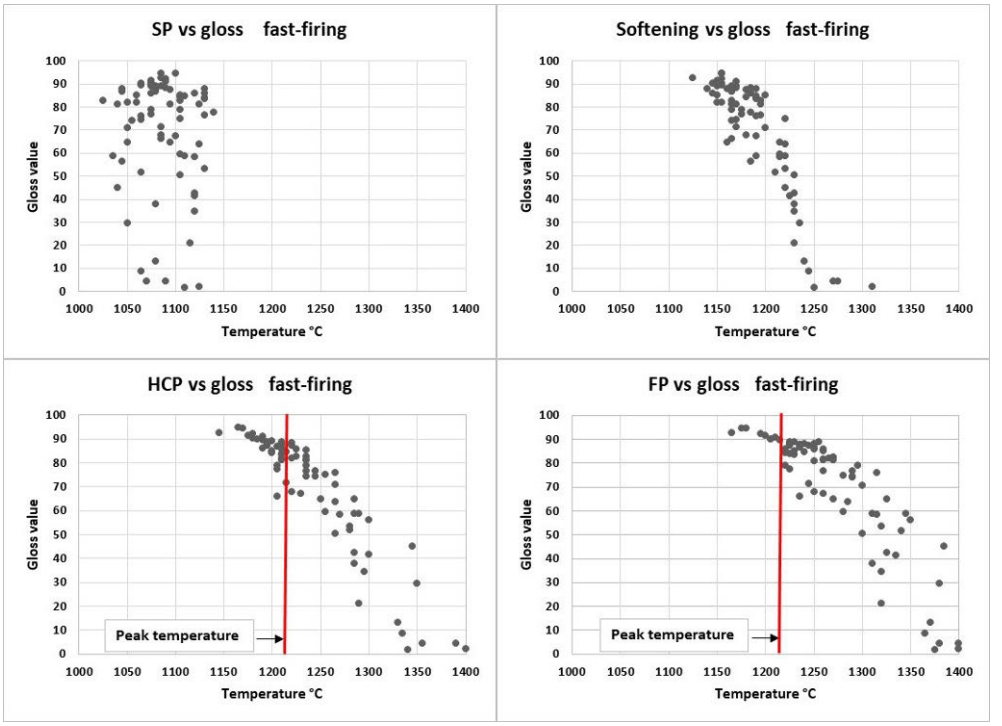

Fig. 16. Correlations between the gloss of fast-fired tiles and the characteristic points (SP, Softening, HCP and FP) of the same glaze compositions measured using HSM (Publication I).

4.2 Influence of firing parameters on phase composition and surface roughness

The crystalline phases developed in fast-firing of raw glazes have been found to depend on the first raw material reactions, whereas crystalline phases developed in longer, traditionally fired glazes correspond to those found in relevant phase diagram [59, 60]. In this chapter, the influence of the soaking time on the phase composition and surface roughness in glazes is discussed. More detailed information is found in Publication II.

4.2.1 Influence of soaking time on phase composition

The effect of soaking time was studied for the glazes in the Series II in several firing schedules: i) firing in an industrial fast-firing kiln with a soaking time of about 2-5 minutes, and ii) firing in a laboratory furnace, fast-firing without a soaking time (0 h) and with soaking times of 1, 4 and 24 hours. The peak temperature in each firing cycle was 1215 °C.

After the industrial fast-firing, the glazes contained crystals of wollastonite, pseudowollastonite or diopside. Also, quartz and corundum, both most likely originating from residuals of unmelted raw materials were found in some of the glazes. In the laboratory fast-firing without a soaking time, the same crystals were found. However, also plagioclase, i.e. anorthite-albite solid solutions, was found in the alumina-rich glazes. The slower heating and cooling rates in the laboratory furnace compared to the industrial kiln were assumed to allow the crystallization of plagioclase and also to enhance crystal growth. In the laboratory firing experiments with longer soaking times wollastonite, pseudowollastonite and diopside gradually dissolved and contributed to the formation of plagioclase. Overall, anorthite and albite were the main crystalline phases in firings with longer soaking times. In the longest soaking time, 24 hours, anorthite was the main crystalline phase.

In general, the crystalline phases found in the final glaze strongly depended on the starting glaze raw material composition as well as on the firing cycle. In lime-rich, magnesia-free glazes (Series II, glazes 5, 6, 9, 13), pseudowollastonite was the main crystalline phase after the shortest soaking times (industrial firing 2-5 min, laboratory furnace 0 h). When the soaking time in the laboratory furnace was increased, the pseudowollastonite crystals gradually melted, if there was not enough alumina present for anorthite formation. In magnesia containing lime-rich glazes (glazes 7 and 11), wollastonite crystals were formed instead of pseudowollastonite for the shortest

soaking time in both the industrial and the laboratory firing. When using longer soaking times, wollastonite was dissolved and anorthite was formed. In lime-rich glazes with high magnesia contents (glazes 3 and 4), both wollastonite and diopside were present in one and the same glaze for glazes fired in the industrial kiln and in the laboratory furnace with no soaking time. In contrast, wollastonite dissolved at longer soaking times in the laboratory furnace experiments. Where the alumina content was high enough, wollastonite and diopside crystals were transformed into anorthite.
Three different routes of plagioclase formation depending on glaze composition were identified:

1) Anorthite-albite solid solution with needle-like network structure was found in feldspar-rich glazes containing corundum. With increased soaking time, the plagioclase composition was transformed towards anorthite.
2) Anorthite was formed by reactions between quartz, corundum and limestone in glazes low in feldspar. After 1 h soaking, the glazes were covered with a network of rectangular flakes, and at a prolonged soaking time also needle-like crystals were present.
3) In glazes with intermediate feldspar and high lime contents, anorthite formation was suggested through a partial dissolution of wollastonite or pseudowollastonite into a feldspar-rich melt. This is an indication of anorthite crystals precipitation from a saturated melt. After 1 h soaking, some anorthite was observed and after 24 h rhombic anorthite crystals were identified.

The predominant crystalline phases in the glazes after each soaking time in both the industrial firing and the laboratory experiments are summarized in the ternary phase diagrams Al_2O_3 – SiO_2 – $MO+MO_2$, where $MO+MO_2$ is the total sum of Na_2O, K_2O, CaO and MgO (Fig. 17). The diagrams suggest that the wollastonite, pseudowollastonite and diopside crystals in the alumina-rich glazes gradually transform into plagioclase with prolonged soaking time. In glazes with low contents of alumina, alkalis and alkaline earths, wollastonite, pseudowollastonite and diopside were also found after a soaking time of 24 h. However, higher contents of alkalis and alkaline earths promoted the formation of plagioclase.

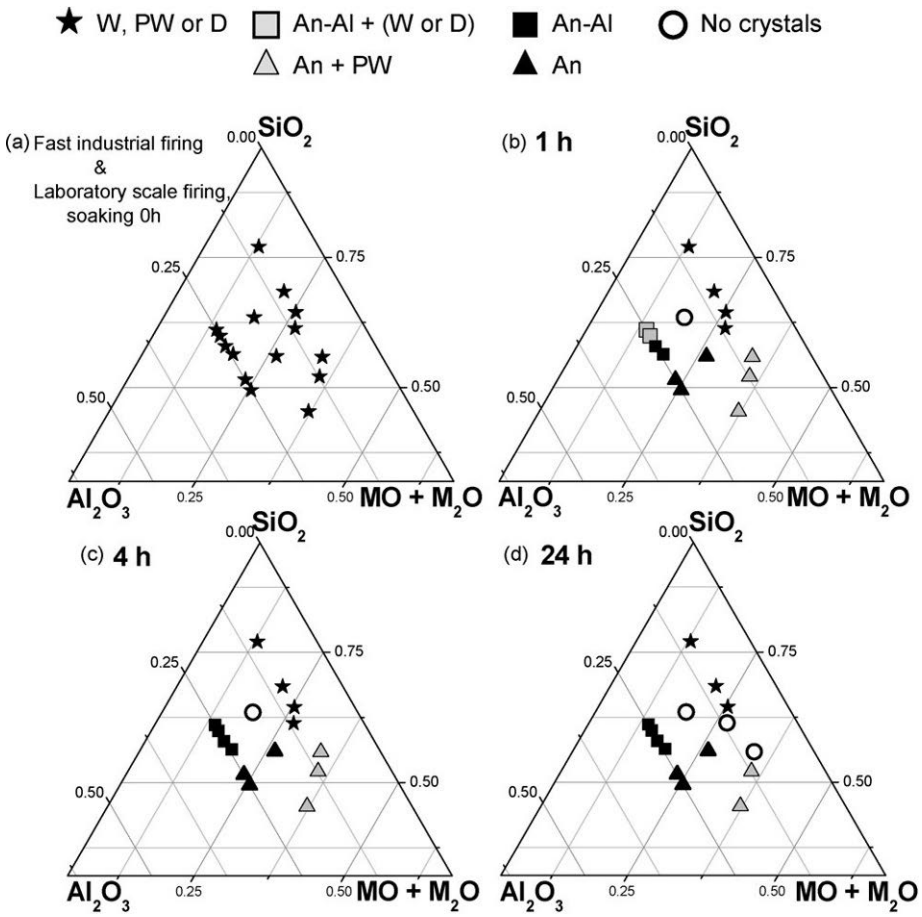

Fig 17. Glaze compositions (wt%) and crystalline phases in the glazes after different firing schedules according to XRD and SEM/EDXA. (a) Industrial fast-firing and laboratory-scale firing including no soaking. Laboratory scale firing soaking (b) 1h, (c) 4h, and (d) 24h. M_2O+MO = Na_2O+K_2O+MgO+CaO. W = wollastonite; PW = pseudowollastonite; D = diopside; An-Al = anorthite–albite. The experimental compositions are from Series II (Publication II).

4.2.2. Influence of soaking time on surface roughness

The size and amount of the crystals in the glazes, and thus the surface topography, varied with the glaze composition and soaking time. The surface roughness was measured with white light confocal microscopy. The highest roughness values were measured for the glazes with unmelted raw materials in the industrial fast-firing.

Anorthite formation also increased surface roughness. The glazes were classified into three groups according to the influence of soaking time on surface roughness.

A. Glazes with diopside, wollastonite or pseudowollastonite as main crystalline phase for all soaking times
B. Glazes with diopside, wollastonite or pseudowollastonite and some plagioclase in fast-firing and transformed into only plagioclase with prolonged soaking time.
C. Glazes with mainly diopside, wollastonite or pseudowollastonite after fast-firing, exhibited a continuous growth, mostly of anorthite, with prolonged soaking time.

The results are summarized in the ternary diagram showing the compositional ranges of groups A, B and C and the graph showing the trends in surface roughness as functions of soaking time (Fig. 18). In group A, the glazes showed sufficient surface crystallization for matte appearance also when no soaking time was used. However, during prolonged soaking times, the crystals partly or completely melted and the surface became smoother. In group B, the crystals had dissolved after a soaking time of 1 h but the formation and growth of plagioclase crystals led to an increased surface roughness with increased soaking time. In group C, the glazes showed continuous growth of crystals with increased soaking times.

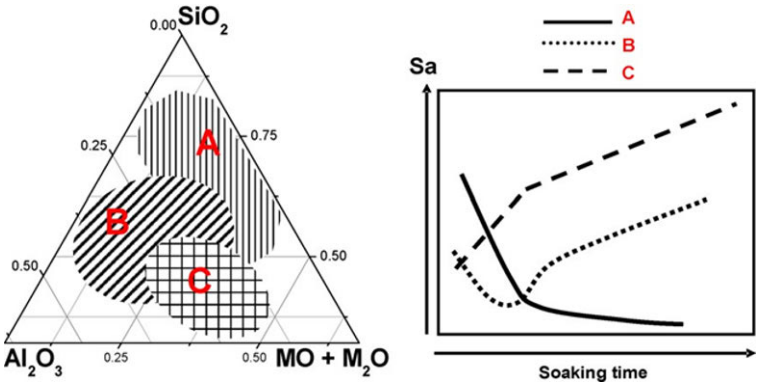

Fig 18. Phase diagram showing the trends in microstructure for different compositions (left). Trends in surface roughness as a function of soaking time for the different compositional areas (right). The groups A, B and C according to the classification in the text (Publication II).

4.3 Influence of wollastonite and dolomite on properties of raw glazes

In Publication I, the results showed that an introduction of dolomite and wollastonite in the recipe enhanced the melting behaviour of the glaze at roughly 1200 °C. However, when the amount of alkaline earths increased, a matte surface appearance was obtained.

A more detailed study on the influence of the alkaline earths (CaO, MgO), added as the raw materials wollastonite and dolomite, on the melting behaviour and surface properties of the fired tiles is reported in Publications III-IV. The glaze compositions included all the combinations of 10, 12, 14, 16 or 18 wt% CaO with 0, 1, 2, 3 or 4 wt% MgO (Series III). The melting behaviour and surface appearance were studied in Publications III-IV and the chemical durability of the glaze surfaces was reported in Publication IV.

4.3.1. Melting behaviour

Hot-stage microscopy was used to describe the melting behaviour of the glazes. The melting behaviour was determined from the sample shapes and the typical sintering curve points as illustrated in Fig. 12.

The measured temperatures describing the melting behaviour of nine glaze compositions are given in Table 8. The sintering point (SP) varied between 1110 and 1140 °C. The sintering point was assumed to correlate with particle-to-particle interactions and was not sensitive to the glaze composition. The softening point (Softening) varied between 1180 and 1230 °C. The highest temperature was measured for the glaze with the lowest content of alkaline earths. The softening point decreased with an increasing total content of the alkaline earths and showed a minimum value at 2 wt% MgO. The half-cone point (HCP) varied between 1200 and 1295 °C and the floating point between 1210 and 1350 °C. These temperatures decreased with increasing amounts of CaO and MgO. The characteristic points from the sintering curve T_1, T_2 and T_3 showed similar behaviour. The temperatures T_2 and T_3 decreased with increasing alkaline earth content. The lowest temperatures were again found with 2 wt% MgO.

Table 8. Temperatures (°C) of the measuring points (exp) described in Fig. 12 of experimental glazes with 10, 14 and 18 wt% CaO and 0, 2, 4 wt% MgO. Corresponding values (model) calculated with Eqs (4-10) are also shown. The temperature measurement accuracy ± 5 °C and the accuracy of the calculated values according to the Eqs. (4-10), pages 53-54.

CaO [wt%]		Temperature [°C]					
		at 0 wt % MgO		at 2 wt% MgO		at 4 wt% MgO	
		exp	model	exp	model	exp	model
10	SP	**1125**	1104	**1135**	1125	**1140**	1147
	Softening	**1230**	1212	**1205**	1198	**1210**	1225
	HCP	**1295**	1294	**1255**	1259	**1245**	1251
	FP	**1340**	1325	**1305**	1292	**1270**	1257
	T_1	**1170**	1146	**1145**	1155	**1150**	1164
	T_2	**1205**	1168	**1180**	1169	**1195**	1194
	T_3	**1240**	1214	**1205**	1195	**1215**	1217
14	SP	**1110**	1108	**1120**	1126	**1130**	1145
	Softening	**1205**	1183	**1185**	1173	**1205**	1205
	HCP	**1250**	1247	**1215**	1217	**1220**	1217
	FP	**1275**	1269	**1240**	1240	**1230**	1215
	T_1	**1155**	1142	**1140**	1152	**1145**	1162
	T_2	**1185**	1156	**1170**	1156	**1190**	1186
	T_3	**1215**	1177	**1185**	1164	**1210**	1194
18	SP	**1125**	1114	**1140**	1131	**1135**	1148
	Softening	**1195**	1177	**1180**	1170	**1190**	1201
	HCP	**1240**	1228	**1210**	1205	**1200**	1205
	FP	**1250**	1235	**1220**	1213	**1210**	1190
	T_1	**1150**	1140	**1140**	1150	**1145**	1160
	T_2	**1185**	1156	**1160**	1159	**1180**	1185
	T_3	**1210**	1172	**1175**	1163	**1190**	1192

The influence of the increased CaO content in the MgO-free glazes on the sintering curves is given in Fig. 19a. The sintering curves, i.e. the sample height as a function of the temperature, show that an increase of CaO and, thus wollastonite, effectively enhanced the fusibility, as also suggested by the equations in Publication I. The influence of increased content of MgO at a constant CaO content is shown in Fig. 19b. The fusibility was enhanced by the addition of up to 2 wt% MgO. This effect can partly depend on the decrease in the liquidus temperature of silicate melts by the addition of

up to 2.5 wt% MgO [172]. A higher content will increase the characteristic points in the HSM curve due to the crystallization of diopside.

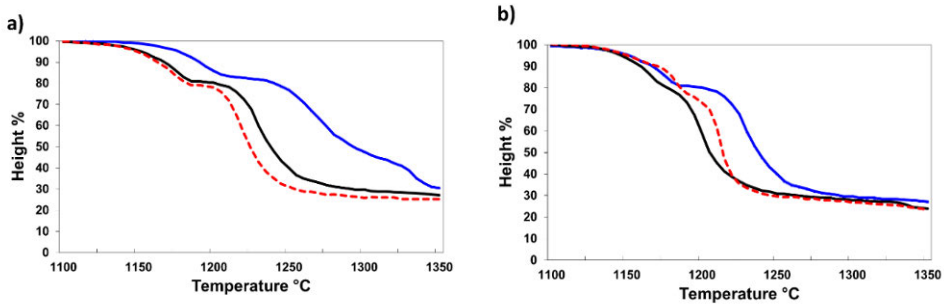

*Fig 19. Sample height as a function of temperature for (a) magnesia–free glazes with 10 wt% CaO (blue), 14 wt % CaO (red) and **18 wt% CaO** (black); (b) glazes with 14 wt% CaO and 0 wt% MgO (blue), 2 wt% MgO (red) and 4 wt% **MgO** (black). (Redrawn from Publication III).*

The corresponding temperatures calculated with Eqs (4-10) showed similar trends (Table 8). However, some of the raw materials used in these experiments were outside the range of the mathematical models. Corundum was used at 11-16 wt% (models 0-10 wt%). The highest content of wollastonite (up to 39 wt%) and dolomite (up to 16 wt%) was also outside the model ranges (wollastonite 0-30 wt%, dolomite 0-10 wt%). Most experimental temperatures are higher than the calculated temperatures likely due to the higher corundum content.

4.3.2. Phase composition and gloss

All compositions in Series III developed a matte surface appearance after fast-firing (50 min) at a peak temperature of 1215 °C in an industrial roller kiln for fast-fired tiles. The crystalline phases present in the glazes were specified from XRD and SEM/EDX analyses. Diopside was identified in the glazes with 2 wt% of MgO and the number of crystals increased with higher MgO contents. The diopside crystals were rather evenly spread in the bulk and also at the surface of the glaze. The crystals were columnar and quite small (1-5 μm), mainly present in clusters of several crystals. Residual quartz particles, surrounded by tiny diopside crystals suggest that the crystallization of diopside was not completed during the firing. All the other

crystalline phases in the glazes were residual raw materials. Wollastonite ($CaO{\cdot}SiO_2$) crystals were present in all glazes and wollastonite was the main crystalline phase in glazes with low MgO contents. Wollastonite crystals were evenly distributed in the glaze. The crystals were columnar and their size varied from 1 μm up to roughly 60 μm. In glazes with MgO < 3 wt%, the amount of wollastonite crystals increased with the wollastonite content in the recipe. However, the SEM images suggest that the crystals had partly dissolved in the melt during the firing. In glazes with higher dolomite contents and accordingly higher MgO contents, more wollastonite had dissolved into the melt and thus both the size and the amount of the wollastonite crystals in the fired glaze were much smaller. It should be observed that the corundum content in the recipes was rather high, 11-17 wt%, in the glazes. Thus, all glazes contained residual corundum after firing. Correspondingly, the amount of quartz, as a raw material, in the recipes was low, 0-17 wt%. Yet, some residual quartz particles were identified in the experimental glazes after the firing. In general, the glazes in this series did not have the fluxing capacity and time enough to dissolve all the corundum and quartz during the fast-firing process. On the other hand, as the fluxing capacity increased with an increasing amount of alkaline earths in the recipe, more corundum and quartz reacted and dissolved in the melt during the firing.

A few of the glazes were also fired in a long firing schedule (25 h) at the peak temperature of 1210 °C in an industrial tunnel kiln for sanitary ware. SEM images showing the difference in surface structure between the fast-firing and the traditional firing are given in Fig. 20. After the longer firing schedule, the glazes contained less residual raw materials because the longer firing time provided a better fusibility (Figs 20b and d). Although the glaze raw materials were assumed to proceed to a greater degree during the longer soaking time, the glazes also crystallized to a greater degree during the slow cooling in the traditional firing. This was seen as the extensive crystallization of diopside More and longer (40-60 μm) needle-shaped diopside crystals were observed in the glazes with more than 2 wt% MgO. Similarly, the amount and size of the wollastonite crystals increased in the traditional long firing.

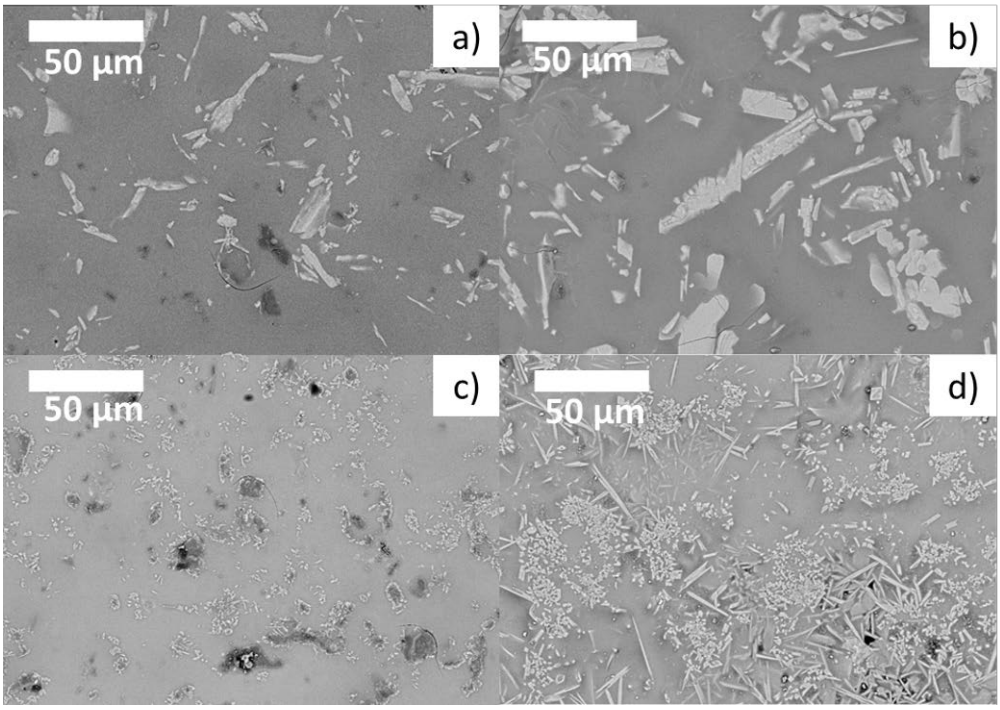

Fig 20. SEM images for (a) fast-fired and (b) traditionally fired glaze A18/0 containing 18 wt% CaO and 0 wt% MgO, and for (c) fast-fired and (d) traditionally fired glaze A14/4 containing 14 wt% CaO and 4 wt% MgO. The bar in the images corresponds to 20 µm. The main crystalline phases: (a) wollastonite, corundum and quartz, (b) wollastonite, (c) diopside, corundum and quartz, and (d) diopside (Publication III).

In fast-firing (50 min), the gloss values of the glazes varied between 20 and 75. Glazes with low contents of CaO and MgO had a low gloss value. SEM images and EDX analyses suggest that these glazes contained large shares of raw materials which had not reacted or dissolved during the firing. This indicates that the fluxing capacity of the glaze is not sufficient when the contents of wollastonite and dolomite, i.e. the calcium and magnesium oxide fluxes, are low in the recipe. With an increasing amount of these raw materials, the amount of amorphous phase, and accordingly the gloss increased. The most glossy glazes contained around 2-3 wt% MgO and about 14 wt% CaO. At higher content of these alkaline earths, increasing amounts of diopside and wollastonite were identified in the glazes. Simultaneously, the gloss of the glazes decreased.

In traditional long firing (25 h), the gloss values showed a different trend than in fast-firing. The highest gloss values were found for glazes with low contents of CaO and MgO. Most of the raw materials had dissolved during the firing and the contents of CaO and MgO were too low to promote crystallization. With increasing contents of MgO and CaO, a more or less homogenous melt with high contents of alkaline earths was formed and lead to extensive crystallisation during the slow cooling in the traditional firing. The very high amount of crystalline phases was shown as a low gloss value.

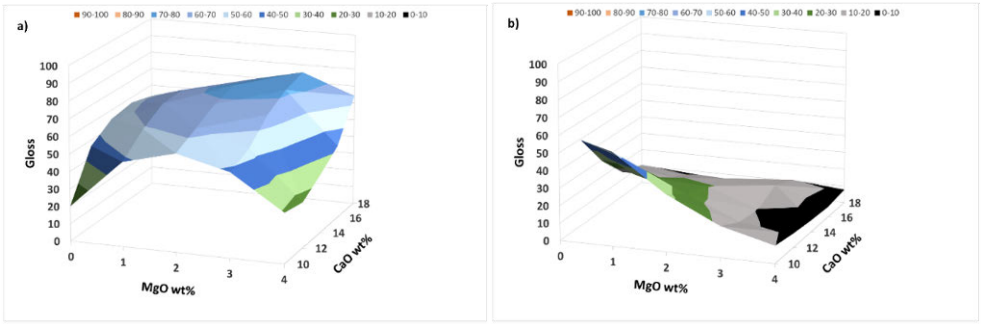

Fig. 21. Gloss values of experimental glazes in (a) fast-firing and (b) traditional firing (Publication III).

4.3.3. Chemical durability

Glaze surfaces are used in everyday environments and must withstand various chemical agents. However, surface pitting and degradation in service diminishes cleanability [94]. Surface degradation might also lead to the opening of closed porosity at the glaze surface, thus leading to micro-scale holes which are often hard to clean by conventional cleaning techniques. The chemical durability of the glazes in the series III fired in an industrial kiln for fast-firing of tiles is reported in detail in Publication IV.

The chemical durability of the glazes was first determined using the ISO 10545-13 standard method. The glazes were exposed to aqueous solutions of hydrochloric acid (original pH = 0.3, exposure time = 4 days), citric acid (original pH = 1.5, exposure time = 24 hours) and potassium hydroxide (original pH = 13.4, exposure time = 4 days). After the specified exposure time, the solution was removed and the surfaces were visually classified. The chemical durability against the hydrochloric acid solution

was poor for most of the glazes. Only a few glazes in each series showed no visual damage to the surface and thus they achieved the best classification. In contrasts, the glazes with high contents of both CaO (16-18 wt%) and MgO (3-4 wt%) were severely damaged. The damage could be visually seen already before the classification procedure. The durability against the citric acid solution was clearly better. Most glazes reached the best classification. The chemical resistance against the potassium hydroxide solution was also very good. The standard method used to measure the durability only studies the visual appearance after the exposures but does not give any detailed information on the extent or mechanism of the surface damage. Thus, it may fail to give indications of minor attacks which affect e.g. attachment of soils on the surfaces or long-term chemical durability of the surfaces. In this work, more detailed information of the surface conditions after the exposures was obtained from analyses with SEM and XRD.

The differences in the morphology and composition of the glazes induced by the aqueous solutions were studied with SEM/EDX analyses. The presence of wollastonite crystals at the glaze surface was found to be the main reason for the observed corrosion attacks by the acidic solutions (Fig. 22). These crystals were severely attacked by the hydrochloric acid solution and partly also by the citric acid solution. The corrosion of wollastonite started at crystals in the glaze top surface. The SEM images suggest that the interfacial thin amorphous layer was first attacked after which the surface of the crystal was exposed to the acid attack. The interfacial amorphous layer with low silica and alumina content compared to the bulk amorphous phase was assumed to form when the wollastonite crystals gradually dissolved in the melt [95]. The SEM images also suggest that the corrosion had started around and along grain boundaries of the polycrystalline wollastonite grains. Based on the images, the corrosion of the wollastonite crystals is suggested to proceed by the gradual dissolution of Ca ions through an ion exchange reaction with protons from the acidic solution leaving a silica-rich residual structure.

Wollastonite crystals showed indications of corrosion in the top layer of the surface in all the experimental glazes after the exposure to the acidic solutions. Tiny columnar crystals have been reported to corrode in acidic to slightly alkaline solutions while larger crystals seen in glazes after longer firing schedules corroded only in acidic solutions [95, 96]. Wollastonite crystals in magnesia-free compositions had the poorest chemical durability [96].

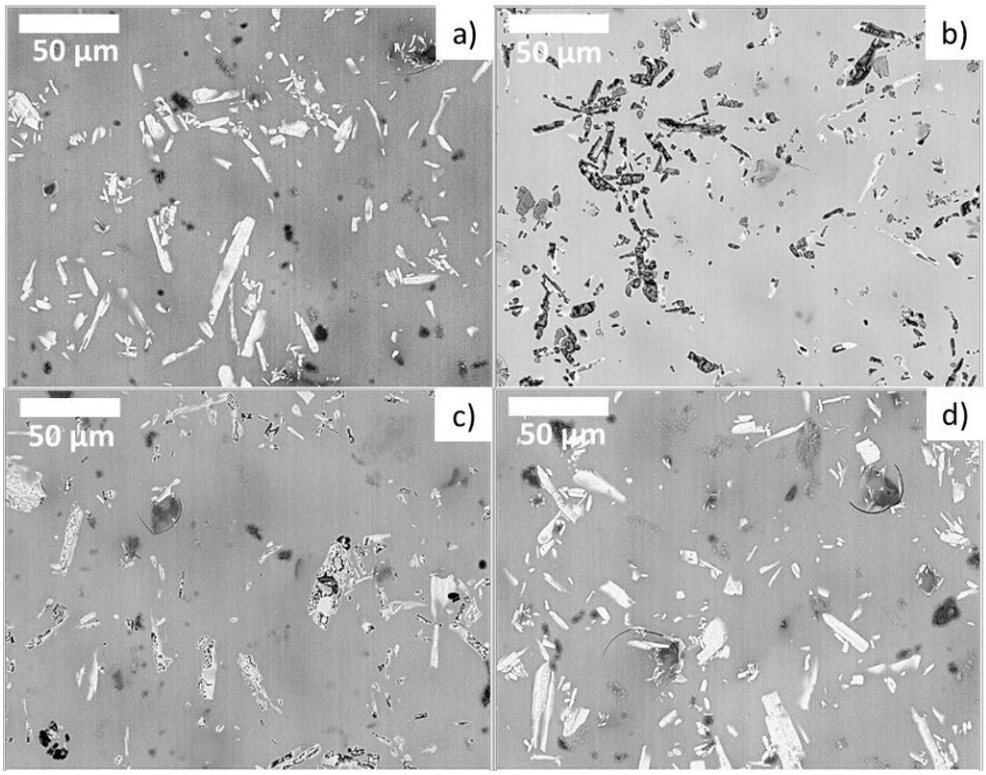

Fig. 22. SEM images of glaze A18/0 (see Appendix III). a) before exposure, b) after exposure to 3 % hydrochloric acid, 4 days. c) after exposure to citric acid (100g/l), 24 hours and d) after exposure to potassium hydroxide (30 g/l), 4 days (Publication IV).

The ions released from the surface into the test solutions were analysed with ICP-AES. Mainly calcium species had leached out from the glazes in the acidic solutions. The result also supports the findings suggested by the SEM/EDX analyses suggesting that calcium had leached out from wollastonite crystals. Similar incongruent dissolution of wollastonite, i.e. faster leaching of calcium, leaving a silica layer on the surface has widely been reported [95, 96, 103, 104, 107, 108]. The low concentrations of Al, Si and Na analyzed in the solution suggest a minor dissolution of the amorphous phase around the wollastonite crystals as also seen in the SEM images.

The diopside crystals that formed during the fast-firing showed good durability in all the solutions. Also, this is in accordance with the previously reported results [96]. However, in hydrochloric acid, some surface pitting of the diopside-containing glazes

was noticed in the SEM images, but this was assumed to depend on corrosion of small wollastonite crystals present at the surface.

The glazes with high contents of CaO and MgO showed also corrosion of the amorphous phase in acidic solutions (Fig. 23). After the hydrochloric acid and citric acid exposures, the surface layer was severely destroyed. Large parts of the surface had been peeled off, leaving cracked remnants consisting mainly of silica. However, some diopside crystals could be identified in the partly peeled surface, thus verifying their high chemical durability. According to the SEM images, the amorphous phase showed the heaviest attack, most likely due to the ion-exchange of H^+-ions for the modifying ions in the structure of the amorphous layer.

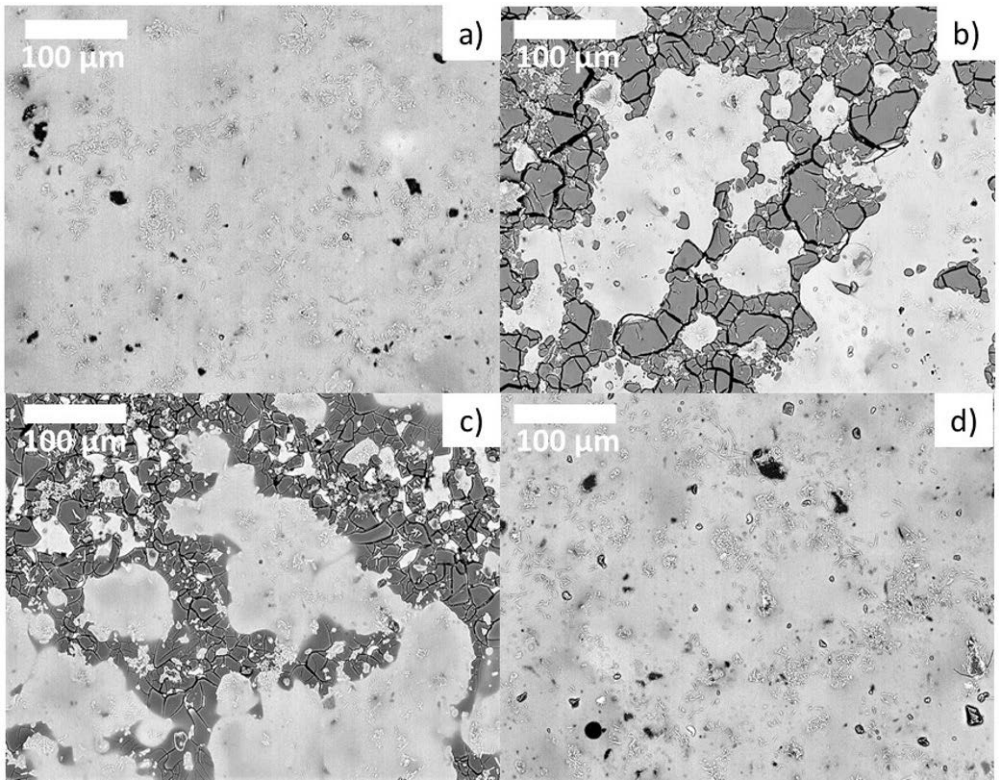

Fig. 23. SEM images of glaze A16/4 (see Appendix III). a) glaze before exposure, b) after exposure to 3 % hydrochloric acid, 4 days. c) after exposure to citric acid (100g/l), 24 hours and d) after exposure to potassium hydroxide (30 g/l), 4 days (from Publication IV, a and b).

Similar dissolution of the alkali and alkaline earth ions leading to a Si-rich surface layer in acidic solutions has been reported for silicate glasses [173]. The most severe attack, seen as the total destruction of the amorphous phase in the glaze after the hydrochloric acid exposure, was seen for the glazes with the highest content of CaO and MgO (Fig. 24). Major corrosion led to almost total destruction of the amorphous phase in the glaze layer and seen as a thick, cracked, Si-rich remnant. According to the SEM/EDX analyses, some diopside and corundum crystals were still left embedded in the Si-rich layer. After the exposure (24h) to citric acid, only the outermost surface showed clear signs of corrosion of the amorphous phase. The milder corrosion can partly be explained by the shorter exposure time, 24 h in citric acid vs. 4 days in hydrochloric acid.

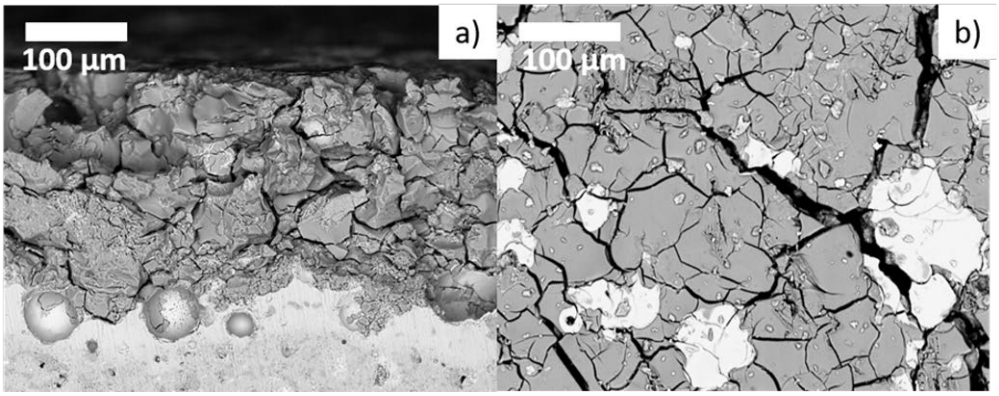

Fig. 24. SEM images of glaze A18/4 after 4 days in 3 % hydrochloric acid: a) cross-section, b) surface.

In the alkaline potassium hydroxide solution, no evidence of corrosion of the glaze surfaces was found in the SEM analyses. However, the ICP-AES analysis of the solutions suggested that a small content of Si, Ca, Na and K species and had leached out, thus indicating minor corrosion of the amorphous phase. In contrast, no traces of Mg species were detected, most likely because, in calcium-rich compositions, dolomite had primarily reacted with quartz to form diopside crystals with a good durability.

The impact of hydrochloric acid strength on the durability as a function of time was studied by exposing the glazes to 3 vol% (pH= 0.3) and 0.1 vol% (pH = 1.4) for 1,3, 7 and 28 days. Wollastonite crystals showed rapid incongruent dissolution of

calcium resulting in a silica-rich remnant at the surface within one day. At pro-longed exposure, the wollastonite crystals gradually dissolved. The dissolution rate depended on the pH of the solution, i.e. the higher the pH the more rapid the dissolution.
The different approaches used to identify corrosion suggested that the ISO standard method is suitable for qualitative estimation of corrosion. As the matte glaze surfaces have heterogeneous composition and different degrees of topographic variations, no reliable indications of minor corrosion could be retrieved from phase analyses using XRD. In contrast, SEM/EDX analyses of the surfaces before and after the exposures to the solutions as well as the ICP-AES analyses of the solutions after the attacks gave quantitative information of the corrosion mechanisms and rates. The minor corrosion detected using e.g. SEM could not be identified by the standard method. The initial minor corrosion can lead to a more severe deterioration of the glaze surface during use in every-day environments. In addition, minor surface pitting can also affect the soil attachment and cleanability.

The results showed that matte glazes with wollastonite crystals at the top surface had poor resistance against acidic aqueous solutions and thus should be avoided. However, the excellent durability of the diopside crystals gives a possibility to further study the diopside formation and its use in matte glazes.

4.4. Effect of an additional functional layer on ceramic glazes

Increasing demands for improved surface properties, such as easier cleanability, have led to the development of functional coatings on traditional glaze surfaces. However, the functionality, as well as the mechanical and chemical durability of these coatings are not yet fully understood or controlled. In this study, reference white sanitary ware glazes were coated with commercial fluoropolymers and new hybrid sol-gel functional coatings, including a TiO_2-based coating. Then, the cleanability and resistance to mechanical and chemical wear of the coated surfaces were measured. The influence of adding a smooth, transparent glaze layer on the top of the reference glaze was also investigated. More detailed information is found in Publications V-VI.

4.4.1. Surface properties

Contact angles of the experimental surfaces used in Publication VI are shown in Figure 25. The reference glaze is rather hydrophilic in nature; its water contact angle varied between 30 and 40°. The fluoropolymer coatings clearly increased the contact angle values to higher than 90°, thus giving the surfaces hydrophobic characteristics. The contact angle of the sol-gel titania coating was rather similar to the uncoated glaze

surface. However, the contact angle decreased to below 20° after the exposure to ultraviolet light. Thus, this coating provided the surfaces with hydrophilic properties and likely also provided active self-cleaning properties. The smoother double glazed surfaces had a slightly lower value than the reference surface and the titania coated surface.

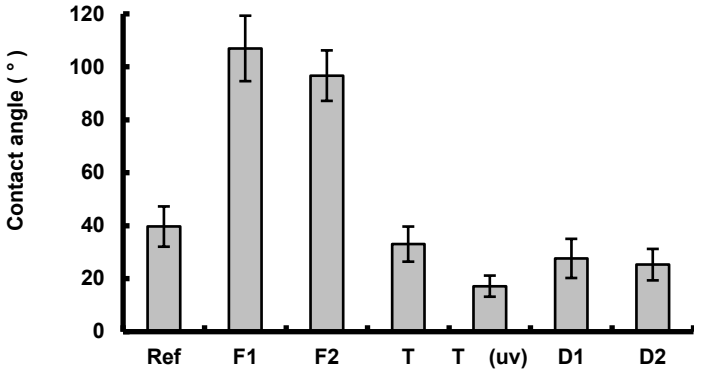

Fig. 25. Average contact angle and standard deviation of the experimental surfaces. F1 and F2 fluoropolymer coatings, T titania coating, T (uv) titania coating after UV-light exposure, D1 and D2 double glazings [122].

The average roughness values (Sa) of the experimental surfaces in Publication VI varied between 0.012 and 0.028 μm (Fig. 26). The double glazing (D1 and D2) clearly decreased the surface roughness; similar values were measured for both single (D1) and double (D2) fired tiles. Thus, the transparent glaze layer covered the zirconium silicate crystals penetrating the first opaque glaze. The more heterogeneous reference glaze surface and the fluoropolymer F1 surfaces gave larger variations in the measured values as indicated by the standard deviation bars in Fig. 26. The coatings had only a slight effect on the roughness. Fluoropolymer coating F1 showed a small increase in the average roughness. This was assumed to depend on small bubbles in the surface, cf. the confocal microscopy (COM) image in Fig. 27. The other two functional coatings (F2 and T) were assumed to cover some small irregularities on the ceramic glaze and thus lead to somewhat smoother surfaces.

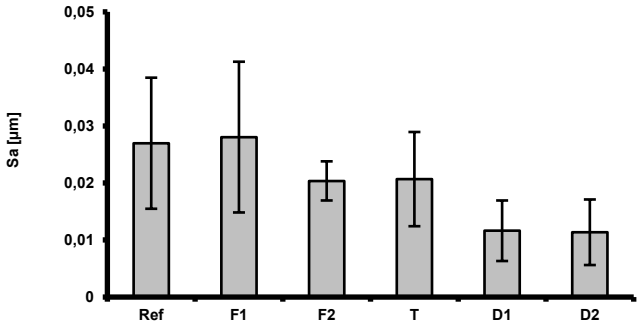

Fig. 26. Surface roughness (Sa) of experimental glazes. F1 and F2 fluoropolymer coatings, T titania coating, D1 and D2 double glazings [122].

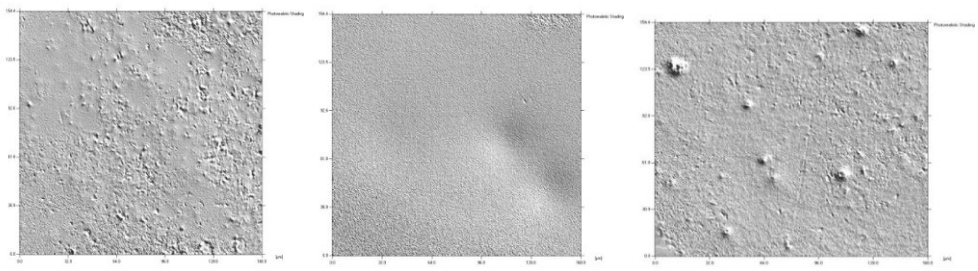

Fig. 27. COM images of experimental surfaces: reference, double-glazed D1 and fluoropolymer F1 (left to right) [122].

Similar results were observed for the surfaces used in Publication V. No changes in the surface roughness of coated samples compared to the reference commercial glaze (R_a=0.059 µm) could be observed, thus indicating that the coatings were very thin. The only exception was the experimental silane-based coating PRO B which gave a smoother surface (R_a=0.039 µm). The coating PRO B covered the whole glaze surface including the zirconium silicate. For the other coatings, some of the zirconium silicate crystals were still uncovered after the coating process. The surface roughness was significantly lower for the double glazed surface D2 (Ra = 0.026 um).

In Publication V, the effect of the coatings on both the hydrophobic and the oleophobic properties was assessed by contact angle measurements of water and oleic acid on the surface as a function of time for the reference glaze and the reference glazes

coated with two experimental silane coatings (PRO A and PRO B), two commercial fluoropolymer coatings (F1 and F2) and double glazing (D2) (Fig. 28). For the reference surface, the resistance against oil and greasy contaminants was weak as is shown by the contact angle measurements.

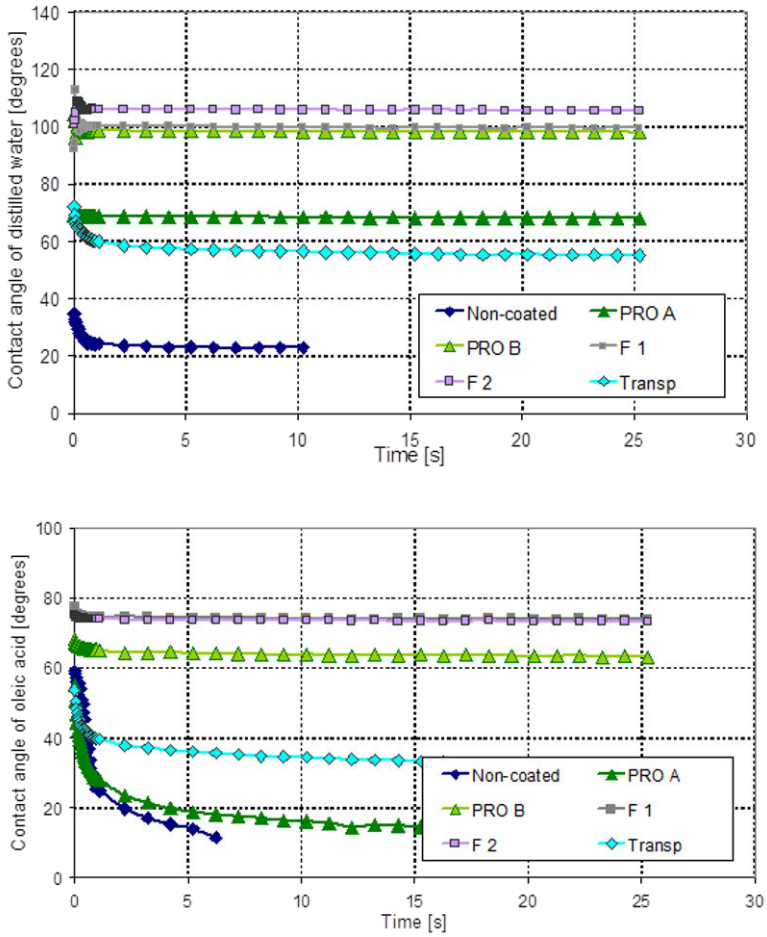

Fig.28. Contact angles of distilled water (a) and oleic acid (b) on uncoated and coated glaze surfaces. PRO A and PRO B experimental silane-based coatings, F1 and F2 commercial fluoropolymer coatings, Transp = D2 double glazing (Publication V).

with oleic acid. The double glazed sample (D2) showed higher hydro- and oleophobic properties. This is likely due to decreased surface roughness. It was also observed that the surface properties depended on the chemical composition of the coating. The

contact angles are reported to be sensitive to surface roughness and chemical heterogeneities [174]. In general, coatings containing high concentrations of functionally modified polymers are hydrophobic. Increase of ceramic components in coatings usually leads to a decrease in the hydrophobicity. Of the two experimental thin coatings, PRO B with further modified polymeric content showed a high hydrophobicity and oleophobicity. The more traditional ceramic nanocomposite coating, PRO A, increased the hydrophobicity but to a lower degree than the other experimental coatings. However, the oleophobicity of PRO A was equal to the reference glaze. The hydrophobicity and oleophobicity of the commercial fluoropolymer coatings used in this study were very good which is typical for coatings based on fluoro-based compounds.

4.4.2. Soiling and cleanability

In Publication V, the anti-soiling properties and cleanability of the surfaces were studied by soil-spot-test developed by VTT and the extent of soil on the surfaces were qualitatively analysed with FTIR mapping method (Fig. 29). The uncoated reference glaze was sensible to oily stains and impurity contamination. Oleic acid drops spread on the surface and formed soiled areas. Wipe cleaning with a dry micro-fibre cloth had no significant cleaning effect of the surface. The anti-soiling properties of the coating with a high content of ceramic components, PRO A, was also poor. All other coatings selected to this study improved the anti-soiling properties of the glaze surface. Oleic acid formed solid spots on the surfaces without any indications of spreading or penetration. The best result was obtained with the organically modified coating PRO B. The FTIR analysis showed that only traces of the oleic acid impurities could be detected after the cleaning with a dry micro-fibre cloth. The anti-soiling properties of the fluoropolymer coatings were clearly better than the soiling properties of the uncoated glaze although a significant amount of oleic acid remained on the surface after the cleaning. The anti-soiling properties of the smooth, double glazed tile were surprisingly equal to the reference glaze. Although the surface roughness was significantly lower, the soil-spot-test showed no improvement in the cleaning properties. The oily nature probably makes the soil sensitive to the oleophobic properties of the surface thus giving no differences in this test.

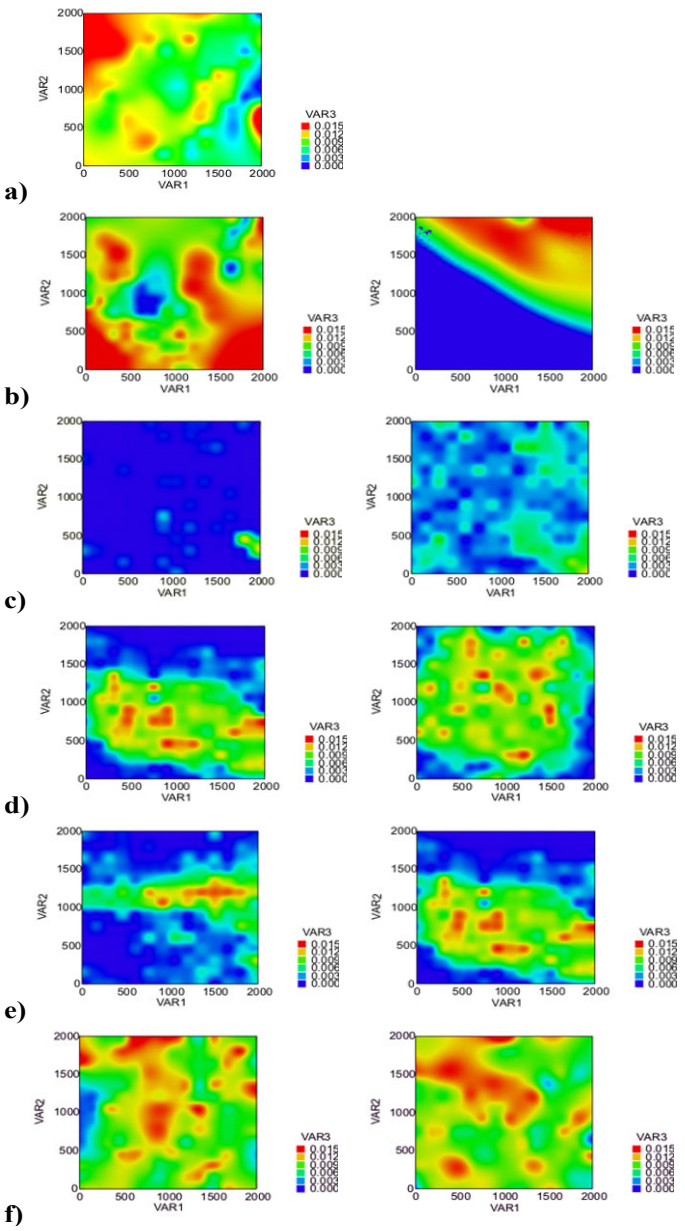

Fig 29. FTIR charts showing oleic acid residues on non-coated and coated glaze surfaces after wiping the grease-covered surfaces with a dry microfiber cloth. The surfaces prior to the wet abrasion test are shown on the left side and the abraded surfaces (700 cycles) on the right side. The light shades reveal that hydrocarbon-based soil is still present on the surface, while the dark (blue) areas are soil-free. a) Ref glaze, b) PRO A, c) PRO B, d) F3, e) F1, f) D2 (Publication V).

In another method used in Publication VI, the cleanability was colourmetrically estimated from the dark colour of the sebum-soot soil mixture for the fluoropolymer, titania coated and double glazed surfaces. The amount of the soil on the surfaces was measured both after the soiling and after the cleaning. The calculated E values (Eqs. 1-3) were used to estimate the amount of soil attached to the surface after the soiling and further to estimate the soil removed and the soil residue after the cleaning step (Fig. 30). The soil attached equally on all surfaces except on the fluoropolymer F1. This fluoropolymer coating showed expected hydrophobic easy-to-clean properties; the coating prevented the attachment of soil on the surface. The other fluoropolymer coating F2 was not found to prevent the attachment of the model soil used. The reason for this behaviour could not be determined in this study. The titania coating clearly increased the cleanability of the surface after exposure to ultraviolet light. The same amount of soil was attached to the surface as for the reference glaze, but almost 80 % of the soil was removed in the cleaning process. The results clearly showed the differences in the cleanability behaviour between an easy-to-clean fluoropolymer coating and a self-cleaning photocatalytic titania coating. Cleanability of the double glazed surfaces was surprisingly low. The smoother double glazed surfaces were expected to increase the cleanability compared to the rougher reference surface. The results correlated with the results in Publication V, in which oil-based contaminants were found to easily attach on double glazed smooth surfaces.

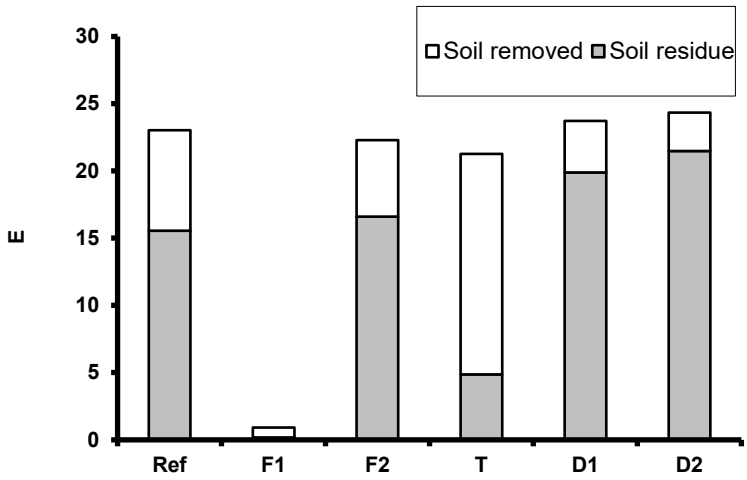

Fig. 30. Cleanability of experimental glazes. The amount of soil on the glazes after soiling (the whole column), soil removed and soil residue [122].

4.4.3. Chemical and mechanical durability and their effect on cleanability

The chemical resistance of all coatings was good in acidic and neutral solutions. No changes in the hydrophobicity or the visual appearance could be detected. Only the fluoropolymer coatings were corroded at pH > 9. After the attack, the surface energy values were similar to the values of the reference glaze. At pH 10, the fluoropolymer coatings were destroyed after two hours and at pH 13 only 30 seconds were needed to destroy the coatings. The poor chemical behaviour of the fluoropolymer coatings in alkaline solutions will put new demands on cleaning instructions for fluoropolymer coated ceramics.

In Publication V, the abrasion resistance of the coatings was evaluated from changes observed in the surface energy values when the coatings were subjected to a wet abrasion test. After 700 abrasion cycles, the anti-soiling properties of the coatings were decreased as shown by the soil-spot-test and the FTIR mapping method (Fig 29). The SEM analyses showed that the coatings were damaged by the abrasion test and were partly peeled off thus revealing the uncoated glaze surfaces. Coatings with a higher content of organic components in the matrix lead to softer surface structures, which were less resistant to abrasion. The results indicated that the polymeric content of the coatings tends to wear. The surface energy values of the coating PRO A remained rather unchanged after 700 abrasion cycles, which is most likely due to the ceramic constituents in the coating. However, signs of wear also in this coating could be seen when the abrasion procedure was continued up to 1400 cycles. Surface properties of the silane-based coating PRO B and fluoropolymer coating F3 showed changes already after 700 abrasion cycles. After doubling the abrasion cycles, the surface energy values of these coatings nearly increased to the values of the non-coated reference glaze. The other fluoropolymer coating F1 was the only one that did not show any significant changes in surface energy after abrasion. Any explanation for the excellent mechanical properties of this coating could not be deduced from the surface analysis done in this work. Detailed compositional information about this commercial product was not available.

In Publication VI, the mechanical wear of the reference glaze and surfaces coated with fluoropolymer F1 and F2, titania T and double glazings D1 and D2 was tested with a microfiber cloth (10 000, 15 000, 20 000 rev.) and steel wool (50, 100, 150 rev.) in a laboratory-scale testing apparatus. The contact angle of the fluoropolymer surface gradually decreased with an increased number of revolutions with both the microfiber cloth and the steel wool. The steel wool was so hard that it even scratched the underlying glaze surface. However, the contact angle values of the fluoropolymer

surfaces after both mechanical tests were still high enough to give some degree of hydrophobicity to the surfaces. Thus, it was assumed that some remnants of the coatings were left on the surface. The sol-gel derived ceramic titania coating was also damaged by the steel wool. No hydrophilic behaviour could be found for the surface abraded with steel wool after the exposure to UV-light, thus indicating that the coating had been destroyed. The microfiber cloth, however, did not affect the contact angle values of the titania coating. Only minor changes in the contact angle were found for the uncoated glaze. The observed small decreases in the contact angle values were assumed to be partly due to the polishing of the surfaces.

Images of the soiled experimental surfaces coatings (Publication VI) before and after the mechanical (150 x steel wool, 20 000 x microfiber) and chemical tests (7 days at pH 9.1) are shown in Fig. 31. The images show the differences in the soil attachment on the surfaces. All additional surface coatings decreased soil attachment. However, the mechanical and chemical wear increased the soil attachment on all surfaces as given by the increase of the darkness in the colour of the surfaces caused by the carbon in the model soil.

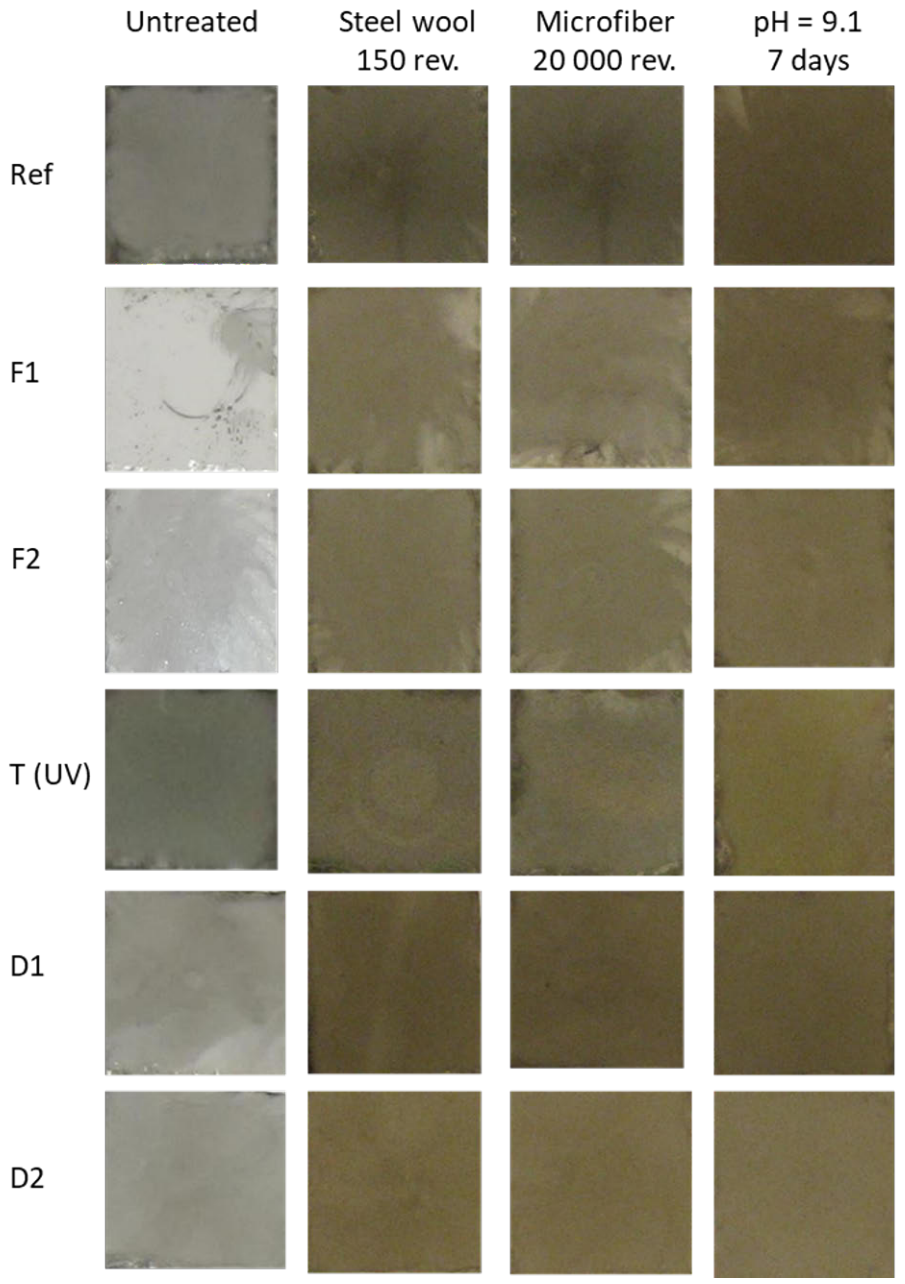

Fig. 31. Camera images of experimental surfaces (2.5 x 2.5 cm) after spin coating with model soil consisting of sebum, ethanol and carbon. Ref = no coating, F1 and F2 fluoropolymer film, T = TiO_2 film, D1 and D2 double glazed surfaces [168].

The cleanability was colourimetrically estimated from the amount of the sebum-soot soil mixture on the surfaces (Fig. 32). Nearly the same amount of soil was attached to the surfaces after the mechanical and chemical treatments. Surprisingly, the uncoated and the fluoropolymer F2 surface showed an increased cleanability after the mechanical and chemical wears. This was assumed to depend on the smoothening of the surface and elimination of some surface heterogeneities. The good cleanability of the fluoropolymer coating F1, which was partially or totally destroyed by the durability tests and the cleanability was back on the same level as the uncoated reference surface. For the double glazed surfaces, no large changes were observed after the durability tests. The decreased surface roughness was not found to decrease the attachment of oil-based contaminants to the surface. The experimental titania coating showed a good long-term performance when exposed to UV light. The hydrophilic and photocatalytic properties of the coating were not destroyed by the microfiber polishing or by the chemical attack. The harsh abrasion with steel wool did not totally destroy the surface, suggesting that the surface would retain its functionality if the abrasion is not very harsh. This coating showed potential as a durable easy-to-clean coating. The results also indicated that the choice of any additional functional coating for a given application should be based on a good understanding of the existing chemical and mechanical conditions present in the application.

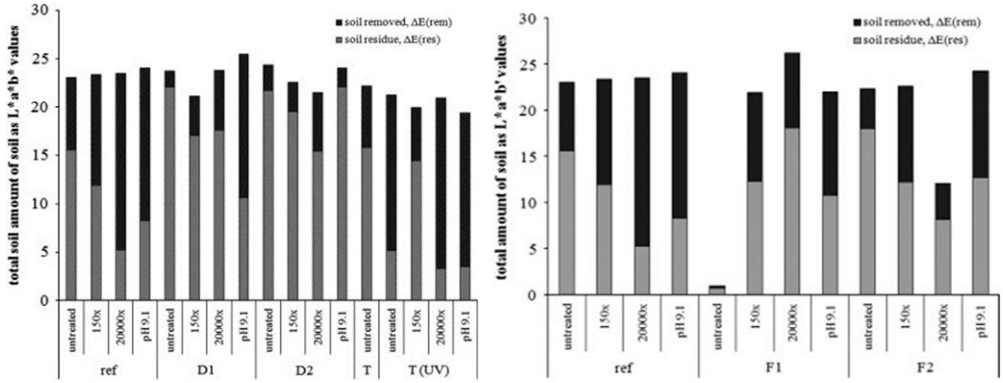

Fig. 32. Cleanability of experimental glazes (untreated, steel wool 150 rev., microfiber cloth 20 000 rev., pH = 9.1, 7 days). The amount of soil on the glazes after soiling (the whole column), soil removed and soil residue (Publication VI)

5. Conclusions

The melting behaviour of raw glazes was described by several characteristic temperature points determined by hot-stage microscopy. The relationship between each temperature point and the composition of the glaze was mathematically modelled. These relationships are valuable tools when designing new glaze compositions for changed requirements in the firing cycle or when comparing the melting behaviour of different raw glazes. Also, the calculated trends can directly be adapted to practical glaze firing processes. Although the relationships were developed for certain raw materials, the trends are likely to be similar also when using other raw materials with slightly different compositions.

The models suggested that zinc oxide, dolomite and wollastonite had the greatest effects on the melting behaviour. Zinc oxide was effective in decreasing all the temperatures from the onset of sintering to the fusion of the raw glaze. Both dolomite and wollastonite decreased the temperatures characterizing the melting behaviour, with an increasing effect starting from the sintering range. By suitably adjusting the raw material composition the desired melting behaviour can be achieved. However, the final surface morphology not given by the equations should also be taken into account when designing the glaze composition.

The gloss of the glazes fired in an industrial fast-firing kiln was modelled as a function of the glaze composition. The gloss clearly correlated with the melting behaviour of the glaze compositions at higher temperatures as suggested by the mathematical models for the melting behaviour. This implies that the hot-stage microscopy can be utilized to predict not only the melting behaviour but also the gloss value of fast-fired raw glazes.

The phase composition and topography of raw glazes depended on the firing cycle. For short firing, e.g. fast-firing typical for floor tiles, the surface morphology depended on initial raw material reactions and melt formation. The most glossy and smooth glazes were obtained for compositions with high feldspar contents. Diopside, wollastonite and pseudowollastonite crystals were formed in glazes rich in wollastonite and dolomite during the initial raw material reactions at temperatures close to the peak firing temperature of floor tiles.

At longer firing cycles typical e.g. for sanitary ware, the surface morphology was controlled by the total oxide composition and equilibrium phase conditions at peak firing temperature. In corundum-free compositions, glossy glazes were formed through gradual melting of the initially formed crystals. For compositions which contained corundum, longer soaking times lead to plagioclase formation. The

feldspar-rich compositions crystallized into plagioclase with prolonged soaking time. Thus, a high corundum content was assumed to aid crystallization of plagioclase.

The impact of wollastonite and dolomite on glaze properties was studied in more detail to gain detailed information about their influence on the fusibility and final surface appearance of raw glazes. Both the total content and the ratio between wollastonite and dolomite were found to be the key controlling factors for the melting behaviour of raw glazes fired to around 1200 °C. The fusibility was increased with wollastonite, and thus, the CaO content in the glaze. Also, MgO introduced as dolomite increased the fusibility of the glazes. In fast-firing, the most pronounced effect on fusibility was found at around 2 wt% MgO. The main crystalline phases in the glazes were wollastonite and diopside. Wollastonite was the main crystalline phase in glazes with low dolomite contents. Diopside crystals were observed in glazes with more than 2 wt% MgO. In fast-firing, the glazes with the lowest contents of the alkaline earths were not totally fused and showed high contents of residual quartz and corundum. The formation of a more or less homogenous melt with a high content of alkaline earths gave extensive crystallisation during the slow cooling in the traditional firing. The results can be applied to adjust the wollastonite and dolomite contents in raw glazes to ensure a proper fusibility and a desired surface structure.

The chemical durability of the fast-fired glazes containing wollastonite crystals at the surface was poor in acidic solutions. The wollastonite crystals at the surface were rapidly attacked and reacted through incongruent dissolution of calcium, thus leaving a silica-rich remnant at the surface. The results showed that marked corrosion was detected already within a one-day exposure in acidic solutions. As the corrosion proceeded, occasionally the whole crystal was dissolved. The dissolution of wollastonite was found to be dependent on the pH of the solution. The glazes with high contents of CaO and MgO showed corrosion of the amorphous phase in acidic solutions. Parts of the surface layer was peeled off, leaving a cracked, mainly Si-containing surface. For the glazes with the highest alkaline earth contents, the whole glaze layer was destroyed. In the alkaline potassium hydroxide solution, no evidence of corrosion of the glaze surfaces was found in the SEM analyses. However, the ICP-AES analyses of the solutions suggested some dissolution of Si species and modifying ions, thus indicating minor corrosion of the amorphous phase. The diopside crystals which formed during the fast-firing showed excellent durability in all acidic to alkaline the solutions. However, for the compositions with high contents of alkaline earths, the amorphous phase was heavily attacked in the acidic solutions and the surface was totally destroyed. Although the overall acid durability was low, the excellent properties

of the diopside crystals are encouraging for further studies of manufacture of diopside-based matte raw glazes, especially in modified composition range with higher silica contents to ensure better durability.

The anti-soiling properties and cleanability of glazed surfaces can be improved by functional thin coatings. The chemical composition of the coating affects both its soil-repelling, chemical and mechanical properties. Sol-gel based coatings with a high content of polymers increased the hydrophobicity and oleophobicity of the surface but decreased its abrasion resistance. The abrasion resistance was improved by increasing the ceramic components in the coating matrix. In general, the fluoropolymer coatings effectively decreased the surface energy, and thus decreased also the soiling of the surfaces. However, not all fluoropolymer coatings were effective in improving the cleanability. Double glazing with a transparent glaze decreased the surface roughness but did not affect the attachment of oil-based contaminants or the cleanability of the surface.

The influence of mechanical abrasion and chemical wear on the surface properties was compared for different additional coatings on a glazed surface. Chemical wear by alkaline solutions (pH < 9) and mechanical abrasion by steel wool was found to severely damage the fluoropolymer coatings. Microfiber cloth abrasion had only a slight effect on the surface properties of the fluoropolymers. Both the sol-gel derived ceramic titania coating and double glazed surfaces had a satisfactory resistance for chemical and mechanical wears.

The increased cleanability by the additional functional films was lost for the surfaces, which were partially or totally destroyed by mechanical or chemical wear. The ability of the sol-gel derived titania coating to resist both chemical and mechanical wear suggested that it would be suitable for harsh environments where UV-light can be utilized for self-cleaning. The results also indicated that the choice of any additional functional film or coating for a given application should be based on a good understanding of the existing chemical and mechanical conditions present in the application. The results are essential for estimating the criteria when tailoring the additional coatings and traditional surfaces for a long-term effect on cleanability in everyday environments.

6. References

1. J. R. Taylor, A.C. Bull, Ceramics Glaze Technology, Pergamon Press Oxford, 1986.
2. P. B. Vandiver, Ancient glazes, Sci. Am. 262 (1990), 106-113.
3. R. A. Eppler, D. R. Eppler, Glazes and Glaze Coatings, Westerville, The American Ceramic Society, 2000.
4. C. B. Carter, M.G. Norton, Ceramic Materials – Science and Engineering, Springer, New York, 2007.
5. H. Seger, Collected writings, vol 2, New York, 1902.
6. R. Casasola, J. Ma. Rincon, M. Romero, Glass-ceramics glazes for ceramic tiles – a review, J. Mat. Sci., 27 (2012), 553-582.
7. S. Ludwig, Coating experiences on ceramic surfaces, cfi/Ber. DKG, No 1-2 (2005), E24-E26.
8. W. H. Zachariasen, The atomic arrangement in glass, J. Am. Ceram. Soc. 54 (1932), 3841-3851.
9. B. E. Warren, Summary of work on atomic arrangement in glass, J. Am. Ceram. Soc. 24 (1941), 256-261.
10. L. Fröberg, T. Kronberg, L. Hupa, Effect of soaking time on phase composition and surface microstructure in vitrocrystalline whiteware glazes, J. Eur. Ceram. Soc., 29 (2009), 2153-2161.
11. W. M. Carthy, M. Katz, J. Gill, The unity molecular formula approach to glaze development, Ceram. Eng. Sci. Proc. 21 (2000), 95-109.
12. S. Stefanov, S. Batschwarov, Keramik-Glasuren Ceramic Glazes, Bauverlag GmbH, Wiesbaden and Berlin, ISBN: 3-7652-2600-1, 1988
13. R. A. Eppler, D. R. Eppler, Formulation of leadless glazes, Ceram. Eng. Sci. Proc. 18 (1997), 150-158.
14. K. Meinssen, Ceramic glaze materials: the top ten list, Ceram. Eng. Sci. Proc. 18 (1997), 308-319.
15. R. A. Eppler, Selecting raw materials for glazes, Ceram. Eng. Sci. Proc. 19 (1998), 9-15.
16. Y. Hutchinson Cuff, Ceramic Technology for Potters and Sculptors, University of Pennsylvania Press, 1996.
17. W. M. Carthy, U. Senapati, Porcelain – raw materials, processing, phase evolution and mechanical behaviour, J. Am. Ceram. Soc. 81 (1998), 3-20.
18. H. Scholze, Glas; Natur, Struktur und Eigenschaften, Springer-Verlag, Berlin, 1988

19. T. Lakatos, L-G Johansson, B. Simmingsköld, Viscosity temperature relations in the glass system SiO_2-Al_2O_3-Na_2O-K_2O-CaO-MgO in the composition range of technical glasses, Glass Techn., 13 (3), (1972), 66-95.
20. T. Lakatos, Viscosity-temperature relations in glasses composed of SiO_2-Al_2O_3-Na_2O-K_2O-Li_2O-CaO-MgO-BaO-ZnO-PbO-B_2O_3, Glast. Tidskr., 31(3), (1976), 51-54.
21. T. Westerlund, L. Hatakka, K.H. Karlsson, A model for optimizing glass batch compositions, J. Am. Ceram. Soc., 66, (1983), 574-579.
22. T. Kronberg, K. Fröberg, L. Hupa, Optimizing glaze properties, Ceram. Eng. Sci. Proc., 22, (2001), 167-177.
23. A. R. Boccaccini, B. Hamann, Review – in situ high-temperature optical microscopy. J. Mater. Sci., 34, (1999), 5419-5436.
24. H. J. Harkort, Dilatometer und Erhitzungsmikroskop in ihrer Anwendung zur Charakterisierung von Kaolinen und Tonen. Keram. Z., 6, (1954), p 315.
25. F. Zapp, J. Domagala, Das Schmelzverhalten von Feldspaten im Erhitzungs-mikroskop. Keram. Z., 6 (10), (1954), 505-508.
26. A. Zwetsch, Untersuchungen zur Kennzeichnung von Feldspaten. Ber. Dtsch. Keram. Ges., 33(11), (1956), 349-386.
27. D. Harkort, D. Paetsch, Zur Untersuchung von Feldspaten im Erhitzungs-mikroskop. Ber. Dtsch. Keram. Ges., 37, (1960), 402-409.
28. H. Scholze, Der Einfluss von Viskosität und Oberflächenspannung auf erhitzungs-mikroskopische Messungen an Gläsern. Ber. Dtsch. Keram. Ges., 39, (1962), 63-68.
29. M. Obst, I. Simon, Untersuchung von Feldspaten mit der erhitzungsmikro-skopischen Methode. Keram. Z., 22 (4), (1970), 209-214.
30. B. Burzacchini, M. Paganelli, H. G. Christ, Examination of fast-fire frits and glazes using a hot stage microscope at different heating rates. Ceram. Eng. Sci. Proc., 17 (1), (1996), 60-66.
31. M. Paganelli, Understanding the behaviour of glazes: new test possibilities using the automated hot stage microscope "Misura". Ind. Ceram., 17, (1997) 69-73.
32. M. Paganelli, D. Sighinolfi, Understanding the behaviour of glazes with the automatic heating microscope, Ceram. Forum Int., 85 (5), (2008), E63-E67.

33. T. Kronberg, K. Fröberg, The melting behaviour in the system wollastonite – feldspar – quartz, Ceram. Eng. Sci. Proc., 22, (2001), 167-177.
34. M. J. Pascual, L. Pascual, A. Duran, Determination of viscosity-temperature curve for glasses on the basis of fixed viscosity points determined by hot stage microscopy. Phys. Chem. Glasses, 42, (2001), 61-66.
35. M. J. Pascual, A. Duran, A. Prado, A new method to determining fixed viscosity points of glasses. Phys. Chem. Glasses, 46, (2005), 512-520.
36. M. Ahmed, D. Earl, Characterizing glaze-melting via HSM. Am. Ceram. Soc. Bull., 81, (2002), 47-51.
37. R. L. Dumitrache, I, Teoreanu, Melting behaviour of feldspar porcelain glazes, U.P.B. Sci. Bull., Series B, Vil 68, No 1, (2006).
38. F. Montanari, P. Misilli, C. Leonelli, C. Boschetti, J. Henderson, P. Baraldi, Calibration and use of the heating microscope for indirect evaluation of the viscosity and meltability of archeological glasses, Int. J. Appl. Glass Sci., 5 (2), (2014), 161-177.
39. W. Panna, P. Wyszomirski, P. Kohut, Application of hot-stage microscopy to evaluating sample morphology changes on heating, J. Therm. Anal. Calorim. 125 (2016), 1053-1059.
40. W. Radmacher, Bestimmung des Asche-Schmelz verhaltens fester Brennstoffe, Brennstoff-Chemie, 30, (1949), 377-384.
41. E. Rousseau, Determination de la fusibilite des cendres de combustibles en atmosphere reductive, Chemie & Ind., 60, (1948). p 124.
42. DIN 51 730, German Norm, 1958.
43. BSS 453, British Norm, 1932.
44. ASTM D 271, American Norm, 1933.
45. E. Vedel, H. Arstila, H. Ylänen, L. Hupa, M. Hupa, Predicting physical and chemical properties of bioactive glasses from chemical composition - Part 1: Viscosity characteristics, Glass Technol. Part A, 49 (6), (2008), 251-259.
46. J. L. Amoros, E. Blasco, A. Moreno, M. P. Gomez-Tena, Sintering of raw glazes for floor and porcelain tiles: A non-isothermal kinetic model, Ceram. Int. 42 (2016), 16169-16179.
47. J.L. Amoros, E. Blasco, A. Moreno, M. P. Gomez-Tena, C. Feliu, Non-isothermal sinter-crystallisation of satin glazes: A kinetic model, Ceram. Int. 44 (2018), 7780-7787.

48. W. D. Kingery, H. K. Bowen, D. R. Uhlman, Introduction to ceramics, 2nd edition, John Wiley & sons (1960, 1976) ISBN: 0-471-47860-1.
49. M. Sheikhattar, H. Attar, S. Sharafi, W. M. Carty, Influence of surface crystallinity on the surface roughness of different ceramic glazes, Mater. Charac.118 (2016), 570-574.
50. J. K. Koenig, F. C. Henderson, Particle size distribution of glazes, J. Am. Ceram. Soc. 24 (1941), 286-297.
51. A. M. Bernadin, The influence of particle size distribution on the surface appearance of glaze, Dye Pigm. 80 (2009), 121-124.
52. E. Rambaldi, A. Tucci, L. Esposito, D. Naldi, G. Timellini, Effects of nano-oxides on the surface properties if ceramic tiles, In proceedings of world congress on ceramic tile quality, Qualicer, (2010).
53. J. Li, J. Liang, L. Wang, F. Wang, Effect of particle-size distribution on the surface appearance of glazed surface, J. Therm. Anal. Calorim. 115 (2014), 1127-1131.
54. J. Partyka, J. Lis, The influence of the grain size distribution of raw materials on the selected surface properties of sanitary glazes, Ceram. Int. 37 (2011), 1285-1292.
55. J. Partyka, M. Gajek, K. Gasek, Effects of quartz grain size distribution on the structure of porcelain glaze, Ceram. Int. 40 (2014), 12045-12053.
56. J. Partyka, M. Gajek, K. Gasek, Study of the topography and roughness of the glaze surface as modified by selection of raw materials grain size, Materialy Ceramiczne/Ceramic Materials 66 (2014), 121-125.
57. A. Tunali, Investigation of methods of reducing the number of pinhole defects in glossy-opaque floor tile glaze by modifying glaze properties, J. Ceram. Process. Res. Vol 15 No 4 (2014), 225-230.
58. J. Li, J. Liang, F. Wang, L. Wang, The role of firing process on bubble formation in a glaze layer of sanitary ware, Thermochim. Acta 588 (2014), 75-80.
59. L. Fröberg, T. Kronberg, L. Hupa, Influence of firing parameters on phase composition of raw glazes, J. Eur. Ceram. Soc. 27 (2007), 1671-1675.
60. L. Fröberg, S. Vane-Tempest, L. Hupa, Surface composition and topography of fast-fired raw glazes, In proceedings of VIII world congress on ceramic tile quality, Qualicer, (2004), P.G1, 143.
61. E. M. Levin, C. R. Robbins, H. F. McMurdie, Phase Diagrams for Ceramist, The American Ceramic Society, Ohio, 1964.

62. M. G. Rasteiro, T. Gassman, R. Santos, E. Antunes, Crystalline phase characterization of glass-ceramic glazes, Ceram. Int., 33 (2007), 345-354.
63. J. J. Reinosa, F. Rubio-Marcos, E. Solera, M. A. Bengochea, J. F. Fernandez, Sintering behaviour of nanostructured glass-ceramic glazes, Ceram. Int., 36 (2010), 1845-1850.
64. A. M. Ferrari, L. Barbieri, C. Leonelli, T. Manfredini, C. Siligardi, A.B. Corradi, Feasibility of using cordierite glass—ceramics as tile glazes, J. Am. Ceram. Soc. 80 (1997), 1757-1766.
65. F.J. Torres, J. Alarcon, Effect of additives on the crystallization of cordierite-based glass-ceramics as glazes for floor tiles, J. Eur. Cer. Soc. 23 (2003), 817-826.
66. F.J. Torres, J. Alarcon, Microstructural evolution in fast-heated cordierite-based glass-ceramic glazes for ceramic tile, J. Am. Ceram. Soc. 87 (2004), 1227-1232.
67. F. J. Torres, J. Alarcon, Effect of MgO/CaO ratio on the microstructure of cordierite-based glass-ceramic glazes for floor tiles, Ceram. Int. (2005), 683-690.
68. G. Baldi, E. Generali, C. Leonelli, T. Manfredini, G.C. Pellacani, C. Silligardi, Effects of nucleating agents on diopside crystallization in new glass-ceramics for tile-glaze applications, J. Mat. Sci., 30 (1995), 3251-3255.
69. M. Romero, J. Ma. Rincon, A. Acosta, Effect on iron oxide content on the crystallization of a diopside glass-ceramic glaze, J. Eur. Ceram. Soc. 22 (2002), 883-890.
70. F. J. Torres, J. Alarcon, Pyroxene-based glass-ceramics as glazes for floor tiles, J. Eur. Ceram. Soc., 25 (2005), 349-355.
71. F. J. Torres, J. Alarcon, Mechanism of crystallization of pyroxene-based glass-ceramic glazes, J. Non-Cryst. Solids, 347 (2004), 45-51.
72. B. E. Yekta, P. Alizadeh, L. Rezazadeh, Floor tile glass-ceramic glaze for improvement of glaze surface properties, J. Eur. Ceram. Soc., 26 (2006), 3809-3812.
73. K. Pekkan, B. Karasu, Zircon-free frits suitable for single fast-firing opaque wall tile glazes and their industrial productions, J. Eur. Ceram. Soc., 29 (2009), 1571-1578.
74. S. Ghosh, K. S. Pal, N. Dandapat, J. Ghosh, S. Datta, Glass-ceramic glazes for future generation floor tiles, J. Eur. Ceram. Soc., 33 (2013), 935-942.

75. E. Suvaci, B. Ylidiz, Roles of CaO, MgO and SiO2 on crystallization and microstructure development in diopside-based glass-ceramics glazes under industrial fast-firing condition, J. Aust. Ceram. Soc., 53 (2017), 75-81.
76. G. Cultrone, C. Rodriguez-Navarro, E. Sebastian, O. Cazalla. M. J. de la Torre, Carbonate and silicate phase reactions during firing, Eur. J. Mineral, 13 (2001), 621-634.
77. G. M. Azarov, E. V. Maiorova, M. A. Oborina, A. V. Belyakov, Wollastonite raw materials and their applications (a review), Glass Ceram. 52 (1995), 237-240.
78. S. Ke, X. Cheng, Y. Wang, Q. Wang, H. Wang, Dolomite, wollastonite and calcite as different CaO sources in anorthite-based porcelain, Ceram. Int. 39 (2013), 4953-4960.
79. W. Foster, The system $NaAlSi_3O_8$-$CaSiO_3$-$NaAlSiO_4$, J. Geol. 50 (1942), 53-73.
80. M. Gajek, J. Lis, J. Partyka, M. Wojczyk, Floor tile glass-ceramic glaze for improvement of the resistance to surface abrasion, IOP Conf. Ser: Mater. Sci. Eng. 18 (2011) 112016
81. R. Condradt, Chemical durability of oxide glasses – a review, J. Am. Ceram. Soc., 91 (2008), 728-735.
82. R.G. Newton, The durability of glass – a review, Glass Technol. Vol 26 (1985), 21-38.
83. H. Scholze, Chemical durability of glasses, J. Non-Cryst. Solids, 52 (1982), 91-103.
84. R. A. Eppler, Corrosion of glazes and enamel, in D. E. Clark, B. K. Zoitos, Corrosion of glass, ceramics and ceramic superconductors, Noyes Publications, Park Ridge, NJ, 1992.
85. T. Toya, Y. Tamura, Y. Kameshima, K. Okada, Preparation and properties of CaO-MgO-Al2O3-SiO2 glass-ceramics from kaolin clay refining waste (kira) and dolomite, Ceram. Int. 30 (2004), 983-989.
86. T. W. Cheng, Effect of additional materials on the properties of glass-ceramic produced from incinerator fly ashes, Chemosphere, 56 (2004), 127-131.
87. T. Toya, A. Nakamura, Y. Kameshima, A. Nakajima, K. Okada, Glass-ceramics prepared from sludge generated by a water purification plant, Ceram. Int., 33 (2007), 573-577.
88. G. Topates, B. Tarhan, M. Tarhan, Chemical durability of zircon containing glass-ceramic glazes, Ceram. Int., 43 (2017), 12333-12337.

89. G. Bolelli, V. Cannilo, L. Lusvarghi, T. Manfredini, C. Siligardi, C. Bartuli, A. Loreto, T. Valente, Plasma-sprayed glass-ceramic coatings on ceramic tiles: microstructure, chemical resistance and mechanical properties, J. Eur. Ceram. Soc., 25 (2005), 1835-1853.
90. S. A. M. Abdel-Hameed, A. A. El-Kheshen, Thermal and chemical properties of diopside-wollastonite glass-ceramics in the SiO2-CaO-MgO system from raw materials, Ceram. Int. 29 (2003), 265-269
91. A. Escardino, J. L. Amoros, A. Gozalbo, M. J. Orts, F. Lucas, A. Belda, Interaction between glaze layers during firing. Chemical resistance of the resulting glazes, In proceedings of VII world congress on ceramic tile quality, Qualicer, (2002), 201-217.
92. T. Kronberg, L. Hupa, K. Fröberg, Durability of mat glazes in hydrochloric acid solutions, Key Eng. Mater., (2004), 1565-1568
93. S. Vane-Tempest, T. Kronberg, L. Fröberg, L. Hupa, Chemical resistance of fast-fired glazes in solutions containing cleaning agents, acids or bases, In proceedings of VIII world congress on ceramic tile quality, Qualicer, (2004), P.G1, 155-164.
94. L. Hupa, R. Bergman, L. Fröberg, S. Vane-Tempest, M. Hupa, T. Kronberg, E. Pesonen-Leinonen, A.M. Sjöberg, Chemical resistance and cleanability of glazed surface, Surf. Sci, (2005), 113-118.
95. L. Fröberg, T. Kronberg, S. Törnblom, L. Hupa, Chemical durability of glazed surfaces, J. Eur. Ceram. Soc., 27 (2007), 1811-1816.
96. L. Fröberg, L. Hupa, M. Hupa, Corrosion of crystalline phases of matte glazes in aqueous solutions, J. Eur. Ceram. Soc., 29 (2009), 7-14.
97. W. McCracken, Corrosion of glass-ceramics, in D. E. Clark, B. K. Zoitos, Corrosion of glass, ceramics and ceramic superconductors, Noyes Publications, Park Ridge, NJ, 1992.
98. J. Partyka, J. Lis, Chemical corrosion of sanitary glazes of variable grain size composition in acid and basic aqueous solution media, Ceram. Int., 38 (2012), 553-560.
99. I. Atkinson, M. E. Smith, M. Zaharescu, Examining correlations between composition, structure and properties in zircon-containing raw glazes, Ceram. Int. 38 (2012), 1827-1833.
100. A. C. Lasaga, R. J. Kirkpatrick, Kinetics of geochemical processes, Rev. Mineral. 8 (1981).
101. W. H. Casey, B. Bunker, Leaching of minerals and glass surfaces during dissolution, Rev. Mineral., (1990), 397-426.

102. W. B. White, Theory of corrosion of glass and ceramics, in D. E. Clark, B. K. Zoitos, Corrosion of glass, ceramics and ceramic superconductors, Noyes Publications, Park Ridge, NJ, 1992.
103. J. Schott, O. Pokrovsky, E. H. Oelkers, The link between mineral dissolution/precipitation kinetics and solution chemistry, Rev. Mineral. Geochem. 70 (2009), 207-258.
104. E. H. Oelkers, S. V. Golubev, C. Chairat, O. S. Pokrovsky, J. Schott, The surface chemistry of multi-oxide silicates. Geochem. Cosmochim. Acta, 65 (2009), 2011-2024.
105. B. C. Bunker, Molecular mechanisms for corrosion of silica and silica glasses, J. Non-Cryst. Solids, 179 (1994), 300-308.
106. C. Cailleteau, F. Angeli, F. Devreux, S. Gin, J. Jestin, P. Jollivet, O. Spalla, Insight into silicate-glass corrosion, Nat. Mater. 7 (2008), 978-983.
107. E. J. Weissbart, J. D. Rimstidt, Wollastonite: incongruent dissolution and leached layer formation, Geochim. Cosmochim. Acta, 64 (2000), 4007-4016.
108. J. Schott, O. S. Pokrovsky, O. Spalla, F. Devreux, A. Gloter, J. A. Mielczarski, Formation, growth and transformation of leached layers during silicate minerals dissolution: the example of wollastonite. Geochim. Cosmochim. Acta, 98 (2012), 259-281.
109. ISO 10545-13. Ceramic tiles – Part 13. Determination of chemical resistance (1996).
110. V. Cannillo, L. Esposito. E. Rambaldi, A. Sola, A. Tucci, Microstructural and mechanical changes by chemical ageing of glazed surfaces, J. Eur. Ceram. Soc., 29 (2009), 1561-1569.
111. L. Fröberg, L. Hupa, Topographic characterization of glazed surfaces, Appl. Surf. Sci. 254 (2008), 1622-1629.
112. L. Hupa, R. Bergman, L. Fröberg, S. Vane-Tempest, M. Hupa, T. Kronberg, E. Pesonen-Leinonen, A.-M. Sjöberg, Chemical resistance and cleanability of glazed surfaces, Surf. Sci. 584 (2005), 113-118.
113. ISO 10545-14. Ceramic tiles – Part 14. Determination of resistance to stains (1996).
114. P. M. Tenerio Cavalcante, M. Dondi, G. Ercolani, G. Guarini, C. Melandri, M. Raimondo, E. Rocha e Almendra, The influence of microstructure on the performance of white porcelain stoneware, Ceram. Int. 30 (2004), 953-963.
115. M. Dondi, G. Ercolani, G. Guarini, C. Melandri, M. Raimondo, E. Rocha e Almendra, P. M. Tenerio Cavalcante, The role of surface

microstructure on the resistance to stains of porcelain stoneware tiles, J. Eur. Ceram. Soc. 25 (2005), 357-365.

116. R. Kuisma, L. Fröberg, H.R. Kymäläinen, E. Pesonen-Leinonen, M. Piispanen, P. Melamies, M. Hautala, A.M. Sjöberg, L. Hupa: Microstructure and Cleanability of Uncoated and Fluoropolymer, Zirconia and Titania Coated Ceramic Glazed Surfaces. J. Eur. Ceram. Soc. 27 (2007) 101-108.
117. T. Kronberg, A.-C. Ritschkoff, R. Mahlberg, J. Mannila, M. Kallio, A. Vesa, L. Hupa, Soil-resistant surfaces for traditional surfaces, J. Eur. Ceram. Soc. 27 (2007), 1775-1780.
118. J. Määttä, Modifications of surface materials and their effect on cleanability as studied by radiochemical methods, PhD Thesis, University of Helsinki, Finland (2007).
119. A. L. da Silva, M. Dondi, M. Raimondo, D. Hotza, Photocatalytic ceramic tiles: Challenges and technological solutions, J. Eur. Ceram. Soc. 38 (2018), 1002-1017.
120. J. Määttä, M. Piispanen, R. Kuisma, H.R. Kymäläinen, A. Uusi-Rauva, K.R. Hurme, S. Areva, A.M. Sjöberg, L. Hupa: Effect of Coating on Cleanability of Glazed Surfaces. J. Eur. Ceram. Soc. 27 (2007), 4555-4560.
121. T. Kronberg, K.Fröberg, The formation of Insoluble Stains on Glass and Glaze Surfaces", 2002 Glass Odyssey, Proceedings: 6th ESG (European Society of Glass Science and Technology) Conference, Montpellier, France, (CD-Rom), 2003.
122. T. Kronberg, M. Piispanen, S. Areva, L. Hupa, Cleanability of functional and traditional ceramic surfaces. Proc. 10th ECerS 2007, Berlin, Germany, ISBN-3-87264-022-4 (CD-Rom), 2008.
123. W. Barthlott, C. Neinhuis, Purity of the Sacred Lotus, or Escape from Contaminants in Biological Surfaces, Planta, 202 (1997), 1–8.
124. A. Fujishima, K. Honda, Electrochemical Photolysis of Water at a Semiconductor Electrode, Nature, 238 (1972), 37–8.
125. A. Fujishima, T.N. Rao, D.A. Tryk: Titanium Dioxide Photocatalysis. J. Photochem. Photobiol. C: Photochem. Rev. 1 (2000) 1-21.
126. A. Fujishima, Z. Zhang, Titanium Dioxide Photocatalysis: Present Situation and Future Approaches. C. R. Chemie 9 (2006) 750-760.
127. A. Mills, M. McFarlane, Current and possible future methods of assessing the activities of photocatalyst films, Catal. Today, 129 (2007), 22-28

128. K. Midtdal, B. P. Jelle, Self-cleaning glazing products: A state-of-the-art review and future research pathways, Sol. Energ. Mat. Sol. C. 109 (2013), 126-141.
129. K. Nakata, A. Fujishima, TiO_2 photocatalysis: design and application, J. Photochem. Photobiol. C Photochem. Rev. 13 (2012), 169-189.
130. G. Varshney, S. R. Kanel, D. M. Kempisty, V. Varshney, A. Agrawal, E. Sahle-Demessie, R. S. Varma, M. N. Nadagouda, Nanoscale TiO_2 films and their applicationin remediation of organic pollutants, Coord. Chem. Rev. 306 (part 1) (2016), 43-64.
131. F. Bondioli, R. Taurino, A. M. Ferrari, Functionalization of ceramic tile surface by sol-gel technique, J. Colloid Interf. Sci. 334 (2009), 195-201.
132. A. M Berto, Ceramic tiles: Above and beyond traditional applications, J. Eur. Ceram. Soc. 27 (2007), 1607-1613.
133. K. Murugan, R. Subasri, T. N. Rao, A. S. Gandhi, B. S. Murty, Syntesis, characterization and demonstation of self-cleaning TiO_2 coatings on glass and glazed ceramic tiles, Prog. Org. Coat. 76 (2013), 1756-1760.
134. V. B. Tezza, M. Scarpato, L. F. S. Oliveira, A. M. Bernadin, Effect of firing temperature on the photocatalytic activity of anatase ceramic glazes, Powder Technol. 276 (2015), 60-65.
135. P. Zhang, J. Tian, R. Xu, G. Ma, Hydrophilicity, photocatalytic activity and stability of tetraethyl orthosilicate modified TiO_2 film on glazed ceramic surface, Appl. Surf. Sci. 266 (2013), 141-147.
136. S. Ke, X. Cheng, Q. Wang, Y. Wang, Z. Pan, Preparation of a photocatalytic $TiO_2/ZnTiO_3$ coating on glazed ceramic tiles, Ceram. Int. 40 (2014), 8891-8895.
137. A. L. da Silva, D. N. F. Muche, S. Dey, D. Hotza, R. H. R. Castro, Photocatalytic Nb_2O_5-doped TiO_2 nanoparticles for glazed ceramic tiles, Ceram. Int. 42 (2016), 5113-5122.
138. A. L. da Silva, M. Dondi, D. Hotza, Self-cleaning ceramic tiles coated with Nb_2O_5-doped-TiO_2 nanoparticles, Ceram. Int. 43 (2017), 11986-11991.
139. V. Vaiano, G. Sarno, D. Sannino, P. Ciambelli, Photocatalytic and antistain properties of ceramic tiles functionalized with tungsten-doped TiO_2, Chemical Engineering Transactions 39 (2014), 499-504.
140. F. Knies, K. Schrantz, C. Aneziris, L. Gauckler, T. Graule, Superhydrophilic ceramic glazes for sanitaryware, J. Ceram. Sci. Tech. 7 (2016), 53-64.

141. A. Nakajima, K. Hashimoto, T. Watanabe, Recent studies on super-hydrophobic films, Monatshefte fur Chemie, 132 (2001), 31-41.
142. A. Nakajima, K. Hashimoto, T. Watanabe, K. Takai, G. Yamauchi, A. Fujishima, Transparent superhydrophobic thin films with self-cleaning properties, Langmuir, 16 (2001), 7044-7047.
143. A. Marmur, E. Bittoun, When Wenzel and Cassie are right: Reconsiling local and global considerations, Langmuir 25 (2009), 1277-1281.
144. N. Takashi, M. Masashi, N. Katsuhiko, M. Motonori, U. Yasukiyo, The lowest surface free energy based on -CF3 alignment, Langmuir, 15 (1999), 4321-4323.
145. I. Cacciotti, F. Nanni, V. Campaniello, F. R. Lamastra, Development of a transparent hydrorepellent modified SiO_2 coatings for glazed sanitarywares, Mater. Chem. Phys. 146 (2014), 240-252.
146. M. Machida, K. Norimoto, T. Kimura, Antibacterial activity of photocatalytic titanium dioxide thin films with photodeposited silver on the surface of sanitary ware, J. Am. Ceram. Soc. 88 (2005), 95-100.
147. N. Baheiraeia, F. Moztarzadeha, M. Hedayati, Preparation and antibacterial activity of Ag/SiO_2 thin film on glazed ceramic tiles by sol-gel method, Ceram. Int. 38 (2012), 2921-2925.
148. M. Kawashita, S. Tsuneyama, F. Miyali, T. Kokubo, H. Kozuka, K. Yamamoto, Antibacterial silver-containing silica glass prepared by sol-gel method, Biomaterials 21 (2000), 393-398.
149. T. Toshikazu, Antimicrobial agent composed of silica-gel with silver complex, Inorg. Mater. 6 (1999), 505-511.
150. S. de Niederhäusern, M. Bondi, Self-cleaning and antibacterial ceramic tile surface, Int. J. Appl. Ceram. Technol. (2013), 949-956.
151. S. -Q. Sun, B. Sun, W. Zhang, D. Wang, Preparation and antibacterial activity of $Ag\text{-}TiO_2$ composite film by liquid phase deposition (LPD) method, Bull. Mater. Sci 31 (2008), 61-66.
152. Q. Wang, X. Guo, W. Wu, S. Liu, Preparation of fine Ag_2WO_4 antibacterial powders and its application in the sanitary ceramics, Adv. Mater. Res. (2011), 1321-1325.
153. A. Bernasconi, V. Diella, N. Marinoni, A. Pavese, F. Francescon, Influence of composition on some industrially relevant properties of traditional sanitary-ware glaze, Ceram. Int. 38 (2012), 5859-5870.
154. S. Wang, C. Peng, Z. Huang, J. Zhou, M. Lu, J. Wu, Clustering of zircon in raw glaze and its influence on optical properties of opaque glaze, J. Eur. Ceram. Soc. 34 (2014), 541-547.

155. I. A. Levitskii, N. V. Mazura, Opacified glazes produced by high-temperature firing for sanitary ceramicware, Glass Ceram. 62 (2003), 215-218.
156. K. Ozbek, N. Ay, Double layer glaze application for the vitrified glazes and surface properties, Key Eng. Mater. 264-268 (2004), 1673-1676.
157. M. Dondi, M. Raimondo, C. Zanelli, Stain resistance of ceramic tiles, Ceramic world review (2007)
158. M. Piispanen, T. Kronberg, S. Areva, J. Pimenoff, L. Hupa, Easy-to-clean coatings on glass and glazed surfaces, Adv. Sci. Technol. 66 (2010), 150-155.
159. M. Piispanen, J. Määttä, S. Areva, A.-M. Sjöberg, M. Hupa, L. Hupa, Chemical resistance and cleaning properties of coated glazed surfaces, J. Eur. Ceram. Soc. 29 (2009), 1855-1860.
160. A. Fujishima, T. N. Rao, D. A. Tryk, TiO_2 photocatalysts and diamond electrodes, Electrochim. Acta 45 (2005), 4683-4690.
161. T. Minabe, D. A. Tryk, P. Sawunyama, Y. Kikuchi, K. Hashimoto, A. Fujishima, TiO_2-mediated photodegradation of liquid and solid organic compounds, J. Photoch. Photobio A 137 (2000), 53-62.
162. K. Guan, Relationship between photocatalytic activity, hydrophilicity and selfcleaning effect of TiO_2/SiO_2 films, Surf. Coat. Tech. 191 (2005), 155-160.
163. N. Yoshida, M. Takeuchi, T. Okura, H. Monma, M. Wakamura, H. Ohsaki, T. Watanabe, Super-hydrophobic photocatalytic coatings utilizing apatite-based photocatalyst, Thin Solid Films 502 (2006), 108-111.
164. J. Määttä, M. Piispanen, H.-R. Kymäläinen, A. Uusi-Rauva, K.-R. Hurme, S. Areva, A.-M. Sjöberg, L. Hupa, Effects of UV-radiation on the cleanability of titanium dioxide-coated glazed ceramic tiles, J. Eur. Ceram. Soc. 27 (2007), 4569-4574.
165. C. Sciancalepore, F. Bondioli, Durability of SiO_2-TiO_2 photocatalytic coatings on ceramic tiles, Int. J. Appl. Ceram. Technol. 12 (2015), 679-684.
166. M. Piispanen, L. Fröberg, T. Kronberg, S. Areva, L. Hupa: Corrosion of Glazes with Functional Films in Detergent Solutions. Adv. Sci. Technol. 45 (2006) 156-161, Trans Tech Publications, Switzerland.
167. M. Piispanen, T. Kronberg, S. Areva, L. Hupa, Effect of mechanical and chemical wear on soil attachment and cleanability of sanitaryware with additional coatings, J. Am. Ceram. Soc. 94(3) (2011) 951-958.

168. M. Piispanen, J. Määttä, T. Kronberg, S. Areva, A-M. Sjöberg, L. Hupa, Effect of mechanical and chemical wear on cleanability of functional and traditional glazed surfaces, Proc. 10th ECerS 2007, Berlin, Germany, ISBN-3-87264-022-4 (CD-Rom), 2008.
169. ISO 10545-7, Ceramic tiles - Part 7: Determination of resistance to surface abrasion for glazed tiles (1996).
170. M. Raulio, V. Pore, S. Areva, M. Ritala, M. Leskelä, J. Linden, J. B. Rosenholm, K. Lounatmaa, M. Salkinoja-Salonen, Destruction of deinococcus geothermalis biofilm by photocatalytic ALD and sol-gel TiO_2 surfaces, J. Ind. Microbiol. Biotechnol. 33 (2006), 261-268.
171. I. Redsven, R. Kuisma, L. Laitala, E. Pesonen-Leinonen, R. Mahlberg, H.-R. Kymäläinen, Application of a proposed standard for testing soiling and cleanability of resilient floor coverings, Tenside Surfact Det. 40 (2003), 346-352.
172. G. W. Morey, The Properties of Glass, 2nd ed, Reinhold Publishing Corporation, New York, 1954.
173. L. Björkvik, X. Wang, L. Hupa, Dissolution of bioactive glasses in acidic solutions with the focus on lactic acid, Int. J. Appl. Glass Sci. 7 (2016), 154-163.
174. C. Della Volpe, A Penati, R. Peruzzi, S. Siboni, L. Tonioli, C. Columbo, The combined effect of roughness and heterogeneity on contact angles: The case of polymer coatings for stone protection, J. Adhes. Sci. Technol. 14 (2000), 273-299.

Appendix I

Glaze	Wo	FS	CC	Do	Co	ZnO	Q	ZS
1	20	20	5	6	0	4	35	10
2	15	45	15	2	6	0	7	10
3	20	20	5	4	8	0	33	10
4	15	25	5	0	2	4	39	10
5	10	30	10	8	0	0	32	10
6	15	20	15	4	2	0	34	10
7	30	25	5	6	0	4	20	10
8	20	40	10	0	0	2	18	10
9	10	50	10	0	2	0	18	10
10	20	35	10	0	2	0	23	10
11	10	20	10	0	4	2	44	10
12	10	40	5	0	0	2	33	10
13	15	20	5	6	10	2	32	10
14	10	45	5	6	10	2	12	10
15	30	20	15	8	6	4	7	10
16	10	25	5	0	8	0	42	10
17	15	25	15	10	0	2	23	10
18	30	40	5	10	0	0	5	10
19	10	25	15	2	2	2	34	10
20	10	25	5	2	2	2	44	10
21	15	25	5	10	2	0	33	10
22	10	20	15	2	10	2	31	10
23	15	25	5	4	10	4	27	10
24	10	35	10	6	2	2	25	10
25	25	35	5	6	6	4	9	10
26	25	20	15	2	10	0	18	10
27	25	30	5	4	8	0	18	10
28	25	30	5	4	0	4	22	10
29	25	45	5	4	8	0	3	10
30	30	20	15	8	8	0	9	10
31	15	30	10	0	6	4	25	10
32	25	40	10	4	4	2	5	10
33	15	50	10	0	4	0	11	10
34	20	40	5	8	4	0	13	10
35	30	40	15	0	0	0	5	10
36	30	35	5	4	0	2	14	10
37	20	25	10	2	2	4	27	10
38	10	50	10	10	4	0	6	10
39	20	35	5	2	10	2	16	10
40	25	30	5	10	4	2	14	10
41	30	25	10	8	4	4	9	10

42	20	35	10	10	2	0	13	10
43	30	35	10	0	4	2	9	10
44	10	30	10	10	6	0	24	10
45	30	40	5	8	2	2	3	10
46	20	35	10	10	8	0	7	10
47	20	30	15	8	6	2	9	10
48	15	35	15	2	8	2	13	10
49	15	45	5	6	6	4	9	10
50	30	20	10	8	10	0	12	10
51	25	25	15	4	0	2	19	10
52	25	40	10	0	6	0	9	10
53	10	40	10	6	4	4	16	10
54	15	30	10	10	2	4	19	10
55	15	30	15	8	6	2	14	10
56	15	45	5	8	10	2	5	10
57	25	30	15	4	4	2	10	10
58	20	45	10	4	4	4	3	10
59	10	50	10	10	6	0	4	10
60	15	20	15	8	8	4	20	10
61	25	20	15	6	6	4	14	10
62	15	40	15	6	0	4	10	10
63	25	30	15	0	8	0	12	10
64	25	40	5	4	8	2	6	10
65	25	35	15	8	6	0	1	10
66	10	45	5	10	10	4	6	10
67	10	35	15	4	4	4	18	10
68	20	25	5	0	10	2	28	10
69	30	40	10	2	2	0	6	10
70	15	45	10	2	2	0	16	10
71	10	25	10	8	4	4	29	10
72	10	50	15	0	10	4	1	10
73	20	45	15	4	4	2	0	10
74	20	40	10	10	8	0	2	10
75	25	30	5	6	8	2	14	10

The raw material compositions (wt%) of experimental glazes (No 1..75) in Publication I. Wo = wollastonite, FS = feldspar, CC = china clay, Do = dolomite, Co = corundum, ZnO = zinc oxide, Q = quartz, ZS = zirconium silicate.

Appendix II

Glaze	Kaolin	Feldspar	Dolomite	Limestone	Corundum	Quartz
1	6.0	74.6	14.5	0.0	0.0	4.9
2	8.0	26.0	15.0	17.8	13.0	20.2
3	8.0	26.2	15.0	17.7	0.3	32.8
4	5.0	42.5	14.5	17.0	0.0	21.0
5	5.0	27.7	0.0	27.0	1.4	38.9
6	5.5	25.9	0.0	43.0	0.9	24.7
7	5.0	26.9	7.5	22.6	14.3	23.7
8	5.0	52.9	8.4	2.9	11.6	19.3
9	5.0	43.0	0.0	41.5	0.0	10.5
10	5.0	78.0	0.0	7.5	7.6	2.0
11	8.0	48.0	7.4	22.1	3.0	11.6
12	8.0	27.2	15.4	0.0	0.6	48.8
13	5.0	45.5	0.0	42.8	3.7	3.1
14	5.0	72.8	15.0	0.0	7.2	0.0
15	5.0	76.6	8.4	2.5	7.4	0.0

Glaze	Na_2O+K_2O	MgO	CaO	Al_2O_3	SiO_2
1	10.0	4.0	5.0	17.5	63.5
2	4.0	4.0	17.5	25.0	49.5
3	4.0	4.0	17.5	10.0	64.5
4	7.0	4.0	17.5	10.0	61.5
5	4.0	0.0	17.5	10.0	68.5
6	4.0	0.0	30.0	10.0	56.0
7	4.0	2.0	17.5	25.0	51.5
8	7.0	2.0	5.0	25.0	61.0
9	7.0	0.0	30.0	10.0	53.0
10	10.0	0.0	5.0	25.0	60.0
11	7.0	2-0	17.5	17.5	56.0
12	4.0	4-0	5.0	10.0	77.0
13	7.0	0.0	30.0	17.5	45.5
14	10.0	4.0	5.0	25.0	56.0
15	10.0	2.0	5.0	25.0	58.0

Raw material composition and oxide composition of experimental glazes in Publication II.

Appendix III

	Raw material composition						Oxide composition					
Glaze	**Wo**	**FS**	**CC**	**Do**	**Co**	**Q**	**CaO**	**MgO**	**SiO_2**	**Al_2O_3**	**Na_2O+K_2O**	**SiO_2/Al_2O_3**
A10/0	21,3	37,6	10,0	0,0	16,6	14,4	9,9	0,1	56,6	28,3	5,0	2,0
A10/1	18,5	36,7	10,0	3,9	16,0	14,9	10,0	1,0	56,0	28,0	5,0	2,0
A10/2	15,1	36,0	10,0	8,2	15,3	15,5	10,0	2,0	55,4	27,6	5,0	2,0
A10/3	11,7	35,3	10,0	12,5	14,5	16,0	10,0	3,0	54,7	27,2	5,0	2,0
A10/4	8,6	34,5	10,0	16,4	13,9	16,6	10,0	4,0	54,1	26,9	5,0	2,0
A12/0	25,8	37,6	10,0	0,0	15,9	10,6	12,0	0,1	55,3	27,6	5,0	2,0
A12/1	22,8	36,7	10,0	3,9	15,3	11,2	12,0	1,0	54,7	27,3	5,0	2,0
A12/2	19,3	35,9	10,0	8,2	14,6	11,9	12,0	2,0	54,0	27,0	5,0	2,0
A12/3	16,0	35,2	10,0	12,4	13,9	12,5	12,1	3,0	53,4	26,6	5,0	2,0
A12/4	12,7	34,5	10,0	16,3	13,3	13,1	12,0	4,0	52,7	26,3	5,0	2,0
A14/0	30,2	37,6	10,0	0,0	15,3	6,9	13,9	0,2	53,9	27,0	5,0	2,0
A14/1	27,3	36,8	10,0	3,7	14,7	7,5	14,0	1,0	53,3	26,7	5,0	2,0
A14/2	23,7	35,9	10,0	8,1	14,0	8,2	14,1	2,0	52,6	26,3	5,0	2,0
A14/3	20,2	35,2	10,0	12,3	13,3	9,0	14,0	3,0	52,0	25,9	5,0	2,0
A14/4	16,9	34,5	10,0	16,2	12,7	9,7	14,0	4,0	51,4	25,6	5,0	2,0
A16/0	34,7	37,6	10,0	0,0	14,6	3,1	16,0	0,2	52,5	26,3	5,0	2,0
A16/1	31,8	36,9	10,0	3,6	14,0	3,7	16,0	1,0	52,0	26,0	5,0	2,0
A16/2	28,0	36,1	10,0	8,0	13,3	4,5	16,0	2,0	51,3	25,7	5,0	2,0
A16/3	24,5	35,3	10,0	12,2	12,7	5,3	16,1	3,0	50,6	25,3	5,0	2,0
A16/4	21,1	34,6	10,0	16,2	11,9	6,2	16,1	4,0	50,1	24,8	5,0	2,0
A18/0	39,1	37,4	10,0	0,0	13,5	0,0	18,0	0,2	51,6	25,2	5,0	2,0
A18/1	36,2	36,8	10,0	3,5	13,4	0,0	18,0	1,0	50,6	25,4	5,0	2,0
A18/2	32,4	36,0	10,0	8,0	12,6	1,1	18,1	2,0	50,0	24,9	5,0	2,0
A18/3	28,6	35,4	10,0	12,0	12,1	1,9	17,9	3,0	49,4	24,7	5,0	2,0
A18/4	25,0	34,6	10,0	16,1	11,5	2,8	17,9	4,0	48,7	24,4	5,0	2,0

Raw material composition and oxide composition for experimental glazes in Publication 3 and 4.

Appendix IV

Glaze	T_1	T_2	T_3	SP	Softening	HCP	FP
1	1100	1135	1160	1060	1150	1210	1260
2	1170	1200	1240	1120	1230	1295	1320
3	1155	1195	1220	1120	1215	1270	1315
4	1065	1140	1200	1045	1185	1300	1350
5	1150	1200	1225	1130	1220	1280	1320
6	1160	1200	1240	1120	1225	1300	1335
7	1095	1130	1150	1065	1145	1180	1205
8	1085	1145	1185	1040	1170	1235	1270
9	1175	1220	1275	1110	1250	1340	1375
10	1165	1200	1240	1120	1230	1285	1325
11	1100	1215	1310	1070	1270	1390	> 1400
12	1085	1160	1245	1040	1220	1345	1385
13	1100	1160	1190	1050	1200	1265	1300
14	1100	1145	1185	1065	1170	1245	1290
15	1125	1150	1155	1100	1155	1170	1180
16	1170	1250	1340	1125	1310	1400	> 1400
17	1130	1165	1190	1090	1185	1220	1250
18	1120	1170	1185	1105	1180	1200	1220
19	1105	1190	1260	1080	1240	1330	1370
20	1070	1170	1250	1050	1235	1350	1380
21	1145	1210	1220	1095	1215	1250	1270
22	1115	1205	1295	1090	1275	1355	1380
23	1080	1135	1170	1055	1165	1235	1290
24	1110	1155	1190	1065	1190	1265	1315
25	1090	1130	1150	1075	1150	1175	1200
26	1160	1190	1220	1105	1215	1255	1280
27	1140	1175	1200	1105	1195	1235	1270
28	1080	1125	1145	1045	1140	1195	1235
29	1130	1165	1180	1095	1180	1220	1245
30	1165	1180	1190	1130	1190	1210	1225
31	1065	1140	1200	1050	1160	1285	1325
32	1110	1140	1160	1065	1155	1190	1215
33	1170	1200	1240	1115	1230	1290	1320
34	1135	1170	1190	1110	1190	1215	1240
35	1155	1185	1205	1105	1200	1235	1260
36	1100	1130	1165	1060	1150	1200	1230
37	1080	1125	1165	1050	1155	1220	1265
38	1140	1175	1200	1125	1195	1235	1260

39	1090	1135	1170	1025	1165	1225	1270
40	1120	1150	1170	1090	1170	1190	1210
41	1115	1145	1150	1085	1155	1165	1175
42	1090	1105	1120	1085	1125	1145	1165
43	1085	1145	1170	1045	1165	1210	1235
44	1160	1195	1220	1125	1220	1265	1285
45	1105	1140	1160	1090	1155	1180	1195
46	1140	1175	1190	1130	1185	1210	1220
47	1130	1160	1175	1105	1175	1205	1220
48	1120	1170	1230	1080	1230	1285	1310
49	1080	1120	1150	1075	1145	1190	1260
50	1160	1180	1190	1130	1190	1210	1225
51	1110	1145	1170	1080	1170	1210	1255
52	1160	1190	1215	1105	1220	1255	1280
53	1090	1135	1175	1075	1165	1235	1295
54	1105	1140	1165	1085	1165	1200	1225
55	1130	1165	1190	1100	1190	1230	1260
56	1115	1145	1170	1095	1165	1210	1250
57	1115	1150	1175	1080	1170	1210	1240
58	1090	1130	1150	1075	1150	1195	1230
59	1145	1175	1195	1130	1195	1235	1260
60	1110	1150	1180	1085	1180	1220	1250
61	1110	1145	1155	1075	1155	1185	1205
62	1095	1130	1165	1080	1165	1205	1250
63	1170	1200	1230	1105	1230	1265	1300
64	1105	1140	1155	1080	1160	1195	1235
65	1155	1175	1185	1140	1185	1205	1225
66	1095	1130	1165	1085	1165	1205	1235
67	1090	1150	1215	1065	1210	1280	1340
68	1085	1160	1215	1035	1190	1290	1345
69	1145	1170	1190	1120	1185	1225	1250
70	1160	1190	1225	1110	1220	1285	1310
71	1095	1145	1185	1075	1175	1245	1290
72	1090	1185	1280	1065	1245	1335	1365
73	1120	1145	1175	1085	1170	1215	1245
74	1140	1170	1185	1130	1190	1210	1230
75	1110	1145	1170	1080	1165	1195	1225

The characteristic point temperatures (℃) of experimental glazes in Series I (Publication I) as given by HSM analyses. T_1, T_2 and T_3 defined according to Fig. 12. Sintering point (SP), softening point (softening), half-cone point (HCP) and floating point (FP) according to Fig. 4.

Appendix V

Glaze	Gloss	Gloss std.dev.	Crystalline phases	PEI hardness
1	82	0,9	Q,Wo	2
2	35	4,0	Q,Wo, FS, Co	4
3	59	5,3	Q, Wo, FS, Co	2
4	56	5,8	Q	3
5	53	8,2	Q, Wo, FS	3
6	42	7,8	Q, Wo, FS	4
7	90	1,2	Q, Wo	2
8	81	1,1	Q, Wo	2
9	2	0,1	Q, FS	5
10	43	3,9	Q, Wo, FS	3
11	5	0,4	Q, FS	5
12	45	1,2	Q, Wo, FS	5
13	71	1,0	Q	3
14	74	0,9	Co, Q, FS	3
15	95	0,8		1
16	2	0,1	Co, Q, FS	4
17	88	0,7	Q	2
18	84	0.9	Wo	1
19	13	4,2	Q, FS	4
20	30	4,0	Q, Wo, FS	4
21	65	1,1	Q, Wo, FS	3
22	5	0,2	Co, Q, FS,	5
23	74	1,2	Q, Co	2
24	76	1,3	Q, FS	3
25	91	0,4		2
26	60	4,8	Co, Q, Wo, FS	3
27	83	0,9	Q, Wo	1
28	88	1,0	Q, Wo	1
29	87	1,0	Wo, Co	2
30	88	1,3	Wo	1
31	65	2,1	Q, Wo, FS	3
32	90	1,2		1
33	21	4,5	Q, Wo, FS	4
34	85	2,6	Q, Wo	1
35	85	0,8	Wo, Q	2
36	85	1,4	Wo	1
37	82	2,3	Q	2
38	81	1,5	Q,FS	2
39	83	0,8	Co, Q, Wo, FS	2
40	91	0,8	Wo	1
41	95	1,6		1
42	93	0,7		1
43	87	1,6	Q, Wo	1
44	64	3,1	Q, Wo, FS	2
45	92	1,0	Wo	1
46	86	2,1		1
47	79	1,5		1
48	38	1,1	Q, Wo, FS, Co	4
49	86	0,6	Q	1
50	84	6,4	Co, Q, Wo	1

51	89	1,2	Q, Wo	2
52	75	4,0	Co, Q, Wo, FS	3
53	79	0,8	Q	2
54	89	0,4	Q	1
55	67	1,8	Q, FS	2
56	81	1,1	Co	1
57	88	0,9		1
58	89	0,7		1
59	77	1,1	FS	2
60	68	1,0	Q, FS	2
61	90	0,5	Q	1
62	87	0,4	Q	2
63	50	5,7	Co, Q, Wo, FS	3
64	88	1,3	Wo	1
65	78	2,5	Wo, FS	2
66	66	1,8		2
67	52	3,0	Q, FS	3
68	59	2,2	Co, Q, Wo, FS	3
69	86	1,1	Q, Wo	2
70	59	6,1	Q, Wo, FS	3
71	77	1,6	Q,	2
72	9	0,8	Co, Wo, FS	4
73	72	2,3	FS	2
74	83	1,9	Wo, FS	2
75	87	1,6	Q, Wo	2

Gloss value, gloss value standard deviation, crystalline phases detected and PEI hardness of experimental glazes in series I (Publication I). Q = quartz, Wo = wollastonite, FS = feldspar, Co = corundum

RECENT REPORTS FROM THE COMBUSTION AND MATERIALS RESEARCH GROUP OF THE JOHAN GADOLIN PROCESS CHEMISTRY CENTRE:

15-01	Petteri Kangas	Modelling the Super-Equilibria in Thermal Biomass Conversion: Applications and Limitations of the Constrained Free Energy Method
15-02	David Agar	The Feasibility of Torrefaction for the Co-Firing of Wood in Pulverised-Fuel Boilers
16-01	Tooran Khazraie Shoulaifar	Chemical Changes in Biomass during Torrefaction
16-02	Hao Wu	Chemistry of Potassium Halides and Their Role in Corrosion in Biomass and Waste Firing
19-01	Jingxin Sui	Initial Stages of Alkali Salt Induced High Temperature Corrosion Mechanisms: Experimental studies using a combination of chronoamperometry, scanning electron microscopy, X-ray photoelectron spectroscopy and time-of-flight secondary ion mass spectrometry
19-02	Hanna Kinnunen	The Role and Corrosivity of Lead in Recycled Wood Combustion
19-03	Jonne Niemi	Effects of Temperature Gradient on Ash Deposit Aging and Heat Exchanger Corrosion
20-01	Meheretu Jaleta Dirbeba	Thermochemical Conversion Characteristics of Vinasse

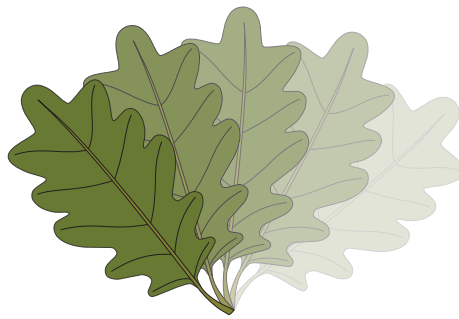

ISBN 978-952-12-3978-6 (printed)
ISBN 978-952-12-3979-3 (digital)
Åbo/Turku, Finland, 2020

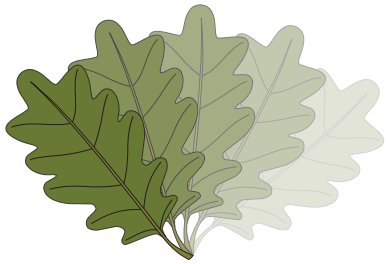

Johan Gadolin
Process Chemistry Centre

ISBN 978-952-12-3979-3